

UCSF

UC San Francisco Electronic Theses and Dissertations

Title

Development of Allosteric Inhibitors Targeting Human Herpesviral Proteases

Permalink

<https://escholarship.org/uc/item/6tq8m54m>

Author

Shahian, Tina

Publication Date

2011

Peer reviewed|Thesis/dissertation

Development of Allosteric Inhibitors Targeting Human Herpesviral Proteases

by

Tina Shahian

DISSERTATION

Submitted in partial satisfaction of the requirements for the degree of

DOCTOR OF PHILOSOPHY

in

Biochemistry and Molecular Biology

in the

GRADUATE DIVISION

of the

UNIVERSITY OF CALIFORNIA, SAN FRANCISCO

PREFACE

I would like to thank my advisor Dr. Charles S. Craik for his constant guidance and mentorship over the past six years. Charly's enthusiasm and love for science always made the lab a stimulating environment to work and learn. I was incredibly fortunate to work among colleagues who were brilliant, fun, and always eager to help. The success of my project would not have been possible without the joint efforts of post doctoral fellows Ana Lazic, Gregory M. Lee, and Aida Baharuddin. Graduate student Jonathan Gable is the newest member of our team and is already taking the project in exciting new directions.

I owe a lot of gratitude to my thesis committee advisors Dr. Brian K. Shoichet and Dr. Don Ganem. They not only helped my project remain on track, but also welcomed me to resources in their respective labs. Their advice has been invaluable to my scientific and professional development. Dr. Kiplin R. Guy, who is the Chair of Chemical Biology & Therapeutics at St. Jude Children's Research Hospital, has been our most important collaborator and I appreciate his wisdom on the project, and especially, his hospitality during my one week visit to their screening center.

My career at UCSF began two years prior to starting graduate school when I was working as a research associate in the new lab of Dr. Geeta Narlikar. Even though I was a novice to basic science research, Geeta entrusted me with a key project and guided my development into an independent scientist. This positive experience in Geeta's lab sparked my interest in research and

motivated me to continue my scientific training in graduate school. Geeta has guided me through some of the tough times in graduate school and her friendship is one that I cherish.

I would not be where I am today if it were not for the unconditional love and support of my parents Nasrin Zamanian and Hamid Shahian. Words cannot describe the extent of their sacrifice so that my sister and I could have a fulfilling and prosperous life. Their strong will and perseverance continues to inspire me. This thesis is dedicated to them for instilling in me the importance of always continuing to learn and follow my dreams. My sister Tara Shahian has been my lifelong friend and partner in crime. She and I have followed very different career paths, but I have learned a lot by watching her make daring career choices, work hard, and gain success in her profession.

Meeting my husband Peter Madrid was the most valuable outcome of my time at UCSF. Dr. Peter B. Madrid is an amazing scientist, an exceptional partner, and as of recently, a devoted father. His support, both personally and scientifically, has been instrumental to my success in graduate school and I am so fortunate to have him in my life. There has been nothing more rewarding than watching my beautiful daughter Leyla S. Madrid grow and reach new milestones over this past year. I hope to be a supportive mother and role model to her so that she can strive to be the best at all her life's passions.

Development of Allosteric Inhibitors Targeting Human Herpesviral Proteases

Tina Shahian

Human herpesviruses (HHVs) make up one of the most prevalent viral families and are the etiological agents of a variety of devastating human illnesses that lack safe and effective treatments. All HHVs express a dimeric serine protease that is essential to the viral life cycle. Kaposi's sarcoma-associated herpesvirus protease (KSHV Pr), a gamma subfamily member, was chosen as the model system for developing broad-spectrum herpesviral inhibitors. Of particular interest are KSHV Pr inhibitors that act allosterically, either by dimer dissociation or other mechanisms. A small-molecule KSHV Pr inhibitor has been identified that traps a transient allosteric pocket at the protease dimer interface. The binding of this molecule (DD2) has been shown to prevent the dimerization of KSHV Pr, which is required for its activation. This novel binding pocket is bioinformatically predicted to be conserved across all HHV proteases and DD2 has been shown to have activity against the serine protease from cytomegalovirus (CMV) a member of the beta herpesvirus subfamily. Additionally, methodologies have been developed to identify new inhibitors via a high throughput screen, elucidate the mechanism and binding modes of screening hits, and test for efficacy in a cell culture viral replication assay. This work presents methodologies and demonstrates the feasibility for identifying and using small-molecule allosteric inhibitors to target a conserved enzyme family that is conserved across a viral family.

TABLE OF CONTENTS

| | |
|--|-----------|
| Preface | iii |
| Abstract | v |
| List of Tables | ix |
| List of Figures | x |
| List of Schemes | xiii |
| Chapter 1: Introduction | 1 |
| References | 13 |
| Figures | 20 |
| Chapter 2: Inhibition of a Viral Enzyme by a Small Molecule Dimer | |
| Disruptor | 23 |
| Abstract | 24 |
| Background | 25 |
| Results | 29 |
| Discussion | 36 |
| Materials and Methods | 40 |
| References | 50 |
| Tables | 57 |
| Figures | 60 |
| Chapter 3: Enzyme Inhibition by Allosteric Capture of an Inactive | |
| Conformation | 75 |
| Abstract | 76 |

| | |
|--|-----|
| Background | 77 |
| Results | 81 |
| Discussion | 92 |
| Materials and Methods | 95 |
| References | 104 |
| Tables | 111 |
| Figures | 118 |
| Chapter 4: A Screening Strategy for Trapping the Inactive Conformer of a Dimeric Enzyme with a Small Molecule Inhibitor | 144 |
| Abstract | 145 |
| Background | 146 |
| Results | 148 |
| Discussion | 152 |
| Materials and Methods | 153 |
| Notes | 165 |
| References | 168 |
| Figures | 171 |
| Chapter 5: Determining the Effects of KSHV Pr Inhibition Using Small Molecules in Cell Culture | 182 |
| Abstract | 183 |
| Background | 184 |
| Results | 186 |

| | |
|--|-----|
| Discussion | 189 |
| Materials and Methods | 190 |
| References | 192 |
| Figures | 196 |
| Chapter 6: Conclusion and Future Directions in Developing Novel | |
| Inhibitors that Target Human Herpesvirus Proteases | 202 |
| References | 208 |
| Tables | 209 |
| Figures | 210 |

LIST OF TABLES

| | | |
|-----------|---|-----|
| Table 2-1 | Summary of inhibition data for all compounds | 57 |
| Table 2-2 | Summary of kinetic data for inhibitor DD1 | 58 |
| Table 3-1 | Summary of Crystallographic Information, 3NJQ | 111 |
| Table 3-2 | Average B-Values: KSHV Pr Δ 196-DD2 | 112 |
| Table 3-3 | Structural Comparison of KSHV Pr Constructs | 113 |
| Table 3-4 | Average ^a Sidechain B-Values of Residues | 114 |
| Table 3-5 | Structural Comparison of KSHV Pr-Bound DD2 Poses | 115 |
| Table 3-6 | Average ^a Sidechain B-values of the Active-Site Residues | 116 |
| Table 3-7 | DD2 Solubility and Cell Permeability | 117 |
| Table 6-1 | The effect of substrate length on DD2 activity | 209 |

LIST OF FIGURES

| | | |
|------------|---|-----|
| Figure 2-1 | KSHV Pr dimer interface and helical mimetic inhibitors of KSHV Pr activity | 60 |
| Figure 2-2 | DD2 does not show evidence of non-specific aggregation with Granzyme B | 62 |
| Figure 2-3 | DD2 disrupts the KSHV Pr dimer | 63 |
| Figure 2-4 | Kinetic studies with DD2 show evidence of mixed-type Inhibition | 65 |
| Figure 2-5 | DD2 disrupts the KSHV Pr M197L dimer | 67 |
| Figure 2-6 | ^1H - ^{15}N -HSQC titration data map the DD2 binding site to the dimer interface | 68 |
| Figure 2-7 | Full ^1H - ^{15}N -HSQC titration data for 170 μM DD2 | 70 |
| Figure 2-8 | ^1H - ^{15}N -HSQC titration data for 17 μM DD2 | 72 |
| Figure 2-9 | Monomer Trap model of inhibition by compound DD2 | 74 |
| Figure 3-1 | Domain diagram of KSHV Pr | 118 |
| Figure 3-2 | The ^{15}N - ^1H HSQC spectra of KSHV Pr truncations | 120 |
| Figure 3-3 | KSHV Pr-DD2 titration | 122 |
| Figure 3-4 | ^{13}C - ^1H HSQC spectra of KSHV Pr truncations | 124 |
| Figure 3-5 | The ^{13}C - ^1H HSQC spectra of the Ile-to-Val mutants | 126 |
| Figure 3-6 | DD2 titration of KSHV Pr M197D-I201V | 128 |
| Figure 3-7 | Structural comparison of the “apo” and DD2-inhibited KSHV Pr monomers | 129 |

| | | |
|-------------|---|-----|
| Figure 3-8 | Comparison of the apo and DD2-bound KSHV Pr crystal Structures | 131 |
| Figure 3-9 | The DD2 binding pocket | 132 |
| Figure 3-10 | The alternate conformation of the KSHV Pr Δ 196-DD2 Complex | 134 |
| Figure 3-11 | The poses of KSHV Pr-bound DD2 | 136 |
| Figure 3-12 | Structural perturbation of the KSHV Pr active site upon DD2 binding | 137 |
| Figure 3-13 | CD spectra of DD2 titrations with KSHV Pr and HCMV Pr | 139 |
| Figure 3-14 | HCMV Pr-DD2 titration data | 141 |
| Figure 3-15 | Structural homology of the HHV protease “hot spots” | 142 |
| Figure 4-1 | Structure of KSHV Pr dimer | 171 |
| Figure 4-2 | The workflow for identifying dimer disruptors of HHV proteases | 172 |
| Figure 4-3 | The structure of DD2 | 173 |
| Figure 4-4 | Plate uniformity layout for H/M/L | 174 |
| Figure 4-5 | Sample plate uniformity data analysis | 175 |
| Figure 4-6 | Scatter plot of screening data | 176 |
| Figure 4-7 | HTS assay quality data | 177 |
| Figure 4-8 | The structure and analysis of hexachlorophene | 178 |
| Figure 4-9 | The structure and analysis of cholanic acid | 179 |
| Figure 4-10 | Hexachlorophene shows evidence of non-specific aggregation with Granzyme B | 180 |
| Figure 4-11 | The 96-well plate arrangement | 181 |
| Figure 5-1 | Cell toxicity data with DD2 | 196 |

| | | |
|------------|--|-----|
| Figure 5-2 | Schematic of KSHV re-infection assay | 197 |
| Figure 5-3 | Latent and Lytic KSHV219 cells | 199 |
| Figure 5-4 | KSHV re-infection assay in the presence of DD2 | 200 |
| Figure 5-5 | Western blot assay to monitor AP cleavage | 201 |
| Figure 6-1 | Substrate iFRET8 sequence and kinetics | 210 |
| Figure 6-2 | Design of KSHV Pr FRET construct | 212 |
| Figure 6-3 | Sequences of hydrocarbon-stapled peptides | 213 |
| Figure 6-4 | Inhibition studies with hydrocarbon-stapled peptides | 214 |

LIST OF SCHEMES

| | | |
|------------|-----------------------------------|----|
| Scheme 2-1 | Synthesis scheme of compounds 1-8 | 59 |
|------------|-----------------------------------|----|

**CHAPTER 1: Introduction to Kaposi's sarcoma
Herpesvirus Protease and targeting
protein-protein interactions with small
molecules**

Portions of this chapter will be published in the Handbook of Proteolytic Enzymes, 3rd Ed.

Herpesviruses make up one of the most prevalent viral families and consist of eight human types that cause a variety of devastating illnesses including mononucleosis (Epstein-Barr virus, EBV), shingles (varicella zoster virus, VZV), genital herpes (herpes simplex virus, HSV), retinitis (cytomegalovirus, CMV), and cancer (Kaposi's sarcoma-associated herpesvirus, KSHV).¹ KSHV is the eighth human herpesvirus (HHV-8) and one of seven currently identified human oncoviruses. It belongs to the gamma herpes subfamily, which along with the alpha and beta subfamilies form the large Herpesviridae family (**Fig. 1-1**). KSHV is the etiological agent of Kaposi's sarcoma (KS), a complex angioproliferative and inflammatory lesion that was first described in the late 19th century by a Hungarian dermatologist Moritz Kaposi.^{2,3} KS is the most common neoplasm of patients with AIDS, and is also associated with primary effusion lymphoma (PEL), a clonal B-cell tumor, and multicentric Castleman's disease.⁴

Classic KS is endemic to the Mediterranean and Africa, where it is non-life threatening and found on the skin of elderly men.^{4,5} The most aggressive forms of the disease are found in patients with compromised immune systems, such as AIDS patients and those receiving organ transplants. The most aggressive forms of the disease are found in individuals with compromised immune systems, such as AIDS patients and those receiving organ transplants.⁶ KS is the most common neoplasm of patients with AIDS.⁶ In the United States and Europe, ~30% of HIV-1 infected homosexual men will develop AIDS-associated KS, which is characterized by aggressive skin lesion formation that can spread to vital organs and lead to high mortality rates.⁷ World-wide, KS is a serious problem, given the increase in HIV-infected individuals and lack of access to effective treatment, particularly in Africa, where

endemic KS is more prevalent in children with approximately 50% of children up to 11 years old are infected.^{8,9} With respect to other HHV-related diseases, infection is common in society. According to the CDC, approximately 1 in 150 children in the United States are born with congenital CMV infection, and of those children 20% develop permanent complications. Nationwide 16.2% of Americans suffer from genital herpes caused by herpes simplex virus type 2 (HSV-2).

When HHV infection is AIDS-related, highly active antiretroviral therapy (HAART) is usually effective at controlling the infection. Otherwise the standard course of treatment involved general-purpose antivirals that target viral DNA replication. To name a few, Ganciclovir is a synthetic analogue of 2'-deoxy-guanosine and is used to treat CMV retinitis in AIDS and transplant patients, and acyclovir is a guanosine analogue commonly used to treat herpes simplex virus (HSV-1, HSV-2) and varicella zoster virus (chickenpox, HHV-3, VZV) infections. Though routinely used, this class of drugs, which also includes foscarnet and cidofovir, suffers from undesirable toxicity and poor bioavailability, and increasing instances drug-resistant virus strains.¹⁰⁻¹³ Therefore there is a need for novel therapies that are specific to HHV.

All HHV, including KSHV, require a 25 kDa maturational serine protease (KSHV Pr) to generate infectious virions.¹⁴⁻¹⁷ The virus has two replication programs, latent and lytic. During latency only a handful of genes are expressed and no virions are produced. Upon induction of the lytic cycle, the viral genome is replicated, structural components are made, and infectious progeny is generated. Studies with genetically modified herpes simplex virus

mutants have indicated that protease function is essential for formation of mature KSHV viral capsids viral replication (**Fig. 1-1**).^{18,19} This process is initiated by the viral assembly protein (AP, ORF17.5), which forms a scaffold on which spherical procapsids assemble.¹⁸ KSHV Pr (ORF17) is expressed from an upstream promoter as an inactive monomer, N-terminally fused to roughly 10% of AP molecules (**Fig. 1-2**).¹⁷ Once translocated to the host nucleus where the immature capsid is being formed, the high local concentration of protease is thought to drive dimerization-dependant protease activation, which results in cleavage at two natural proteolysis sites (**Fig. 1-2**).²⁰⁻²³ AP is cleaved at the maturation site (M-site, Ala512*Ser513) near its C-terminus. Additionally, KSHV Pr cleaves itself away from the precursor fusion protein (Pr/AP) at the release site (R-site, Ala230*Ser231), which separates all herpesviral protease domains from their AP constituents.^{17,24-27} These cleavage events are necessary for the maturation of the viral procapsids into structures receptive to DNA packaging.²⁰⁻²³ Based on this evidence HHV proteases including KSHV Pr have been implicated as potential therapeutic targets.²⁸

The first reported structure at 2.2 Å resolution was solved for the protease dimer (**Fig. 1-3**).¹⁶ Each monomeric unit of KSHV Pr is composed of a seven-stranded, predominantly antiparallel, β -barrel and six α -helices. The structural similarity among herpesviral proteases is strongest within the core β -barrel, and diverges in the surrounding helices and loops. There are two independent catalytic triads, one in each monomer. Each non-canonical Ser-His-His catalytic triad is located on two solvent exposed β -barrels, within a shallow pocket surrounded by α -helices 5 and 6. The S1 binding pocket and oxyanion loop are formed and available for substrate binding and catalysis. The 2500 Å² dimer interface is formed primarily

by α -helices 1 and 5. The crossing angle of each monomer's α -helix 5 is similar to that of beta herpesvirus proteases, while the orientation of the β -barrels across the interface is most similar to the alpha herpesvirus proteases.

The activity of HHV proteases *in vitro* are regulated by concentration. Although HHV proteases are initially expressed as a monomer, studies with recombinant protease have demonstrated the dimerization dependence of enzyme activity.^{15,16,29-34} Mutagenesis studies with KSHV and other HHV proteases have shown that the dimer interface is very sensitive to genetic perturbation where a single point mutation leads to loss of dimerization and enzyme activity.^{15,29} When analyzed by sedimentation equilibrium a weak K_D of $1.7 \pm 0.9 \mu\text{M}$ is reported for KSHV Pr. An independent kinetic study in buffer with higher pH and ionic strength yielded a K_D of $0.56 \pm 0.14 \text{ nM}$.³⁵ The 3-fold discrepancy in the above reported dimerization affinities are due to varied assay buffer conditions, which is also observed with HSV-1 and hCMV Pr.^{31,34} An array of structural studies have suggested a model where protease dimerization induces folding of both the interfacial and C-terminal α -helices, which positions the oxyanion loop within the active-site and activates the enzyme.^{29,33,35,36} Furthermore, a strong structural link between the active-site serine and the dimer interface has been demonstrated.^{35,37} Kinetic, spectroscopic, and structural evidence with a hexapeptide diphenylphosphonate inhibitor illustrate how substrate binding to the active-site leads to conformational rearrangements that stabilize the oxyanion loop, as well as the dimer.¹⁷

The non-canonical Ser-His-His catalytic triad in KSHV Pr results in a severely disabled protease with a catalytic efficiency (k_{cat}/K_M) approximately four orders of magnitude reduced when compared with digestive serine proteases, such as trypsin.^{38,39} KSHV Pr cleaves itself and its native substrate assembly protein (AP), at the maturation (M), release (R), and dime disruptor (D) sites. Within the HHVs, the M and R sites exhibit consensus cleavage sequences of (Val/Leu)-(Asn/Gln/Glu)-Ala*Ser and Tyr-(Val/Leu/Ile)-(Lys/Gln)-Ala*Ser respectively, where (*) marks the scissile bond and (-) separate the P1, P2, and P3 positions.⁴⁰ Kinetic studies with recombinant protease and a synthetic oligopeptide substrate containing a fluorescence donor-quencher pair flanking the native KSHV R-site sequence Tyr-Leu-Lys-Ala*Ser-Gln-Phe-Pro yield a k_{cat}/K_M of $0.52 \times 10^3 \text{ M}^{-1} \text{ min}^{-1}$.¹⁴ The assay was performed at 20 °C in buffer consisting of 25 mM potassium phosphate (pH 7.0), 25% (v/v) glycerol, 150 mM KCl, 0.1 mM EDTA, and 1 mM 2-mercaptoethanol. Optimizing the assay conditions to 0.7 M potassium phosphate (pH 8.0) results in a marked increase in the k_{cat}/K_M to $2.2 \times 10^4 \text{ M}^{-1} \text{ min}^{-1}$, with a K_M of $2.9 \pm 1.3 \text{ }\mu\text{M}$ and a k_{cat} of $0.064 \pm 0.01 \text{ min}^{-1}$.¹⁵

A substrate profiling study using a Positional Scanning Synthetic Combinatorial Library (PS-SCL) revealed KSHV Pr to be a highly specific protease.³⁵ Consistent with the strongly conserved P1-alanine seen in all herpesvirus protease cleavage site sequences, alanine is the preferred amino acid at the P1 position, while P4 shows a strong preference for aromatic residues. The PS-SCL data has been used to develop optimal substrates with the fluorogenic reporter group 7-amino-4-carbamoyl-methylcoumarin (ACC) to monitor enzyme activity spectroscopically.^{35,37} Kinetic studies with an acetylated tetrapeptide substrate Ac-Tyr-tBug-Gln-Ala-ACC yield a K_M of $80 \pm 8.8 \text{ }\mu\text{M}$ and a k_{cat} of $0.0084 \pm 0.0003 \text{ s}^{-1}$.^{35,37} Analysis of

peptide substrates of varied lengths shows an 18.2-fold increase in catalytic efficiency for heptameric compared to tetrameric substrates.^{35,37} The enhanced catalytic efficiency comes solely from improved K_M values, whereas the turnover rate, k_{cat} remains virtually unchanged. This suggests that the energy of binding to the extended sites is sufficient to improve K_M values, and illustrates how extended substrate binding helps achieve specificity and effective proteolysis.

Although natural inhibitors of KSHV Pr are not known, synthetic inhibitors have been reported. Available substrate specificity information was the basis for the design of a potent hexapeptide organophosphonate inhibitor with the sequence Ac-Pro-Val-Tyr-tBug-Gln-AlaP-(OPh)^{2,17}. Incubation of KSHV Pr with the diphenylphosphonate revealed time-dependent inhibition of enzymatic activity with $k_{obs}/[I]$ of $6\text{ M}^{-1}\text{s}^{-1}$. On a streptavidin blot a biotinylated organophosphonate inhibitor failed to show binding to a protease mutant lacking the catalytic serine, thus confirming covalent attachment to the active-site.

The second 1.7 Å resolution, crystal structure of KSHV Pr in complex with the hexapeptide transition state analogue Ac-Pro-Val-Tyr-tBug-Gln-AlaP-(OPh)² that stabilizes the dimeric state has also been reported.³⁷ The overall fold of the KSHV protease/inhibitor structure is similar to that of the apo protease dimer. Previously observed disordered regions in the extended binding sites are present in this structure and in addition to the S4 pocket, provide a complete description of the S3, S5 and S6 sub-sites. A deep S4 pocket is formed upon inhibitor binding to accommodate a large Tyr residue, explaining the molecular basis of the previously reported strong preference for large hydrophobic residues at position P4.³⁵

Furthermore, binding of the peptide phosphonate inhibitor enhances dimer stabilization through a network of interactions established by induced conformational changes both at the active-site and the dimer interface.

Initial attempts to target the active-site of cytomegalovirus (CMV) protease lead to variety of peptidic and mechanism-based inhibitors with modest potencies.²⁸ A series of non-peptidic molecules developed based on the mechanism-based β -lactam inhibitors of the serine protease human leukocyte elastase, showed low micromolar potencies in vitro, but poor efficacy in plaque reduction assays.^{41,42} A newer generation of inhibitors based on this scaffold have shown good efficacy and pharmacokinetics in dogs, but have not lead to a clinical trial candidate.^{43,44} Recently a RNase P ribozyme (M1GS RNA) was generated to target the overlapping mRNA sequence of the murine cytomegalovirus (MCMV) protease.⁴⁵ This knockdown in protease expression resulted in reduced viral growth in both cell culture and MCMV-infected SCID mice. These studies serve to validate herpesvirus proteases as valid drug targets for the development of antivirals. Yet, this class of proteases has been deemed undruggable because past pharmaceutical attempts have focused solely on the active-site. Based on the observed strong linkage between the KSHV Pr dimer interface and the active site, inhibitors that disrupt dimerization are of great interest.

Traditionally, synthetic small-molecule inhibitors have been targeted to deep well-defined pockets, such as the active-site of an enzyme. However, the therapeutic potential of targeting protein-protein interactions, despite their inherent un-druggable molecular architecture, is becoming more apparent.⁴⁶ Unlike the conventional drug targets, the contact interfaces of

protein complexes are large and shallow, some as large as 3000 Å².^{47,48} Fortunately studies using alanine scanning mutagenesis have revealed that in most instances a subset of all interacting residues carry the bulk of this binding energy.^{49,50} A growing body of evidence suggests that protein complexes can be disrupted by targeting such “hot spot” residues.⁴⁶ Importantly, small molecules can take advantage of protein dynamics, to trap transient pockets that are otherwise absent from both the free and bound protein states.⁵¹⁻⁵³ Examples of successes include, cytokine interleukin-2 (IL-2) and the IL-2 receptor α -chain (IL-2R α); B-cell lymphoma protein (Bcl-X_L) and the pro-apoptotic molecule Bcl-2 antagonist of cell death (BAK); the oncogene human protein double minute 2 (HDM2) and the tumor suppressor protein p53; and the human papilloma virus transcription factor E2 complex and the viral helicase E1.⁴⁶ An inhibitor of the Bcl-X_L–BAK interaction has entered phase 1 and 2 clinical trials.⁵⁴

Although there are exceptions, high throughput (HTS) screening of large un-biased compound libraries has been for the most part unsuccessful in generating protein-protein interaction inhibitors.⁵⁵ This is due to the fact that the chemotypes of these libraries originate from drug discovery efforts with traditional targets, such as G-protein coupled receptors. A rational approach to this problem is to design inhibitors that mimic the structural domains interacting with the protein of interest. Protein secondary structure motifs play vital roles at the interface of protein complexes.⁴⁷ In particular, α -helices make up the largest class of protein secondary structure and are commonly found at the interface of protein-protein interactions. Therefore significant effort has been aimed at stabilizing peptides in the helical conformation, or developing non-peptide small molecule mimetics of α -helices.⁵⁶⁻⁵⁹

Examples of stabilized helical peptides and unnatural helices are β -peptide helices, mini-proteins, peptoid helices, and side-chain crosslinked α -helices.⁵⁶ Alternatively, helix surface mimetics have a characteristic rigid scaffold with functionalities presented in the same orientation as the i , $i + 3$ or $i + 4$, and $i + 7$ residue positions on an α -helix. The chemotypes of commonly reported scaffolds include biphenyls, allenes, alkylidene cycloalkanes, spiranes, benzylideneacetophenones, trisubstituted imidazole, indanes, polycyclic ethers, benzodiazepines and teraryl units.^{59,60} We have used numerous of these approaches for developing inhibitors that target the dimer interface of KSHV Pr.

The first successful physical disruption of KSHV Pr dimerization was achieved with a 30-amino acid protein, Avian pancreatic polypeptide (aPP), which contains an internally stabilized α -helix.⁶¹ aPP was used as a scaffold to design a KSHV Pr α -helix 5 mimetic. The resulting peptide fully disrupts KSHV Pr dimerization, and at approximately a 200-fold molar excess inhibited protease activity by 50%. The dissociation constant was estimated at 300 μ M. This study proved that targeting the dimer interface is a viable route for developing novel KSHV Pr inhibitors.

Chapters 2 and 3 will discuss the discovery and characterization of a small-molecule dimer disruptor of KSHV Pr.⁶² The two α -helices at the dimer interface of KSHV Pr were the basis for screening a library of small molecule helical mimetics. This biased library was originally developed by computational design to disrupt the interacting α -helix of p53 tumor suppressor protein with oncoprotein MDM2.⁶³ Inhibitor DD2 was identified with an IC_{50} of 3.0 ± 0.2 μ M and later shown to inhibit KSHV Pr dimerization. A variety of 2D-NMR strategies as

well as x-ray crystallography mapped the inhibitor binding site to a novel allosteric pocket at the dimer interface.^{62,64} A “monomer-trap” mode of inhibition was proposed where DD2 captures a pre-existing monomeric protease conformation in which α -helices 5 and 6 are unfolded and unable to stabilize the active dimeric state.⁵³

A key finding discussed in Chapter 3 is a 2.0 Å resolution crystal structure of a C-terminal truncated KSHV Pr in complex with a small molecule dimer disruptor, DD2, maps the binding pocket at the dimer interface and displays significant conformational perturbations at the active site.⁶⁴ This was the first report of a crystallographic structure of an allosterically inhibited HHV Pr monomer. Co-crystallization with DD2 was greatly aided by removing a portion of the disordered C-terminal domain, which hindered crystal lattice formation. In contrast to the active dimeric protease structure, the hot spot Trp109 indole ring adopts an open state in the inhibited protease structure, creating a hydrophobic cavity that acts as the DD2 binding pocket. Importantly the absence of the C-terminal α -helix 6 leads to conformational rearrangements in the active-site that collapse the substrate binding pocket and occludes the catalytic triad. Moreover, the highly conserved Arg142 and Arg143 side chains that point towards the active-site and support the oxyanion loop in the dimeric state, are pointing away in this structure. This observation with the truncated variant, which mimics an unstructured C-terminus in the monomeric state, supports the role of DD2 as an allosteric inhibitor that traps the monomer in an inactive state.

The poor efficacy, solubility, and permeability of DD2 were the limiting factor for follow-up studies in cell culture. Chapter 4 covers the optimization of a high throughput screening

assay for the purpose of screening large compound libraries. A fluorogenic protease activity assay was adapted for screening in a 384-well-plate assay platform. The substrate used is an optimized peptide sequence attached to 7-amino-4-carbamoylmethyl coumarin (ACC).^{35,37} Cleavage at the scissile bond releases the ACC group, resulting in increased fluorescence signals. DMSO tolerance, signal drift, reagent stability, and reaction times were optimized to achieve an assay fitness Z prime score of 0.7 or greater. Our fully characterized inhibitor DD2 was used as the positive control. The robustness of this assay was validated in a pilot screen of a small collection (~4000) of molecules with known bioactivities.

A critical step in validating dimer disruption as a novel approach for the development of a novel anti-herpes therapeutic is demonstrating efficacy in cell culture. Chapter 5 describes two assays that may be used to assess the anti-viral activity of protease inhibitors in the SLK cell culture model for KSHV. The first is a viral re-infection assay that measures the formation of infectious viral progeny. The second is a functional assay that monitors the cleavage of protease substrate, AP, by western blot analysis.

HHV proteases are key targets in the development of anti-herpes therapies. The following chapters will describe our strategy for developing allosteric inhibitors to this class of proteases that have been branded as “undruggable”. Chapter 6 will touch on future directions as we exploit a novel allosteric pocket at the dimer interface of KSHV Pr, with the goal of developing inhibitors with pan-specificity towards all HHV proteases.

REFERENCES

1. Fields, B.N. et al. *Fields Virology*, 3177 (Lippincott Williams & Wilkins, Philadelphia 2006).
2. Kaposi, M. Idiopathisches multiples pigmentsarkom her haut. *Arch Dermatol Shypilol* **4**, 265-273 (1872).
3. Chang, Y. et al. Identification of herpesvirus-like DNA sequences in AIDS-associated Kaposi's sarcoma. *Science* **266**, 1865-9 (1994).
4. Ganem, D. Kaposi's sarcoma-associated herpesvirus. in *Fields Virology*, Vol. 1 (eds. Knipe, D.M. & Howley, P.M.) (Lippincott, Williams and Kluwer, Philadelphia, PA, 2007).
5. Herndier, B. & Ganem, D. The biology of Kaposi's sarcoma. *Cancer Treat Res* **104**, 89-126 (2001).
6. Mitsuyasu, R.T. AIDS-related Kaposi's sarcoma: a review of its pathogenesis and treatment. *Blood Rev* **2**, 222-31 (1988).
7. Mayama, S. et al. Prevalence and transmission of Kaposi's sarcoma-associated herpesvirus (human herpesvirus 8) in Ugandan children and adolescents. *Int J Cancer* **77**, 817-20 (1998).
8. Renwick, N. et al. Seroconversion for human herpesvirus 8 during HIV infection is highly predictive of Kaposi's sarcoma. *Aids* **12**, 2481-8 (1998).
9. Renwick, N. et al. Kaposi's sarcoma and human herpesvirus 8 infection do not protect HIV-1 infected homosexual men from AIDS dementia complex. *Aids* **15**, 2165-9 (2001).

10. Eid, A.J., Arthurs, S.K., Deziel, P.J., Wilhelm, M.P. & Razonable, R.R. Emergence of drug-resistant cytomegalovirus in the era of valganciclovir prophylaxis: therapeutic implications and outcomes. *Clin Transplant* **22**, 162-70 (2008).
11. Eid, A.J. & Razonable, R.R. New developments in the management of cytomegalovirus infection after solid organ transplantation. *Drugs* **70**, 965-81.
12. Morfin, F. & Thouvenot, D. Herpes simplex virus resistance to antiviral drugs. *J Clin Virol* **26**, 29-37 (2003).
13. Reusser, P. Oral valganciclovir: a new option for treatment of cytomegalovirus infection and disease in immunocompromised hosts. *Expert Opin Investig Drugs* **10**, 1745-53 (2001).
14. Pray, T.R., Nomura, A.M., Pennington, M.W. & Craik, C.S. Auto-inactivation by cleavage within the dimer interface of Kaposi's sarcoma-associated herpesvirus protease. *J Mol Biol* **289**, 197-203 (1999).
15. Pray, T.R., Reiling, K.K., Demirjian, B.G. & Craik, C.S. Conformational change coupling the dimerization and activation of KSHV protease. *Biochemistry* **41**, 1474-82 (2002).
16. Reiling, K.K., Pray, T.R., Craik, C.S. & Stroud, R.M. Functional consequences of the Kaposi's sarcoma-associated herpesvirus protease structure: regulation of activity and dimerization by conserved structural elements. *Biochemistry* **39**, 12796-803 (2000).
17. Unal, A. et al. The protease and the assembly protein of Kaposi's sarcoma-associated herpesvirus (human herpesvirus 8). *J Virol* **71**, 7030-8 (1997).
18. Gao, M. et al. The protease of herpes simplex virus type 1 is essential for functional capsid formation and viral growth. *J Virol* **68**, 3702-12 (1994).

19. Preston, V.G., Coates, J.A. & Rixon, F.J. Identification and characterization of a herpes simplex virus gene product required for encapsidation of virus DNA. *J Virol* **45**, 1056-64 (1983).
20. Sheaffer, A.K. et al. Evidence for controlled incorporation of herpes simplex virus type 1 UL26 protease into capsids. *J Virol* **74**, 6838-48 (2000).
21. Sheaffer, A.K. et al. Herpes simplex virus DNA cleavage and packaging proteins associate with the procapsid prior to its maturation. *J Virol* **75**, 687-98 (2001).
22. Weinheimer, S.P. et al. Autoproteolysis of herpes simplex virus type 1 protease releases an active catalytic domain found in intermediate capsid particles. *J Virol* **67**, 5813-22 (1993).
23. Welch, A.R., Woods, A.S., McNally, L.M., Cotter, R.J. & Gibson, W. A herpesvirus maturational proteinase, assemblin: identification of its gene, putative active site domain, and cleavage site. *Proc Natl Acad Sci U S A* **88**, 10792-6 (1991).
24. Baum, E.Z. et al. Expression and analysis of the human cytomegalovirus UL80-encoded protease: identification of autoproteolytic sites. *J Virol* **67**, 497-506 (1993).
25. DiIanni, C.L. et al. Identification of the herpes simplex virus-1 protease cleavage sites by direct sequence analysis of autoproteolytic cleavage products. *J Biol Chem* **268**, 2048-51 (1993).
26. Robertson, B.J. et al. Separate functional domains of the herpes simplex virus type 1 protease: evidence for cleavage inside capsids. *J Virol* **70**, 4317-28 (1996).
27. Welch, A.R., McNally, L.M., Hall, M.R. & Gibson, W. Herpesvirus proteinase: site-directed mutagenesis used to study maturational, release, and inactivation cleavage

- sites of precursor and to identify a possible catalytic site serine and histidine. *J Virol* **67**, 7360-72 (1993).
28. Waxman, L. & Darke, P.L. The herpesvirus proteases as targets for antiviral chemotherapy. *Antivir Chem Chemother* **11**, 1-22 (2000).
 29. Batra, R., Khayat, R. & Tong, L. Molecular mechanism for dimerization to regulate the catalytic activity of human cytomegalovirus protease. *Nat Struct Biol* **8**, 810-7 (2001).
 30. Buisson, M. et al. Functional determinants of the Epstein-Barr virus protease. *J Mol Biol* **311**, 217-28 (2001).
 31. Darke, P.L. et al. Active human cytomegalovirus protease is a dimer. *J Biol Chem* **271**, 7445-9 (1996).
 32. Margosiak, S.A., Vanderpool, D.L., Sisson, W., Pinko, C. & Kan, C.C. Dimerization of the human cytomegalovirus protease: kinetic and biochemical characterization of the catalytic homodimer. *Biochemistry* **35**, 5300-7 (1996).
 33. Nomura, A.M., Marnett, A.B., Shimba, N., Dotsch, V. & Craik, C.S. Induced structure of a helical switch as a mechanism to regulate enzymatic activity. *Nat Struct Mol Biol* **12**, 1019-20 (2005).
 34. Schmidt, U. & Darke, P.L. Dimerization and activation of the herpes simplex virus type 1 protease. *J Biol Chem* **272**, 7732-5 (1997).
 35. Marnett, A.B., Nomura, A.M., Shimba, N., Ortiz de Montellano, P.R. & Craik, C.S. Communication between the active sites and dimer interface of a herpesvirus protease revealed by a transition-state inhibitor. *Proc Natl Acad Sci U S A* **101**, 6870-5 (2004).

36. Nomura, A.M., Marnett, A.B., Shimba, N., Dotsch, V. & Craik, C.S. One functional switch mediates reversible and irreversible inactivation of a herpesvirus protease. *Biochemistry* **45**, 3572-9 (2006).
37. Lazic, A., Goetz, D.H., Nomura, A.M., Marnett, A.B. & Craik, C.S. Substrate modulation of enzyme activity in the herpesvirus protease family. *J Mol Biol* **373**, 913-23 (2007).
38. Khayat, R., Batra, R., Massariol, M.J., Lagace, L. & Tong, L. Investigating the role of histidine 157 in the catalytic activity of human cytomegalovirus protease. *Biochemistry* **40**, 6344-51 (2001).
39. Register, R.B. & Shafer, J.A. A facile system for construction of HSV-1 variants: site directed mutation of the UL26 protease gene in HSV-1. *J Virol Methods* **57**, 181-93 (1996).
40. Gibson, W., Welch, A. R. & Hall, M. R. T. *Perspect. Drug Discov. Design* **2**, 413–426 (1994).
41. Yoakim, C. et al. Potent beta-lactam inhibitors of human cytomegalovirus protease. *Antivir Chem Chemother* **9**, 379-87 (1998).
42. Yoakim, C. et al. beta-Lactam derivatives as inhibitors of human cytomegalovirus protease. *J Med Chem* **41**, 2882-91 (1998).
43. Borthwick, A.D. Design of transactam HCMV protease inhibitors as potent antivirals. *Med Res Rev* **25**, 427-52 (2005).
44. Borthwick, A.D. et al. Design and synthesis of pyrrolidine-5,5'-trans-lactams (5-oxo-hexahydropyrrolo[3,2-b]pyrroles) as novel mechanism-based inhibitors of human

- cytomegalovirus protease. 4. Antiviral activity and plasma stability. *J Med Chem* **46**, 4428-49 (2003).
45. Bai, Y. et al. Effective inhibition in animals of viral pathogenesis by a ribozyme derived from RNase P catalytic RNA. *Proc Natl Acad Sci U S A* **105**, 10919-24 (2008).
46. Wells, J.A. & McClendon, C.L. Reaching for high-hanging fruit in drug discovery at protein-protein interfaces. *Nature* **450**, 1001-9 (2007).
47. Jones, S. & Thornton, J.M. Principles of protein-protein interactions. *Proc Natl Acad Sci U S A* **93**, 13-20 (1996).
48. Lo Conte, L., Chothia, C. & Janin, J. The atomic structure of protein-protein recognition sites. *J Mol Biol* **285**, 2177-98 (1999).
49. Bogan, A.A. & Thorn, K.S. Anatomy of hot spots in protein interfaces. *J Mol Biol* **280**, 1-9 (1998).
50. DeLano, W.L. Unraveling hot spots in binding interfaces: progress and challenges. *Curr Opin Struct Biol* **12**, 14-20 (2002).
51. Brown, S.P. & Hajduk, P.J. Effects of conformational dynamics on predicted protein druggability. *ChemMedChem* **1**, 70-2 (2006).
52. Eyrisch, S. & Helms, V. Transient pockets on protein surfaces involved in protein-protein interaction. *J Med Chem* **50**, 3457-64 (2007).
53. Lee, G.M. & Craik, C.S. Trapping moving targets with small molecules. *Science* **324**, 213-5 (2009).
54. Tse, C. et al. ABT-263: a potent and orally bioavailable Bcl-2 family inhibitor. *Cancer Res* **68**, 3421-8 (2008).

55. Cochran, A.G. Antagonists of protein-protein interactions. *Chem Biol* **7**, R85-94 (2000).
56. Henchey, L.K., Jochim, A.L. & Arora, P.S. Contemporary strategies for the stabilization of peptides in the alpha-helical conformation. *Curr Opin Chem Biol* **12**, 692-7 (2008).
57. Jochim, A.L. & Arora, P.S. Assessment of helical interfaces in protein-protein interactions. *Mol Biosyst* **5**, 924-6 (2009).
58. Jochim, A.L. & Arora, P.S. Systematic analysis of helical protein interfaces reveals targets for synthetic inhibitors. *ACS Chem Biol* **5**, 919-23.
59. Garner, J. & Harding, M.M. Design and synthesis of alpha-helical peptides and mimetics. *Org Biomol Chem* **5**, 3577-85 (2007).
60. Davis, J.M., Tsou, L.K. & Hamilton, A.D. Synthetic non-peptide mimetics of alpha-helices. *Chem Soc Rev* **36**, 326-34 (2007).
61. Shimba, N., Nomura, A.M., Marnett, A.B. & Craik, C.S. Herpesvirus protease inhibition by dimer disruption. *J Virol* **78**, 6657-65 (2004).
62. Shahian, T. et al. Inhibition of a Viral Enzyme by a Small Molecule Dimer Disruptor. *Nature Chemical Biology* **5**, 640-646 (2009).
63. Lu, F. et al. Proteomimetic libraries: design, synthesis, and evaluation of p53-MDM2 interaction inhibitors. *J Comb Chem* **8**, 315-25 (2006).
64. Lee, G.M. et al. Enzyme Inhibition by Allosteric Capture of an Inactive Conformation. *Journal of Molecular Biology* (In Press).

Figure 1-1

The role of KSHV protease in the viral lytic phase. KSHV Pr (blue) is expressed from ORF17 fused to an assembly protein (AP, purple). AP is also expressed more abundantly from ORF17.5. The Pr is translocated into the host nucleus (green) where precapsid shells (light purple) are being generated. There the activity of KSHV Pr is necessary for DNA encapsulation and angularization of mature capsids (orange).

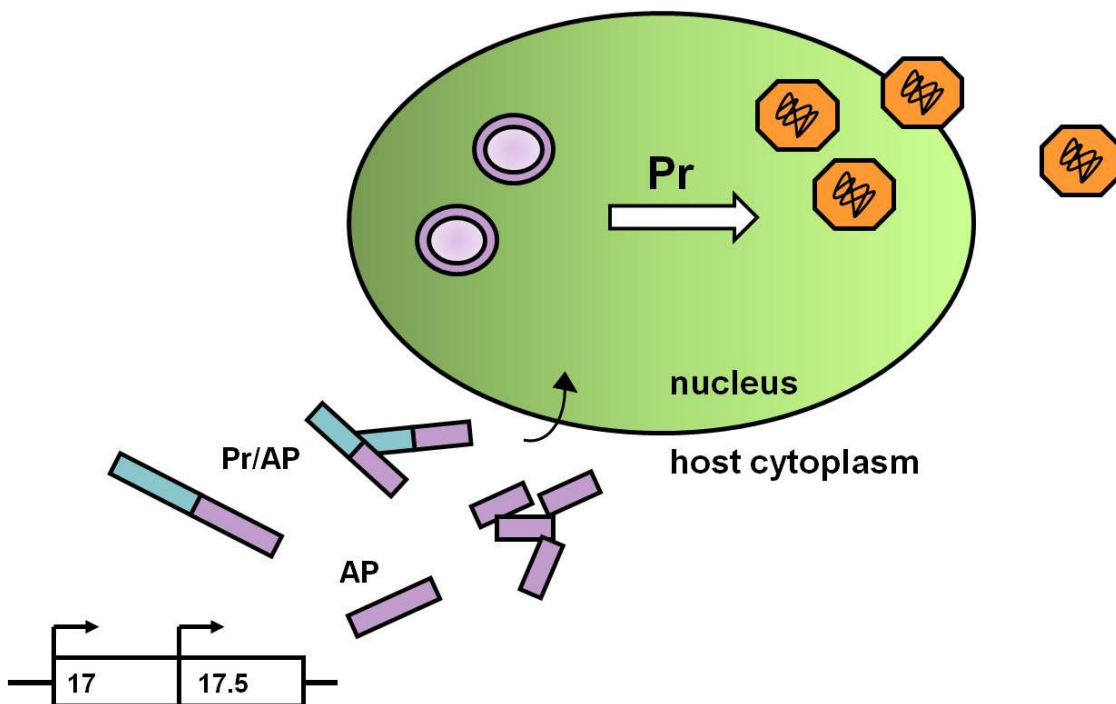


Figure 1-2

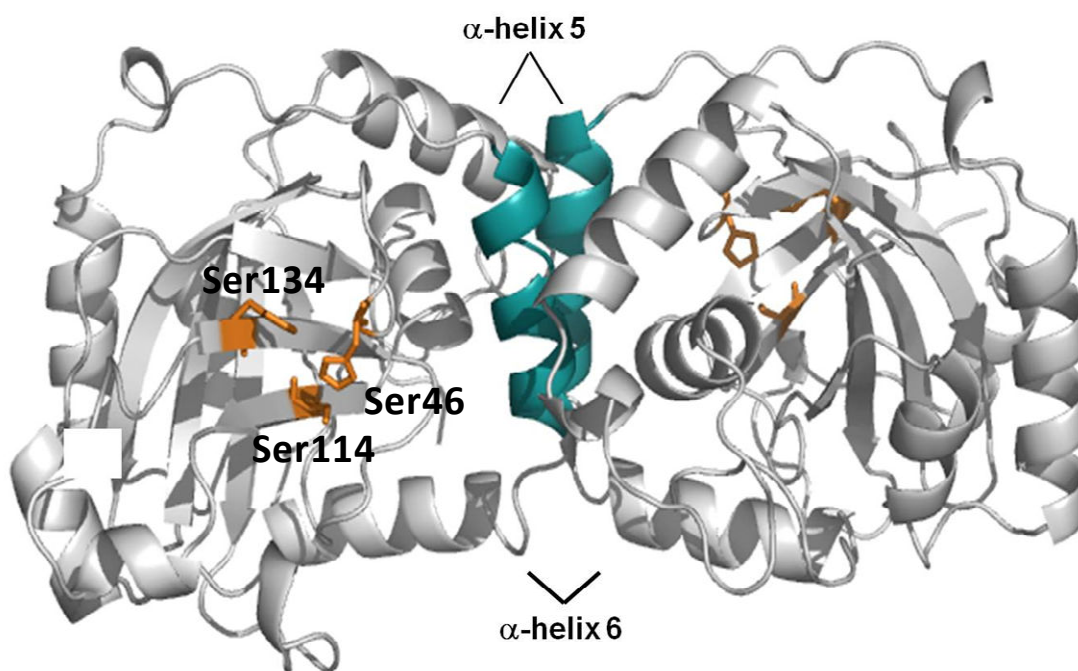
Open reading frame of KSHV Pr and AP. The complete DNA sequence of ORF17 is shown (orange and black). When expressed from the Met1 (M1, blue) the PR and AP fusion product is generated. AP is also expressed more abundantly from ORF17.5 (black). Met247 of ORF17.5 is shown in blue. In red are Ala203 = dimer disruptor site, Ala230 = R site, and Ala512 = M site.

MAAQGLYVGGFVDVVSCPKLEQELYLDPDQVTDYLPVTEPLPITIEHLPETEVGWTGLGFQ
VSGIFCTGAITSPAFLELASRLADTSHVARAPVKNLPKEPLLEILHTWLPGLSLSSIHPREL
SQTPSGVFQHVSLCALGRRRGTVAVYGHDAEWWVSRFSSVSKSERAHILQHVSSCRLED
LSTPNFVSPLETLMKAID**A**SFIRDRLDLLKTDRGVASILSPVYL**K****A**SQFPAGIQAVTPPRP
A**M**NSSGQEDIISIPKSAFLSMLQSSIDGMKTTAAKMSHTLSGPGLMGCQGMMFPTDHHL
SYVSNPAPPYGYAYKNPYDPWYYSPQLPGYRTGKRKRGAEDEGHLFPGEEPAYHKDIL
SMSKNIAEIQSELKEMKLNWHAGPPSSSSAAAAAVDPHYRPHANSAAPCQFPTMKEHG
GTYYHPPIYVQAPHGQFQQAAPILFAQPHVSHPPVSTGLAVVGAPPAEPTPASSTQSIQQQ
APETTHTPCAAVEKDAPTPNPTSNRLE**A**SSRSSPKSKIRKMFCEELLNKQ

M1 = ORF17, **M247** = ORF17.5, **A203** = dimer disruptor site, **A230** = R site, **A512** = M site

Figure 1-3

Crystal structure of KSHV Protease dimer. Alpha helices 5 and 6 are labeled. Alpha helix 5, which is located at the dimer interface, is highlighted in blue. The active site of each monomer acts independently and is composed of a non-canonical Ser114-His46-His134 catalytic triad (orange). The crystal structure of KSHV protease dimer is shown.¹⁶



CHAPTER 2: Inhibition of a Viral Enzyme by a Small Molecule Dimer Disruptor

Tina Shahian¹, Gregory M. Lee², Ana Lazic², Leggy A. Arnold³, Priya Velusamy³, Christina M. Roels³, R. Kiplin Guy³, Charles S. Craik²

¹Graduate Group in Biochemistry and Molecular Biology, University of California, San Francisco, 600 16th St., Genentech Hall, San Francisco, CA 94143, USA

²Department of Pharmaceutical Chemistry, University of California, San Francisco, 600 16th St., Genentech Hall, San Francisco, CA 94143, USA

³ Department of Chemical Biology and Therapeutics, St. Jude Children's Research Hospital, 262 Danny Thomas Place, Memphis, TN 38105, USA

This chapter is reformatted from “Inhibition of a viral enzyme by a small-molecule dimer disruptor”, Nature Chemical Biology 5, 640 - 646 (2009)

ABSTRACT

Small molecule dimer disruptors that inhibit an essential dimeric protease of human Kaposi's sarcoma-associated herpesvirus (KSHV) were identified by screening an α -helical mimetic library. Subsequently, a second generation of low micromolar inhibitors with improved potency and solubility was synthesized. Complementary methods including size exclusion chromatography and ^1H - ^{13}C HSQC titration using selectively labeled ^{13}C -Met samples revealed that monomeric protease is enriched in the presence of inhibitor. ^1H - ^{15}N -HSQC titration studies mapped the inhibitor binding-site to the dimer interface, and mutagenesis studies targeting this region were consistent with a mechanism where inhibitor binding prevents dimerization through the conformational selection of a dynamic intermediate. These results validate the interface of herpesvirus proteases and other similar oligomeric interactions as suitable targets for the development of small molecule inhibitors.

BACKGROUND

Targeting protein-protein interactions for a therapeutic purpose is an attractive idea that has proved to be extremely challenging in practice. This is due to the large and flat landscape of most contact surfaces that make them less amenable to intervention by a small molecule.¹⁻⁴ However, in recent years a growing body of evidence has demonstrated that small molecules can disrupt such large and complex protein interactions by binding to interface “hotspots” with drug-like potencies.⁵ Examples include interactions involving cytokine interleukin-2 (IL-2), with the IL-2 receptor α -chain (IL-2R α) ; B-cell lymphoma protein (Bcl-X_L), with pro-apoptotic molecule Bcl-2 antagonist of cell death (BAK); the oncogene human protein double minute 2 (HDM2), with tumor-suppressor protein p53; and the human papilloma virus transcription factor E2 complex with viral helicase E1.⁵ Notably, an inhibitor of Bcl-X_L/BAK interaction has entered phase I/II clinical trials.⁶ In this study we have identified the first of such small molecule protein interaction inhibitors for the family of herpesvirus proteases.

Herpesviruses make up one of the most prevalent viral families including eight human types that cause a variety of devastating illnesses including mononucleosis (Epstein-Barr virus, EBV), shingles (varicella zoster virus, VZV), genital herpes (herpes simplex virus, HSV), retinitis (cytomegalovirus, CMV), and cancer (Kaposi’s sarcoma-associated herpesvirus, KSHV).⁷ The standard course of treatment for common herpesviral infections, a class of broad-acting viral DNA replication inhibitors such as ganciclovir and foscarnet, though widely used, exhibit undesirable toxicity, poor oral bioavailability, and in some cases inadequate efficacy.⁸ With the incidents of drug resistance also on the rise and no other

specific antivirals available, there is a need for the identification of new human herpesvirus (HHV) therapeutic targets.

All herpesviruses express a structurally and functionally conserved dimeric serine protease that plays an essential role in capsid assembly during the lytic stage.⁹⁻¹³ Efforts by pharmaceutical companies to specifically target the active site of human cytomegalovirus protease with small molecule inhibitors has lead to either covalent inhibitors or molecules with non-ideal pharmacological properties.^{8,14-18} In light of evidence supporting a strong linkage between the dimer interface and the protease active site, we have focused our efforts on the dimer interface for identifying novel allosteric inhibitors.

Although HHV proteases are initially expressed as a monomer, studies with recombinant protease have demonstrated the dimerization dependence of enzyme activity.¹⁹⁻²⁶ An array of structural studies has suggested a model where protease dimerization induces folding of both the interfacial and the C-terminal α -helices, which positions the oxyanion loop within the active site and activates the enzyme.^{19,23,27,28} Interestingly, the non-cannonical Ser-His-His catalytic triad of each monomer is located 15Å away from the dimer interface and acts independently (**Fig. 2-1a**).^{25,29-34} Considering the extensive mechanistic knowledge of the human Kaposi's sarcoma-associated herpesvirus protease (KSHV Pr), we chose it as a candidate for the development of dimerization inhibitors for modulating the function of this enzyme family.

The KSHV Pr dimer interface covers approximately 2500 Å², and includes the α-helix 5 of each monomer as the major constituent (**Fig. 2-1a**).²⁵ Mutagenesis studies with KSHV and other HHV proteases have shown that the dimer interface is very sensitive to genetic perturbation where a single point mutation leads to loss of dimerization and enzyme activity.^{19,24} Importantly, this dimerization affinity is weak with a reported *in vitro* K_D of 1.7 μM for KSHV Pr.^{24,35} Hence, the protease is thought to be regulated by concentration-driven zymogen activation, where initially it exists as an inactive monomer in the host cytosol, but achieves dimerization and activation upon reaching a high local concentration inside the pre-capsid. These observed characteristics define the dimer interface as a critical allosteric regulatory site and a potential candidate for inhibition by small molecule dimer disruptors.

Recently we reported evidence for sterically disrupting the dimer interface of a herpesvirus protease.³⁶ Avian pancreatic polypeptide, aPP, a 30-amino acid peptide containing an internally stabilized α-helix, is used as a scaffold to design a KSHV Pr α-helix 5 mimetic. The resulting peptide fully disrupts KSHV Pr dimerization and inhibits activity, demonstrating that in addition to the active site, the protease dimer interface is a potential target for the development of small molecule inhibitors.

In this study we report a small molecule inhibitor of KSHV Pr dimerization. Inhibitors of KSHV Pr activity were obtained by screening a helical mimetic compound library. The top hits were subsequently assayed for dimer disruption and characterized for mode of binding. Our data supports a mechanism of inhibition where inhibitor binding to critical interfacial

residues on the protease monomer prevents dimerization. These studies illustrate that the dimer interface of HHV proteases is amenable to targeting by small molecule inhibitors.

RESULTS

Identification of inhibitors by high throughput screening.

Given that two α -helices are a major component of the KSHV Pr dimer interface, we screened a library of small molecule helical mimetics. This library of 182 compounds was originally developed by computational design to disrupt the interacting α -helix of p53 tumor suppressor protein with oncoprotein MDM2.³⁷ Our experimental design was based on the knowledge that interactions in both complexes are dominated by an α -helical motif.

Screening was performed in a 96-well plate format using a fluorogenic activity assay. The substrate used is an optimized peptide sequence attached to 7-amino-4-carbamoylmethyl coumarin (ACC), where cleavage at the scissile bond releases the ACC group resulting in increased fluorescence.^{38,39} We identified six molecules that inhibited KSHV Pr activity by at least 50%, the most potent compound being DD1, (**1**), with an IC_{50} of $8.8 \pm 0.3 \mu M$ (**Fig. 2-1b** and **Table 2-1**). DD1 was not found to inhibit the interaction of p53-MDM2, suggesting these proteomimetic molecules can potentially discriminate between different intermolecular interactions involving an α -helix.³⁷ A series of DD1 analogs was designed to explore modifications around the 4-benzoylamino-benzoic acid scaffold using previously reported synthetic methods (**Scheme 2-1**).³⁷

Further screening of eight DD1 structural analogues yielded additional hits, the most potent being (**2**) with an IC_{50} of $3.1 \pm 0.2 \mu M$, and (**3**) with an IC_{50} of $16.4 \pm 0.7 \mu M$ (**Fig. 2-1b** and **Table 2-1**). The improved IC_{50} of the top inhibitor, DD2, (**2**) is possibly due to the hydrogen bonding capabilities of the added pyridine nitrogen to residues on the protease. Additionally,

the structure-activity relationship (SAR) for this series indicated that correct positioning of the cyclohexylmethyl side chain is critical, where substitution from its original *meta* position to either the *para* (**4**) or the *ortho* (**5**) positions diminished inhibition (**Fig. 2-1b** and **Table 2-1**). This effect is consistent with the original design rationale of the helical mimetic molecules, where the spatial and angular arrangement of the side chains on the scaffold were fixed to mimic the *i* and *i*+4 residues of an α -helix. It is also in agreement with a specific mechanism of inhibition whereby the cyclohexylmethyl side chain makes critical hydrophobic interactions with KSHV Pr residues.

Compounds were tested for non-specific aggregation by assessing their behavior in the presence of a non-ionic detergent.⁴⁰ KSHV Pr was substituted with an unrelated serine protease Granzyme B, which unlike KSHV Pr, tolerates detergents in assays for biochemical activity. In a spectrophotometric activity assay monitoring Granzyme B activity, DD2 failed to show evidence of inhibition in the presence or absence of detergent, while a known aggregator, hexachlorophene, inhibited Granzyme B activity only in the absence of detergent (**Fig. 2-2**). DD2 also did not show evidence of particle formation when analyzed by dynamic light scattering. Collectively, this data suggests that DD2 acts by a specific mechanism to inhibit KSHV Pr activity.

Helical mimetic inhibitors disrupt protease dimerization.

To assess the dimerization state of KSHV Pr in the presence of DD2, we took two complementary approaches. The first approach used a size exclusion chromatography assay where the dimeric and monomeric protease populations are monitored by their distinct

elution profiles.^{24,28} At a concentration of 5 μ M, KSHV Pr eluted as two separate peaks corresponding to the dimeric and monomeric species, respectively (**Fig. 2-3a**). As expected for a sample concentration above the recorded K_D of 1.7 μ M, a larger fraction of the protease appeared in the dimer peak. However, when pre-incubated with 30 μ M DD2, KSHV Pr eluted predominantly as a monomer (**Fig. 2-3a**). The enrichment of monomeric KSHV Pr strongly suggests that DD2 acts as a dimer disruptor.

As an alternate approach to evaluating protease dimerization, we performed 2-D nuclear magnetic resonance (NMR) assays using selectively isotope-labeled KSHV Pr.²⁸ In this experiment, methionine, which occurs in the sequence only at the N-terminus (Met1) and at the dimer interface (Met197) was used as a probe to evaluate monomer-dimer transitions (**Fig. 2-1a**). Heteronuclear single quantum coherence (HSQC) spectra of selectively labeled ¹³C-Met KSHV Pr exhibits resonances corresponding to the methyl group of Met1 as well as Met197 in both the monomeric and dimeric conformations (**Fig. 2-3c**). Overlaid spectra of the titration data reveal that increasing DD2 concentrations induces a chemical shift perturbation and increase in the peak volume of the Met197-monomer resonance. Concomitantly, we observed a decrease in the peak volume of the M197-dimer peak, which broadens beyond detection at 1 molar equivalence inhibitor (24 μ M). Inhibitor concentrations up to 2 molar equivalence resulted in no additional change. The Met1 resonance remained unchanged throughout the titrations and served as an internal control. The data further confirms that DD2 disrupts the protease dimer and highlights changes in the local conformational environment of the interfacial Met197. DD1 produced similar results in both the size exclusion chromatography as well as the HSQC experiments (data not shown). These

results are consistent with a model of helical mimetic inhibitors of KSHV Pr activity acting via a mechanism of dimer disruption.

DD2 shows characteristics of mixed inhibition.

The activation mechanism of KSHV Pr involves a series of allosteric conformational changes that link the dimer interface to positioning of the oxyanion loop in the active site 15Å away. Binding of a covalent and irreversible peptide phosphonate inhibitor to the KSHV Pr active site promotes enzyme dimerization, illustrating communication between the two sites.²⁸ In such a complex system, an inhibitor acting as a dimer disruptor is expected to show properties of mixed-type inhibition, with a characteristic change in both K_M for substrate and maximum reaction velocity, V_{max} . We performed kinetic assays to measure the Michaelis-Menten constants for substrate in the presence of increasing concentrations of DD2, and plotted the initial reaction velocities as a function of substrate concentration in Lineweaver-Burk format (**Fig. 2-4a**). A 1 -10 μ M concentration range of DD2, caused a 2.5 fold increase in K_M and a 3 fold decrease in V_{max} (**Table 2-2**). This effect on both the K_M and the V_{max} is conceivable since dimer dissociation dismantles the structural framework responsible for forming the KSHV Pr active site. Based on this data, DD2 is a dimer disruptor that acts as a mixed-type inhibitor by preventing the formation of a conformationally stable active site.

DD2 is weaker against a tighter- K_D KSHV Pr variant.

In order to verify that DD2 acts at the dimer interface, we tested its inhibitory activity against a KSHV Pr variant with a lower K_D . Previously we showed that replacing the interfacial Met197 with a leucine results in approximately 4 fold improvement in binding affinity

between KSHV Pr monomers ($K_D = 0.4 \mu\text{M}$).³⁶ In a comparative activity assay with wild-type and M197L KSHV Pr, DD2 exhibited IC_{50} values of $2.6 \pm 0.4 \mu\text{M}$ and $7.3 \pm 0.8 \mu\text{M}$, respectively (**Fig. 2-4b**). Size exclusion chromatography studies with KSHV Pr M197L confirmed that DD2 still acts by dimer dissociation but less efficiently (**Fig. 2-5**). The observation that DD2 was proportionally less active against a tighter-binding dimer interface, suggests that both DD2 and a KSHV Pr monomer are competing for overlapping binding sites on a second KSHV Pr monomer. We observed similar properties in previous studies with a peptidic α -helix 5 mimetic that disrupts the KSHV Pr dimer.³⁶ Consistent with earlier experiments, the finely tuned potency of DD2 and the varied slopes of the IC_{50} curves suggest an inhibitory mechanism that is not aggregation-based, where minute alterations are not expected to alter the overall kinetics of inhibition. The fact that DD2 remained active against the M197L variant also shows that Met197 is not a critical residue for inhibitor binding. We conclude that DD2 is a specific inhibitor of KSHV Pr that disrupts protease dimerization by binding to interfacial residues on the KSHV monomer, excluding Met197.

Residues interacting with DD2 map to the dimer interface.

To obtain a higher resolution map of the DD2 binding site on KSHV Pr we utilized the technique of chemical shift perturbation mapping. Importantly, NMR was our method of choice as the partially disordered state of KSHV protease presents a challenge for crystallographic studies.⁴¹ In the absence of significant conformational perturbations, this method detects changes in the electronic environment of protein backbone amides that occur as a consequence of small molecule binding, and translates them into altered chemical shifts on a ^1H - ^{15}N -HSQC spectrum. For this experiment we used an obligate monomer variant of

KSHV Pr, M197D, for which over 90% of the backbone chemical shifts are assigned²⁷. Based on data showing that DD2 remained active against KSHV Pr M197L, we hypothesized that the M197D point mutation would cause little interference with inhibitor binding. The overlaid ¹H-¹⁵N-HSQC spectra of KSHV Pr M197D in the absence and presence of ~1 molar equivalence (170 μ M) DD2 displayed extensive conformational peak broadening in the backbone amides of interface residues (**Fig. 2-6a** and **Fig. 2-7**). The observed peak-broadening phenomenon is due to conformational exchange on an intermediate NMR time scale. The chemical shift of residues in the saturated bound state cannot be observed because the solubility limit of DD2 does not allow for collecting spectra with a 5-10 fold excess of inhibitor concentrations under the current experimental conditions.

When mapped to the monomeric unit of the KSHV Pr crystal structure,³⁹ the most significantly perturbed residues were clustered at the dimer interface, where both the resident α -helix 5 and the α -helix 5 of the second monomer form key interactions (**Fig. 2-6b**). Importantly, the protease active site residues, Ser114, His46, His134, and Arg143, did not participate in inhibitor binding. The peak broadening of active site residue Arg142 that was observed at saturating DD2 concentrations is likely attributed to allosteric conformational effects propagating from the primary binding site. Notably, the Trp109 indole side chain NH signal exhibited the greatest conformational peak broadening, with over 90% loss of peak intensity in the presence of 1 molar equivalence DD2 (**Fig. 2-6b**). A similar high response was observed with concentrations as low as 0.1 molar equivalence DD2 (**Fig. 2-8**). Trp109 resides in close proximity to the resident α -helix 5 and engages in key intermolecular interactions across the dimer interface (**Fig. 2-1a**). The titration data with KSHV Pr M197D

also provides conclusive evidence that DD2 binds to a monomeric unit of KSHV Pr. We hypothesize that DD2 inhibits KSHV Pr by strongly associating with Trp109 and other interface residues on the monomer, thus preventing dimerization.

A point mutation on Trp109 disrupts KSHV Pr dimerization.

The results of the ^1H - ^{15}N -HSQC titration experiments demonstrate that Trp109 plays a critical role in KSHV Pr dimerization. To test this hypothesis, we monitored protease activity and dimerization on a variant with an alanine substitution of Trp109. KSHV Pr W109A was completely inactive when tested at concentrations up to 30 μM , and eluted as a monomer by size exclusion chromatography (**Fig. 2-3b**). This data suggests that Trp109 participates in essential dimer-promoting interactions, which are disrupted upon DD2 binding.

DD2 inhibits the activity of a related herpesvirus protease.

All known HHV proteases are structurally and functionally conserved. Therefore it is conceivable to identify a broad-acting inhibitor against this family of enzymes. To examine this notion, we tested DD2 for inhibition of human cytomegalovirus protease (CMV Pr) using the KSHV Pr fluorogenic assay discussed previously. DD2 showed activity inhibition with an IC_{50} of $5.0 \pm 0.5 \mu\text{M}$ (**Table 2-1**). We conclude that while DD2 is an inhibitor of KSHV Pr, it is also active against the related CMV Pr.

DISCUSSION

Proteases are attractive drug targets, but conventional approaches aimed at the active site can be challenging due to structural similarities in the substrate-binding pockets of related family members. We have reported a small molecule inhibitor of the herpesvirus protease family that acts at a novel allosteric site by a mechanism of dimer dissociation. Additional work is needed to improve the drug-like properties of these compounds, but they have been instrumental in revealing this regulatory binding site. To our knowledge DD2 is the first small molecule inhibitor of a herpesvirus protease to not only act outside the active site, but also select for the partially unfolded zymogen. This illustrates how the inherent conformational dynamics of proteins that are critical to their function also offer opportunity for allosteric regulation.

A dimerization driven disorder-to-order conformational switch regulates the activity of KSHV Pr. The two α -helices at the dimer interface became our rationale for screening a helical mimetic library for inhibitors. We optimized our initial hit, DD1, to produce our top inhibitor, DD2, with an IC_{50} of $3.1 \pm 0.2 \mu M$. Using a combination of gel filtration chromatography, 2D NMR spectroscopy, mutagenesis, and kinetic methods we demonstrated that DD2 acts at the interface, to inhibit protease dimerization, and in turn prevent formation of the active site.

Trp109 is a critical residue in the formation of the dimer, as well as its dissociation by DD2. A survey of the dimeric KSHV Pr X-ray crystal structure placed Trp109 behind the resident α -helix 5 with its indole ring extended towards the hydrophobic side chains of Met197 and

Ile201 on the second interfacial α -helix 5 (**Fig. 2-1a**). Therefore, we hypothesize that DD2 disrupts protease dimerization by associating with interface residues, including Trp109, and interrupting critical dimer-stabilizing interactions. Interestingly, Met197 and Ile201 assume the i and $i+4$ positions on α -helix 5. In following with the design of the helical mimetic compounds, we speculate the hydrophobic side chains on DD2 mimic these residues and interact with Trp109 in a similar fashion. A homologous binding pocket does not exist in the p53-MDM2 interface, which could explain why this subset of helical mimetic compounds failed to inhibit that interaction⁴².

Based on these studies we propose a “monomer trap” model of inhibition by DD2 (**Fig. 2- 9**). In the absence of inhibitor, inactive KSHV Pr monomer is in equilibrium with active dimer with a weak K_D of 1.2 μ M. DD2 competes with this process and binds to one of the pre-existing zymogen conformations, thus interfering with interactions critical for dimerization and trapping the monomer in an inactive partially disordered state.

An intriguing possibility is a broad-acting inhibitor that targets the protease dimer interface in all eight known HHVs in the alpha, beta, and gamma sub-families. While in all cases the protease is structurally and functionally conserved, the highest amino acid identity observed across sub-families is at 37% between (γ) KSHV Pr and (β) CMV Pr. In our initial studies with CMV Pr, DD2 showed inhibitory activity with an IC_{50} of $5.0 \pm 0.5 \mu$ M. Close analysis of the CMV Pr structure reveals interface residues engaged in similar hydrophobic interactions involving an aromatic residue. In this case Leu222, Val226, and Tyr128 of CMV Pr are homologous to Met197, Ile201, and Trp109 in KSHV Pr.^{33,43} The more distant relative

(α) VZV Pr, with 30% KSHV Pr identity, also reveals a similar interaction with Leu203, Val207, and Tyr115, while the closest relative (γ) EBV Pr, with 44% KSHV Pr identity, virtually replicates the interaction with Ile202, Ile206, and Trp111. We hypothesize that DD2 inhibits both KSHV Pr and CMV Pr by the same mechanism, and suggest that this allosteric site could be targeted across all HHV protease sub-families to develop a novel and broad-spectrum drug.

From a drug-design viewpoint, drugs targeted to a protein-protein interaction as opposed to an enzyme active site could be less prone to drug resistant mutations. This is because acquiring a drug-resistant point mutation, unaccompanied by the right compensatory mutations, is less likely to be tolerated by a complex protein-protein interface. This adaptability is highly dependant on the natural prevalence of amino acid variation across protease residues. For the extensively catalogued Human Immunodeficiency Virus Type 1 (HIV-1) protease the rate of natural variation at its β -sheet dimer interface is highly uncommon.⁴⁴ Furthermore, given the past challenges of developing therapies aimed at the active site of HHV proteases, our findings introduce a new approach to this previously validated target. In terms of drug accessibility, targeting the inactive protease monomer is especially attractive for HHVs. While the active dimer acts on capsid formation in the host nucleus, the inactive monomer, which exhibits a high *in vitro* K_D , is believed to exist in the host cytosol as a mechanism for concentration-dependant zymogen activation.^{24,35}

By identifying allosteric regulatory sites in KSHV Pr we have gained a better understanding of its structure and discovered additional avenues for inhibition. In other enzyme targets such

as caspase-3 and caspase-7, the disulfide trapping approach was used to identify allosteric ligands that bind to the intact dimer interface and trap the enzymes in their zymogen conformation.^{45,46} Similarly, in the case of HIV-1 protease, crosslinked interface peptides and derivatives were developed that bind to the antiparallel β -sheet interface, sterically inhibiting dimerization and thereby formation of the neighboring active site.^{47,48} We have identified a novel inhibitor of HHV proteases that acts by combining both mechanisms. This approach can potentially be used for developing novel inhibitors for HHV proteases as well as other systems involving a similar protein-protein interaction motif.

MATERIALS AND METHODS

Protein Expression and Purification

Wild-type and M197L KSHV Pr were prepared as described previously.^{35,49} All protease constructs carry the S204G mutation, which prevents autolysis while maintaining other proteolytic functions. The W109A construct was created with the QuikChange® Multi Site-Directed Mutagenesis Kit (Stratagene). KSHV Pr wild-type (S204G) construct was used as the parent template for mutagenesis using primer: 5'-ggagatactccacacggcgctcccggggctgtc-3' (Integrated DNA Technologies, Inc.). Protein expression and purification was carried out following the same protocol as that of wild-type protease. CMV Pr protease was expressed following a previously described protocol.⁵⁰ All kinetic assays were performed using KSHV Pr assays and reagents.

Selectively ¹³C-methionine labeled wild-type KSHV Pr and uniformly ¹⁵N-labeled monomeric KSHV Pr M197D was expressed in M9 minimal media and purified as previously described.²⁷ In the former, 250 mg ¹³C-labeled methionine (Cambridge Isotope Laboratories) was added to 1 L minimal media 1 hour prior to IPTG induction. Final sample concentrations were quantified by measuring UV absorbance at 280 nm using a predicted extinction coefficient of 23950 M⁻¹ cm⁻¹ (<http://ca.expasy.org/tools/protparam.html>).

Kinetic Assays

Helical mimetic screen: Protease was diluted to a final concentration of 2 µM in assay buffer (25 mM potassium phosphate pH 8, 150 mM KCl, 0.1 mM EDTA, and 1mM DTT) and 198 µl was dispensed in each well of a black round-bottom 96-well plate (Corning). 1 µl of

compound, provided as 2 mM DMSO stocks, was transferred to each well for a final compound concentration of 10 μ M. Following a 30-minute incubation at 30°C, enzyme activity was initiated by adding 1 μ l fluorogenic hexapeptide substrate to a final concentration of 160 μ M. The substrate (also referred to as P6) 7-amino-4-carbamoylmethyl coumarin (ACC) coupled to Ac-Pro-Val-Tyr-tert-butylglycine-Gln-Ala (Ac-PVYtQA-ACC), was prepared as described previously.^{38,39} Enzyme activity was monitored for 1 hour at 30°C on the Spectra MAX Gemini EM Fluorescence Microplate Reader (Molecular Devices) using excitation and emission wavelength of 380 nm and 460 nm, respectively. Hits were identified as compounds that reduced the initial reaction velocity by at least 50% when compared to control (uninhibited) reaction. The final reaction volume and DMSO concentration were 200 μ l and 1% respectively.

IC₅₀ determination: For each compound a 3-fold dilution series DMSO stock was prepared in a concentration range of 10 mM – 0.014 mM. 1 μ l of each compound dilution was added to 98 μ l of 1 μ M KSHV Pr (wild-type or M197L) in assay buffer to give a final compound concentration of 100 μ M – 0.14 μ M. Following a 30-minute incubation at 30°C, enzyme activity was initiated by adding P6 substrate to a final concentration of 100 μ M. Endpoint fluorescence was recorded after a 1 hour incubation at 30°C (reaction progress curves were linear at the time of measurement). The final reaction volume and DMSO concentration were 100 μ l and 2% respectively. The ratio F/F₀ was plotted as a function of inhibitor concentration and fitted to equation (1) using KaleidaGraph® (Synergy Software). F and F₀ correspond to the endpoint fluorescence measurement of the experimental reaction and the endpoint fluorescence measurement of the control (uninhibited) reaction, respectively. Y,

M0, M1, M2, M3, and M4 correspond to F/F0, compound concentration, maximum endpoint fluorescence, minimum endpoint fluorescence, IC₅₀, and Hill slope, respectively. All IC₅₀ values represents mean values ± s.d. (n=3).

Equation (1)

$$Y = M1 + \frac{M2 - M1}{1 + 10^{((\log M3 - \log M0) \times M4)}}$$

Inhibition kinetics: A standard 100 µl enzyme assay was performed using 1 µM KSHV Pr in assay buffer. Final substrate concentrations of 80, 40, 30, 20, 10, 6, 4, and 2 µM were tested across inhibitor concentrations of 10, 7, 5, 3, 1, and 0 µM (48 total reactions). Initial reaction velocity V0 in units of rfu/sec was converted to µM substrate/sec using the conversion factor (2364 rfu) / (µM substrate). Double-reciprocal plots were fit to a linear equation to determine the K_M and V_{max}. The ratio V_{max} / [dimer] was used to calculate k_{cat}, where the dimer concentration was determined to be 0.26 µM using equation (2). K_D is the dimerization constant for KSHV Pr and E_t is the total enzyme concentration. Data represents mean values ± s.d. (n=3).

Equation (2)

$$[\text{dimer}] = \frac{(K_D + 4 [E_t]) - (K_D + 8K_D [E_t])^{1/2}}{8}$$

Gel Filtration

Size exclusion chromatography was performed using a ÄKTAexplorerTM (GE Healthcare) equipped with Superdex®75 column. KSHV Pr diluted to 5 µM in assay buffer (25 mM potassium phosphate pH 8, 150 mM KCl, 0.1 mM EDTA, and 1mM DTT) was combined

with 30 μ M compound and incubated at 30°C for 30 minutes. The final reaction volume and DMSO concentration were 200 μ l and 1% respectively. Sample was then loaded onto a gel filtration column pre-equilibrated with 30 μ M compound in assay buffer at room temperature. In control experiments, DMSO was used instead of compound.

NMR data acquisition

All spectra were acquired on cryoprobe-equipped Varian Inova 600 MHz or Bruker Avance 800 MHz spectrometers at 27 °C. Typical NMR samples used for the ^1H - ^{13}C -HSQC dimer disruption assays consisted of 0.02 – 0.03 mM selectively labeled with ^{13}C -methionine wild-type KSHV Pr in 0.45 – 0.50 mL buffer. Standard assay buffer consisted of 25 mM phosphate buffer (pH 8.0), 150 mM NaCl, 0.1 mM EDTA, 5 mM DTT, and 10% (v/v) $^2\text{H}_2\text{O}$. Powdered inhibitor was first dissolved in d_6 -DMSO (Cambridge Isotope Laboratories) to create a 10 mM solution, then serially diluted to 5 mM, 1 mM and 0.5 mM stocks. Titrations were performed by adding variable μL aliquots of inhibitor stocks in a step-wise manner until 2 – 4 molar equivalents were reached.

Sample concentrations used for the ^1H - ^{15}N -HSQC backbone mapping of the monomeric KSHV Pr M197D-dimer disruptor interactions were 0.15 – 0.20 mM uniformly ^{15}N -labeled protease in 0.45 – 0.50 mL buffer. Due to significant solvent exchange peak broadening observed at pH 8.0, NMR samples were buffer exchanged to 25 mM phosphate buffer (pH 7.0) using Amicon Ultra 10K Centrifugal Filter Devices (Millipore Corp.). Buffer conditions and titration methodologies were otherwise identical to those used for the ^{13}C -methionine HSQC assays.

External ^{13}C and ^1H chemical shift referencing was performed using a 10 mM sample of 2,2-dimethyl-2-silapentane-5-sulfonate, sodium salt (Cambridge Isotope Laboratories). External ^{15}N chemical shift referencing was performed using $^{15}\text{NH}_3$. ^1H - ^{13}C -heteronuclear single quantum coherence (HSQC) spectra were acquired at 600 MHz with 72 scans, and 1024 t_1 and 96 t_2 complex points. Spectral widths were 3000 Hz and 7200 Hz in the ^{13}C and ^1H dimensions, respectively. ^1H - ^{15}N -HSQC spectra were acquired at 800 MHz with 8 scans, and 1024 t_1 and 256 t_2 complex points. Spectral widths were 2757 Hz and 12820.5 Hz in the ^{15}N and ^1H dimensions, respectively.

Spectral processing and analysis were performed with NMRpipe⁵¹ and Sparky.⁵² Sidechain ^1H - ^{13}C methionine ϵ -methyl and backbone ^1H - ^{15}N spectral assignments were as previously reported^{27,28}. ^1H - ^{15}N peak volumes were normalized against the HSQC spectrum of the apo protease and were mapped onto a monomeric unit of the X-ray crystal structure of wild-type KSHV Pr (PDB accession code: 1FL1.pdb) using either MolMol⁵³ or PyMol⁵⁴.

Granzyme B aggregation test

The expression and purification of Granzyme B, as well as assays for activity were carried out as described previously.⁵⁵ Enzyme (20 nM) was combined with either DD2 (30 μM) or hexachlorophene (30 μM) in assay buffer and incubated for 20 minutes at room temperature. Standard assay buffer consisted of 50 mM NaHEPES buffer (pH 8.0), 100 mM NaCl, \pm 0.01% or 0.03% Triton X-100. Enzyme activity was initiated by adding Ac-IEPD-*p*NA (*p*NA) substrate (500 μM). Hydrolysis of substrate was monitored spectrophotometrically at a wavelength of 405 nm and endpoint absorbance values were recorded after 30. The ratio

of experimental end-point absorbance (A) and un-inhibited end-point absorbance (A0) were plotted as bar graphs. Data represents mean values \pm s.d. (n=3).

Synthesis of helical mimetic compounds

The synthesis of helical mimetic compounds was adapted from word described previously.³⁷ The commercially available compounds **10a-h** were reacted with (cyclohexylmethyl)zinc bromide in the presence of NiCl₂(dppp) to form the corresponding Negishi coupling products in 23-90% yield after 18 hours. Side products, besides the unconverted starting materials, included the biaryl coupling adduct and the dehalogenated esters. The following hydrolysis was carried out under basic conditions affording the corresponding acids **11a-h**. The reaction between **11a-h** and **12**⁵⁶ in the presence of N,N'-dimethylaminopyridine and solid supported p-toluenesulfonic chloride gave the corresponding amides in 10-53% yield after 18 hours together with unconverted starting materials. The alternative conversion of **11b** into the acid chloride in the presence of SOCl₂ followed by the addition of **12**, gave the corresponding amide in 93% yield. The subsequent saponification resulted in the formation of compounds 2-8 discussed in the paper.

¹H-NMR, ¹³C-NMR, & MS characterization of helical mimetic compounds & synthesis intermediates

1: white solid; ¹H NMR (400 MHz, DMSO) δ 12.87 (broad, 1H), 9.91 (s, 1H), 7.88-7.82 (m, 1H), 7.79-7.73 (m, 1H), 7.65-7.61 (m, 2H), 7.56 (s, 1H), 7.46-7.33 (m, 2H), 7.26 (m, 2H), 7.21-7.11 (m, 3H), 4.13 (s, 2H), 2.51-2.48 (m, 2H), 1.69-1.55 (m, 6H), 1.20-1.11 (m, 3H), 0.98-0.85 (m, 2H); ¹³C NMR (101 MHz, DMSO) δ 166.96, 165.73, 141.03, 140.44, 139.61,

135.80, 134.16, 132.36, 131.37, 128.67, 128.41, 128.10, 128.05, 127.87, 127.79, 126.12, 126.08, 125.06, 43.00, 38.88, 36.83, 32.46, 26.03, 25.67; MS = 428.2 (H^+).

2: white solid; 1H NMR (400 MHz, DMSO) δ 10.79 (s, 1H), 8.78-8.72 (m, 1H), 8.43-8.31 (m, 4H), 7.96-7.91 (m, 1H), 7.75-7.60 (m, 5H), 4.61 (s, 2H), 3.15-3.08 (m, 2H), 2.21-1.96 (m, 6H), 1.64-1.56 (m, 3H), 1.45-1.32 (m, 2H); ^{13}C NMR (101 MHz, DMSO) δ 167.36, 161.77, 159.88, 148.11, 145.65, 139.18, 138.40, 134.90, 131.82, 130.52, 128.63, 128.24, 127.18, 126.48, 120.84, 120.79, 119.54, 44.74, 37.74, 36.67, 32.43, 25.93, 25.59; MS = 429.2 (H^+).

3: white solid; 1H NMR (400 MHz, DMSO) δ 9.73 (s, 1H), 7.84-7.73 (m, 3H), 7.65-7.60 (m, 1H), 7.58-7.56 (m, 1H), 7.28-7.24 (m, 2H), 7.20-7.12 (m, 3H), 7.06-7.04 (m, 1H), 4.11 (s, 2H), 3.87-3.78 (m, 3H), 2.51-2.49 (m, 2H), 1.69-1.54 (m, 6H), 1.19-1.07 (m, 3H), 1.01-0.86 (m, 2H); ^{13}C NMR (101 MHz, DMSO) δ 166.99, 165.12, 160.06, 139.65, 135.70, 131.31, 130.06, 128.67, 128.50, 128.40, 127.76, 127.31, 126.12, 125.96, 125.67, 110.19, 55.67, 39.72, 37.66, 36.85, 32.69, 26.07, 25.72; MS = 428.2 (H^+).

4: white solid; 1H NMR (400 MHz, DMSO) δ 12.81 (broad, 1H), 9.93 (s, 1H), 7.88-7.59 (m, 5H), 7.33-7.11 (m, 7H), 4.11 (s, 2H), 2.52-2.50 (m, 2H), 1.72-1.47 (m, 6H), 1.26-1.06 (m, 3H), 1.02-0.87 (m, 2H); ^{13}C NMR (101 MHz, DMSO) δ 166.94, 165.53, 144.96, 140.48, 139.64, 136.04, 131.73, 131.19, 129.15, 128.95, 128.78, 128.44, 127.79, 127.68, 127.54, 126.14, 42.93, 38.88, 36.68, 32.46, 26.00, 25.64; MS = 428.1 (H^+).

5: white solid; 1H NMR (400 MHz, DMSO) δ 12.86 (broad, 1H), 10.06 (s, 1H), 7.88-7.83 (m, 1H), 7.72-7.69 (m, 1H), 7.68-7.6 (m, 1H), 7.42-7.28 (m, 3H), 7.27-7.20 (m, 4H), 7.19-7.14 (m, 2H), 4.14 (s, 2H), 2.51-2.50 (m, 2H), 1.64-1.49 (m, 6H), 1.14-0.98 (m, 3H), 0.96-0.81 (m, 2H); ^{13}C NMR (101 MHz, DMSO) δ 168.41, 166.92, 140.23, 139.76, 138.80, 136.81,

135.56, 131.34, 130.61, 129.29, 128.76, 128.47, 127.84, 127.68, 127.28, 126.16, 125.91, 125.51, 40.14, 38.88, 36.37, 32.64, 25.95, 25.71; MS = 428.2 (H^+).

6: white solid; 1H NMR (400 MHz, DMSO) δ 12.90 (s, 1H), 10.14 (s, 1H), 8.80 (s, 1H), 8.55 (s, 1H), 7.92-7.84 (m, 2H), 7.83-7.80(m,1H), 7.61-7.55 (m, 1H), 7.24-7.22 (m, 2H), 7.20-7.10 (m, 3H), 4.14 (s, 2H), 2.51-2.48 (m, 2H), 1.72 – 1.55 (m, 6H), 1.25-1.05 (m, 3H), 1.02-0.88 (m, 2H); ^{13}C NMR (101 MHz, DMSO) δ 167.03, 164.32, 152.65, 146.21, 139.61, 136.08, 135.84, 135.41, 131.47, 129.52, 128.64, 128.38, 127.83, 126.42, 126.10, 40.14, 38.71, 36.90, 32.28, 25.95, 25.59; MS = 428.8 (M^+).

7: white solid; 1H NMR (400 MHz, DMSO) δ 12.87 (broad, 1H), 10.11 (s, 1H), 8.88 (d, 1H), 8.07-8.04 (m, 1H), 7.85-7.81 (m, 1H), 7.76-7.74 (m, 1H), 7.61-7.57 (d, 1H), 7.36-7.33 (m, 1H), 7.27-7.21 (m, 2H), 7.19-7.09 (m, 3H), 4.10 (s, 2H), 2.67 (d, $J = 7.2$, 2H), 1.69-1.51 (m, 6H), 1.20-1.10 (m, 3H), 1.01-0.90 (m, 2H); ^{13}C NMR (101 MHz, DMSO) δ 166.92, 163.97, 154.43, 148.22, 144.54, 139.95, 139.61, 136.21, 135.44, 131.30, 128.76, 128.72, 128.40, 127.72, 126.44, 126.12, 122.98, 40.42, 37.87, 36.73, 32.52, 25.95, 25.64; MS = 428.8 (H^+).

8: white solid; 1H NMR (400 MHz, DMSO) δ 9.90 (s, 1H), 7.88-7.81 (m, 2H), 7.71-7.62 (m, 2H), 7.53 (s, 1H), 7.42-7.32 (m, 2H), 7.26-7.22 (m, 2H), 7.21-7.10 (m, 3H), 4.15 (s, 2H), 3.83 (s, 3H), 2.50 (m, 2H), 1.70-1.51 (m, 5H), 1.32-1.12 (m, 4H), 1.00-0.89 (m, 2H); ^{13}C NMR (101 MHz, DMSO) δ 165.86, 165.74, 141.03, 140.89, 139.50, 135.86, 134.11, 132.40, 131.24, 128.61, 128.41, 128.11, 128.04, 127.71, 126.59, 126.15, 126.12, 125.06, 52.06, 42.98, 38.88, 36.80, 32.45, 26.03, 25.66; MS = 442.2 (H^+).

11a: white solid; 1H NMR (400 MHz, DMSO) δ 12.94 (s, 1H), 7.84-7.76 (m, 2H), 7.48-7.42 (m, 2H), 2.59-2.56 (m, 2H), 1.75-1.65 (m, 6H), 1.30-1.10 (m, 3H), 1.05-0.94 (m, 2H); ^{13}C

NMR (101 MHz, DMSO) δ 167.44, 141.13, 133.51, 130.56, 129.71, 128.29, 126.71, 40.14, 38.88, 32.39, 26.01, 25.64; MS = 218.9 (M^+).

11b: white solid; ^1H NMR (400 MHz, DMSO) δ 7.71-7.65 (m, 2H), 7.29-7.23 (m, 1H), 2.52-2.46 (m, 2H), 1.62-1.35 (m, 6H), 1.06-0.90 (m, 3H), 0.88-0.74 (m, 2H); ^{13}C NMR (101 MHz, DMSO) δ 166.32, 160.77, 147.86, 137.30, 126.70, 122.00, 39.72, 38.88, 32.49, 25.98, 25.62; MS = 219.8 (M^+).

11c: white solid; ^1H NMR (400 MHz, DMSO) δ 7.91-7.65 (m, 2H), 7.06-6.98 (m, 1H), 3.88-3.80 (m, 3H), 2.49-2.44 (m, 2H), 1.70-1.40 (m, 6H), 1.28-0.90 (m, 5H); ^{13}C NMR (101 MHz, DMSO) δ 160.72, 131.71, 131.30, 129.21, 128.41, 110.22, 55.60, 39.26, 37.54, 37.16, 32.66, 26.04, 25.69; MS = 249.0 (M^+).

11d: white solid; ^1H NMR (400 MHz, DMSO) δ 12.57 (broad, 1H), 7.93-7.83 (m, 2H), 7.33-7.20 (m, 2H), 2.51-2.46 (m, 2H), 1.71-1.48 (m, 6H), 1.27-1.05 (m, 3H), 1.01-0.87 (m, 2H); ^{13}C NMR (101 MHz, DMSO) δ 167.75, 146.00, 129.16, 129.08, 40.14, 39.93, 32.46, 25.99, 25.64; MS = 218.9 (M^+).

11e: ^1H NMR (400 MHz, DMSO) δ 12.79 (s, 1H), 7.80-7.72 (m, 1H), 7.47-7.40 (m, 1H), 7.30-7.20 (m, 2H), 2.86-2.80 (m, 2H), 1.72-1.43 (m, 6H), 1.18-0.87 (m, 5H); ^{13}C NMR (101 MHz, DMSO) δ 169.08, 141.57, 131.57, 131.00, 129.99, 125.79, 39.09, 38.88, 32.63, 26.05, 25.75; MS = 218.9 (M^+).

11f: ^1H NMR (400 MHz, DMSO) δ 13.48 (broad, 1H), 8.93 (s, 1H), 8.65 (s, 1H), 8.14 (s, 1H), 2.69-2.59 (m, 2H), 1.71-1.54 (m, 6H), 1.25-1.04 (m, 3H), 1.02-0.87 (m, 2H); ^{13}C NMR (101 MHz, DMSO) δ 166.05, 152.57, 146.84, 138.08, 136.78, 126.56, 40.14, 38.88, 32.16, 25.92, 25.54; MS = 219.9 (H^+).

AKNOWLEDGMENTS

The authors thank W. Gibson (The Johns Hopkins University School of Medicine) for providing us with the CMV protease expression plasmid and for valuable feedback on the manuscript. This work was funded by US National Institutes of Health grants T32 GMO7810 and AIO67423 (C.S.C.) and by the American Lebanese and Syrian Associated Charities and the St. Jude Children's Research Hospital (R.K.G.). We also thank the University of California, San Francisco–Gladstone Institute for Virology and Immunology/Center for AIDS Research for the Clinical Science Pilot Award (P30-AI027763 to G.M.L.).

REFERENCES

1. Jones, S. & Thornton, J.M. Principles of protein-protein interactions. *Proc Natl Acad Sci U S A* **93**, 13-20 (1996).
2. Hopkins, A.L. & Groom, C.R. The druggable genome. *Nat Rev Drug Discov* **1**, 727-30 (2002).
3. Lo Conte, L., Chothia, C. & Janin, J. The atomic structure of protein-protein recognition sites. *J Mol Biol* **285**, 2177-98 (1999).
4. Berg, T. Modulation of protein-protein interactions with small organic molecules. *Angew Chem Int Ed Engl* **42**, 2462-81 (2003).
5. Wells, J.A. & McClendon, C.L. Reaching for high-hanging fruit in drug discovery at protein-protein interfaces. *Nature* **450**, 1001-9 (2007).
6. Tse, C. et al. ABT-263: a potent and orally bioavailable Bcl-2 family inhibitor. *Cancer Res* **68**, 3421-8 (2008).
7. Fields, B.N. et al. *Fields Virology*, 3177 (Lippincott Williams & Wilkins, Philadelphia 2006).
8. Gopalsamy, A. et al. Design and syntheses of 1,6-naphthalene derivatives as selective HCMV protease inhibitors. *J Med Chem* **47**, 1893-9 (2004).
9. Gao, M. et al. The protease of herpes simplex virus type 1 is essential for functional capsid formation and viral growth. *J Virol* **68**, 3702-12 (1994).
10. Preston, V.G., Coates, J.A. & Rixon, F.J. Identification and characterization of a herpes simplex virus gene product required for encapsidation of virus DNA. *J Virol* **45**, 1056-64 (1983).

11. Sheaffer, A.K. et al. Evidence for controlled incorporation of herpes simplex virus type 1 UL26 protease into capsids. *J Virol* **74**, 6838-48 (2000).
12. Weinheimer, S.P. et al. Autoproteolysis of herpes simplex virus type 1 protease releases an active catalytic domain found in intermediate capsid particles. *J Virol* **67**, 5813-22 (1993).
13. Welch, A.R., Woods, A.S., McNally, L.M., Cotter, R.J. & Gibson, W. A herpesvirus maturational proteinase, assemblin: identification of its gene, putative active site domain, and cleavage site. *Proc Natl Acad Sci U S A* **88**, 10792-6 (1991).
14. Borthwick, A.D. et al. Design and synthesis of pyrrolidine-5,5-trans-lactams (5-oxohexahydropyrrolo[3,2-b]pyrroles) as novel mechanism-based inhibitors of human cytomegalovirus protease. 2. Potency and chirality. *J Med Chem* **45**, 1-18 (2002).
15. Borthwick, A.D. et al. Pyrrolidine-5,5-trans-lactams as novel mechanism-based inhibitors of human cytomegalovirus protease. Part 3: potency and plasma stability. *Bioorg Med Chem Lett* **12**, 1719-22 (2002).
16. Borthwick, A.D. et al. Design and synthesis of monocyclic beta-lactams as mechanism-based inhibitors of human cytomegalovirus protease. *Bioorg Med Chem Lett* **8**, 365-70 (1998).
17. Ogilvie, W. et al. Peptidomimetic inhibitors of the human cytomegalovirus protease. *J Med Chem* **40**, 4113-35 (1997).
18. Waxman, L. & Darke, P.L. The herpesvirus proteases as targets for antiviral chemotherapy. *Antivir Chem Chemother* **11**, 1-22 (2000).

19. Batra, R., Khayat, R. & Tong, L. Molecular mechanism for dimerization to regulate the catalytic activity of human cytomegalovirus protease. *Nat Struct Biol* **8**, 810-7 (2001).
20. Buisson, M. et al. Functional determinants of the Epstein-Barr virus protease. *J Mol Biol* **311**, 217-28 (2001).
21. Darke, P.L. et al. Active human cytomegalovirus protease is a dimer. *J Biol Chem* **271**, 7445-9 (1996).
22. Margosiak, S.A., Vanderpool, D.L., Sisson, W., Pinko, C. & Kan, C.C. Dimerization of the human cytomegalovirus protease: kinetic and biochemical characterization of the catalytic homodimer. *Biochemistry* **35**, 5300-7 (1996).
23. Nomura, A.M., Marnett, A.B., Shimba, N., Dotsch, V. & Craik, C.S. Induced structure of a helical switch as a mechanism to regulate enzymatic activity. *Nat Struct Mol Biol* **12**, 1019-20 (2005).
24. Pray, T.R., Reiling, K.K., Demirjian, B.G. & Craik, C.S. Conformational change coupling the dimerization and activation of KSHV protease. *Biochemistry* **41**, 1474-82 (2002).
25. Reiling, K.K., Pray, T.R., Craik, C.S. & Stroud, R.M. Functional consequences of the Kaposi's sarcoma-associated herpesvirus protease structure: regulation of activity and dimerization by conserved structural elements. *Biochemistry* **39**, 12796-803 (2000).
26. Schmidt, U. & Darke, P.L. Dimerization and activation of the herpes simplex virus type 1 protease. *J Biol Chem* **272**, 7732-5 (1997).

27. Nomura, A.M., Marnett, A.B., Shimba, N., Dotsch, V. & Craik, C.S. One functional switch mediates reversible and irreversible inactivation of a herpesvirus protease. *Biochemistry* **45**, 3572-9 (2006).
28. Marnett, A.B., Nomura, A.M., Shimba, N., Ortiz de Montellano, P.R. & Craik, C.S. Communication between the active sites and dimer interface of a herpesvirus protease revealed by a transition-state inhibitor. *Proc Natl Acad Sci U S A* **101**, 6870-5 (2004).
29. Buisson, M. et al. The crystal structure of the Epstein-Barr virus protease shows rearrangement of the processed C terminus. *J Mol Biol* **324**, 89-103 (2002).
30. Qiu, X. et al. Unique fold and active site in cytomegalovirus protease. *Nature* **383**, 275-9 (1996).
31. Qiu, X. et al. Crystal structure of varicella-zoster virus protease. *Proc Natl Acad Sci U S A* **94**, 2874-9 (1997).
32. Shieh, H.S. et al. Three-dimensional structure of human cytomegalovirus protease. *Nature* **383**, 279-82 (1996).
33. Tong, L. et al. A new serine-protease fold revealed by the crystal structure of human cytomegalovirus protease. *Nature* **383**, 272-5 (1996).
34. Hoog, S.S. et al. Active site cavity of herpesvirus proteases revealed by the crystal structure of herpes simplex virus protease/inhibitor complex. *Biochemistry* **36**, 14023-9 (1997).
35. Pray, T.R., Nomura, A.M., Pennington, M.W. & Craik, C.S. Auto-inactivation by cleavage within the dimer interface of Kaposi's sarcoma-associated herpesvirus protease. *J Mol Biol* **289**, 197-203 (1999).

36. Shimba, N., Nomura, A.M., Marnett, A.B. & Craik, C.S. Herpesvirus protease inhibition by dimer disruption. *J Virol* **78**, 6657-65 (2004).
37. Lu, F. et al. Proteomimetic libraries: design, synthesis, and evaluation of p53-MDM2 interaction inhibitors. *J Comb Chem* **8**, 315-25 (2006).
38. Backes, B.J., Harris, J.L., Leonetti, F., Craik, C.S. & Ellman, J.A. Synthesis of positional-scanning libraries of fluorogenic peptide substrates to define the extended substrate specificity of plasmin and thrombin. *Nat Biotechnol* **18**, 187-93 (2000).
39. Lazic, A., Goetz, D.H., Nomura, A.M., Marnett, A.B. & Craik, C.S. Substrate modulation of enzyme activity in the herpesvirus protease family. *J Mol Biol* **373**, 913-23 (2007).
40. Feng, B.Y. & Shoichet, B.K. A detergent-based assay for the detection of promiscuous inhibitors. *Nat Protoc* **1**, 550-3 (2006).
41. Lee, G.M. & Craik, C.S. Trapping moving targets with small molecules. *Science* **324**, 213-5 (2009).
42. Kussie, P.H. et al. Structure of the MDM2 oncoprotein bound to the p53 tumor suppressor transactivation domain. *Science* **274**, 948-53 (1996).
43. Chen, P. et al. Structure of the human cytomegalovirus protease catalytic domain reveals a novel serine protease fold and catalytic triad. *Cell* **86**, 835-43 (1996).
44. Wu, T.D. et al. Mutation patterns and structural correlates in human immunodeficiency virus type 1 protease following different protease inhibitor treatments. *J Virol* **77**, 4836-47 (2003).
45. Hardy, J.A., Lam, J., Nguyen, J.T., O'Brien, T. & Wells, J.A. Discovery of an allosteric site in the caspases. *Proc Natl Acad Sci U S A* **101**, 12461-6 (2004).

46. Scheer, J.M., Romanowski, M.J. & Wells, J.A. A common allosteric site and mechanism in caspases. *Proc Natl Acad Sci U S A* **103**, 7595-600 (2006).
47. Bannwarth, L. & Reboud-Ravaux, M. An alternative strategy for inhibiting multidrug-resistant mutants of the dimeric HIV-1 protease by targeting the subunit interface. *Biochem Soc Trans* **35**, 551-4 (2007).
48. Lee, S.G. & Chmielewski, J. Rapid synthesis and in situ screening of potent HIV-1 protease dimerization inhibitors. *Chem Biol* **13**, 421-6 (2006).
49. Unal, A. et al. The protease and the assembly protein of Kaposi's sarcoma-associated herpesvirus (human herpesvirus 8). *J Virol* **71**, 7030-8 (1997).
50. Brignole, E.J. & Gibson, W. Enzymatic activities of human cytomegalovirus maturational protease assemblin and its precursor (pPR, pUL80a) are comparable: [corrected] maximal activity of pPR requires self-interaction through its scaffolding domain. *J Virol* **81**, 4091-103 (2007).
51. Delaglio, F. et al. NMRPipe: a multidimensional spectral processing system based on UNIX pipes
J. Biomol. NMR **6**, 277 (1995).
52. Goddard, T.D. & Kneller, D.G. Sparky 3 3.0 edn (University of California San Francisco, San Francisco, 1999).
53. Koradi, R., Billeter, M. & Wuthrich, K. MOLMOL: A program for display and analysis of macromolecular structures. *J. Mol. Graphics* **14**, 51 (1996).
54. DeLano, W.L. The PyMOL Molecular Graphics System. (DeLano Scientific, San Carlos, CA, 2002).

55. Harris, J.L., Peterson, E.P., Hudig, D., Thornberry, N.A. & Craik, C.S. Definition and redesign of the extended substrate specificity of granzyme B. *J Biol Chem* **273**, 27364-73 (1998).
56. Baudoin, O., Guenard, D. & Gueritte, F. Palladium-catalyzed borylation of ortho-substituted phenyl halides and application to the one-pot synthesis of 2,2'-disubstituted biphenyls. *J Org Chem* **65**, 9268-71 (2000).
57. Feng, B.Y., Shelat, A., Doman, T.N., Guy, R.K. & Shoichet, B.K. High-throughput assays for promiscuous inhibitors. *Nat Chem Biol* **1**, 146-8 (2005).

Table 2-1**Summary of inhibition data for all compounds.**

Inhibition data for compound **1-8** against KSHV Pr and human CMV Pr. Percent inhibition values were calculated using a fluorogenic activity assay with 1 μ M KSHV Pr, 10 μ M compound, and 160 μ M P6 substrate. IC₅₀ values were determined using a similar assay with a final compound concentration range of 100 μ M – 0.14 μ M. Data represents mean values \pm s.d. (n=3). Experimental methods are described in main paper.

| Target | Compound ID | % Inhibition | IC ₅₀ (μ M) |
|---------|----------------|--------------|-----------------------------|
| KSHV Pr | 1 (DD1) | 56.6 | 8.8 \pm 0.3 |
| | 2 (DD2) | 82.7 | 3.1 \pm 0.2 |
| | 3 | 51.1 | 16.4 \pm 0.7 |
| | 4 | 24.0 | |
| | 5 | 14.8 | |
| | 6 | 7.9 | |
| | 7 | 10.0 | |
| | 8 | 9.4 | |
| CMV Pr | 2 (DD2) | 92.0 | 5.0 \pm 0.5 |

Table 2-2

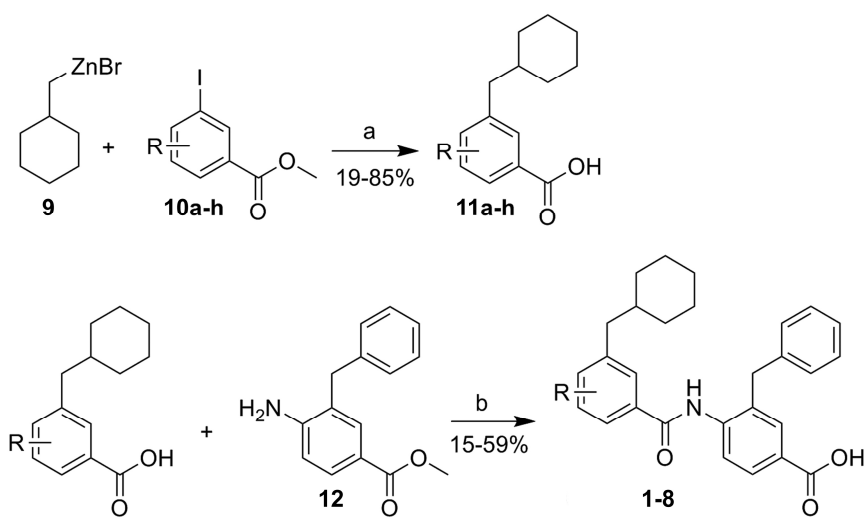
Summary of kinetic data for inhibitor DD1.

A 100 μl enzyme assay was performed using 1 μM KSHV Pr in assay buffer. Final substrate concentrations of 80, 40, 30, 20, 10, 6, 4, and 2 μM were tested across inhibitor concentrations of 10, 7, 5, 3, 1, and 0 μM (48 total reactions). Experimental methods are described in main paper. Values represent mean values \pm s.d. (n=3).

| [DD2] | K_M (μM) | V_{max} ($\mu\text{M} / \text{sec}$) | k_{cat} (s^{-1}) | K_{cat}/K_M ($\text{M}^{-1} \text{s}^{-1}$) |
|---------|-------------------------|---|--------------------------------------|--|
| 0 | 11.0 ± 3.8 | $0.0033 \pm 5.4\text{E-}05$ | $0.013 \pm 2.0\text{E-}04$ | 1136 ± 37 |
| 1uM | 13.6 ± 0.9 | $0.0035 \pm 3.0\text{E-}05$ | $0.013 \pm 1.2\text{E-}04$ | 997 ± 66 |
| 3uM | 16.5 ± 2.2 | $0.0029 \pm 2.2\text{E-}04$ | $0.011 \pm 8.3\text{E-}04$ | 673 ± 58 |
| 5uM | 21.2 ± 3.8 | $0.0021 \pm 6.9\text{E-}05$ | $0.008 \pm 2.7\text{E-}04$ | 398 ± 63 |
| 7uM | 23.9 ± 5.7 | $0.0017 \pm 9.4\text{E-}05$ | $0.006 \pm 3.6\text{E-}04$ | 280 ± 55 |
| 10uM | 27.4 ± 4.2 | $0.0011 \pm 1.5\text{E-}05$ | $0.004 \pm 5.8\text{E-}04$ | 153 ± 23 |

Scheme 2-1

Synthesis scheme of compounds 1-8.



Reagents and conditions: (a) 1) NiCl_2dppp (0.05 eq), THF, rt, 18h; 2) 1M NaOH(aq) , MeOH, THF, 40°C , 2h; (b) 1) DMAP, p-TsCl, DCM, 40°C , 18h; 2) 1M NaOH(aq) , MeOH, THF, 40°C , 2h.

Figure 2-1

KSHV Pr dimer interface and helical mimetic inhibitors of KSHV Pr activity. (a) The interface of monomer A (gray) and the α -helix 5 of monomer B (blue) is shown from two viewpoints. The α -helix 5 (dark gray) and other interface residues (orange) on monomer A form key contacts with α -helix 5 of monomer B. Interfacial residues Met197 (gray and blue), Trp109 (orange), and Ile201 (green) are highlighted throughout the paper. The active site (red) is located 15Å away from the dimer interface. (b) Chemical structures of KSHV Pr activity inhibitors identified by screening an α -helical mimetic library. Compounds **2-8** are structural analogues of initial hit compound **1**.

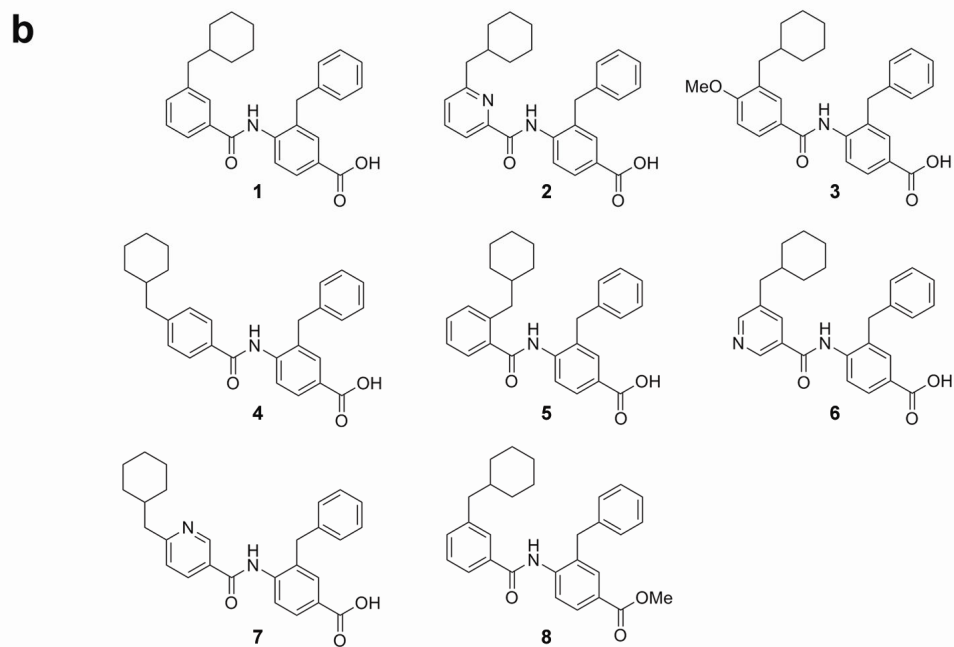
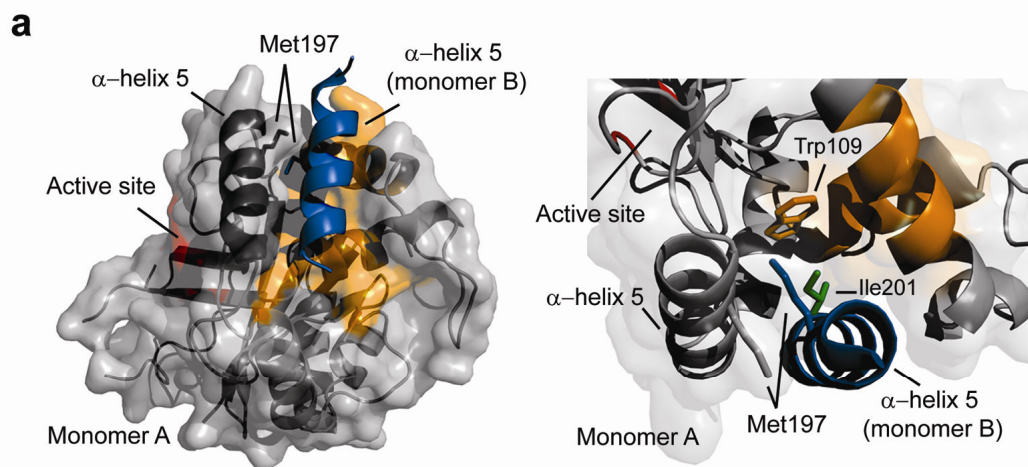


Figure 2-2

DD2 does not show evidence of non-specific aggregation with Granzyme B.

The inhibitory activity of DD2 and the known aggregator hexachlorophene (HEX)⁵⁷ was tested against Granzyme B (GrB) protease in an activity assay. GrB (20 nM), *p*NA substrate (500 μ M), and either DD2 (30 μ M) or HEX (30 μ M) were assayed in buffer with varied amounts of detergent Triton X-100.^{40,57} Bar graphs show the ratio of experimental end-point absorbance (A) and un-inhibited end-point absorbance (A0), recorded 30 minutes after addition of substrate. Data represents mean values \pm s.d. (n=3).

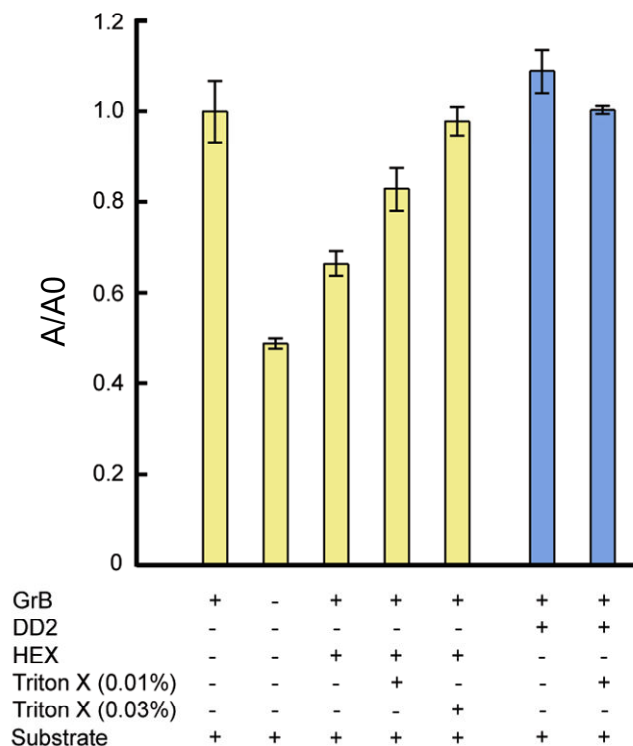


Figure 2-3

DD2 disrupts the KSHV Pr dimer. (a) Wt KSHV Pr (5 μ M) was incubated with either DMSO (dotted) or 30 μ M DD2 (solid). Mixtures were loaded onto a size exclusion chromatography column, pre-equilibrated with running buffer containing either DMSO or 30 μ M DD2 respectively. (b) The elution profile of KSHV Pr variant W109A (5 μ M) in buffer alone indicated the absence of the dimeric species. (c) The overlaid ^1H - ^{13}C HSQC spectra of selectively labeled ^{13}C methionine wt KSHV Pr (23 μ M) in the presence of 0 μ M (red), 6 μ M (yellow), 12 μ M (green) and, 24 μ M (blue) DD2. The spectra of apo protease (red) exhibited individual resonances for the N-terminus Met1 (M1), as well as the interfacial Met197 in the dimeric and monomeric states.

Figure 2-3

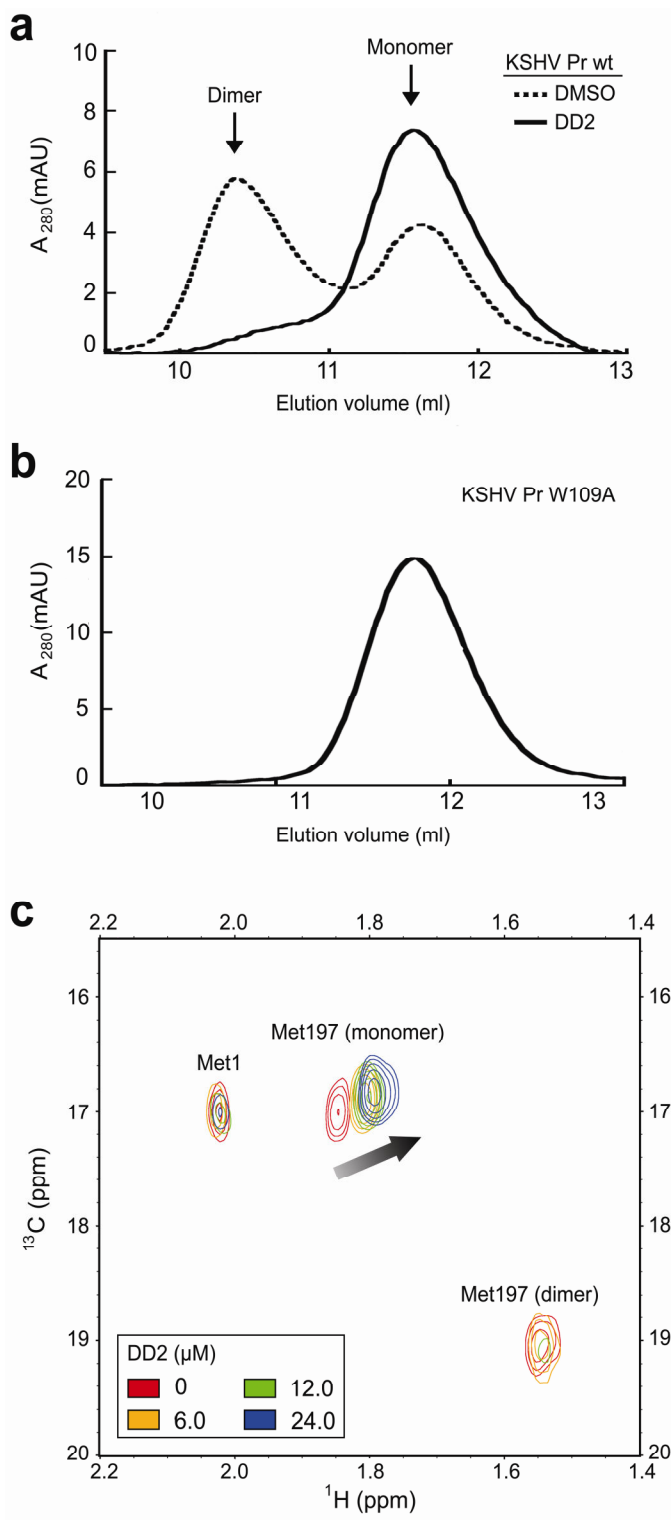


Figure 2-4

Kinetic studies with DD2 show evidence of mixed-type inhibition. (a) A standard enzyme assay was performed using 1 μM KSHV Pr with final substrate (P6) concentration range of 80 μM - 2 μM , across inhibitor concentrations of 10 (orange), 7 (brown), 5 (purple), 3 (green), 1 (blue), and 0 (red) μM . Double-reciprocal plots of initial reaction velocities are shown. (b) IC_{50} of inhibition by DD2 is higher for the tighter- K_D KSHV Pr variant. Activities of wt and M197L KSHV protease at 1 μM were monitored in the presence of increasing concentrations of DD2 ($\sim 0.14\mu\text{M}$ – $100\mu\text{M}$). Data is plotted as the ratio of experimental end-point fluorescence (F), and un-inhibited end-point fluorescence (F_0), as a function of increasing inhibitor concentration. The IC_{50} of inhibition were $2.6 \pm 0.4 \mu\text{M}$ and $7.3 \pm 0.8 \mu\text{M}$ for wt (dotted) and M197L (solid) KSHV Pr respectively. Data represents mean values \pm s.d. (n=3).

Figure 2-4

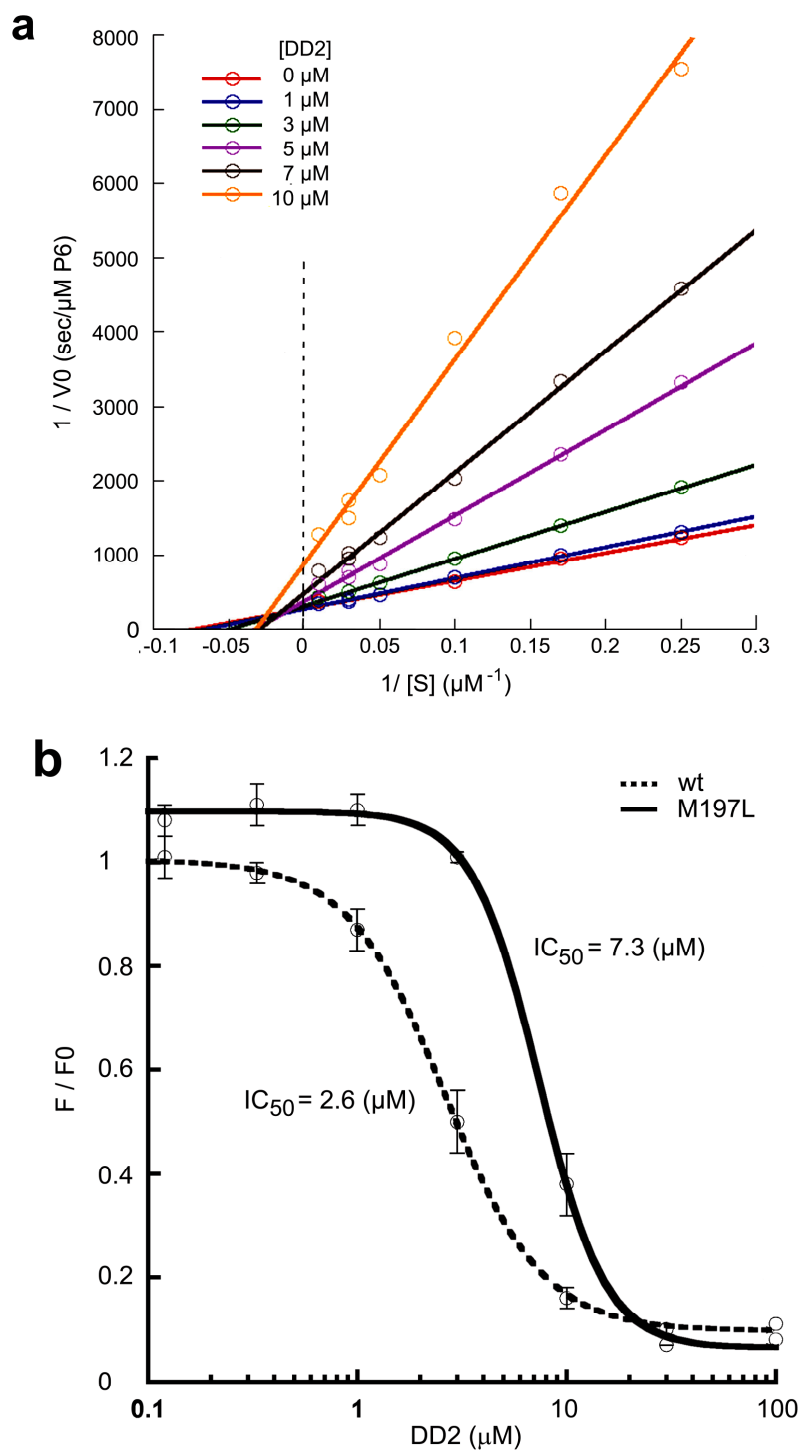


Figure 2-5

DD2 disrupts the KSHV Pr M197L dimer.

The dimerization state of KSHV Pr wt and M197L is monitored by size exclusion chromatography. Protease (5 μ M) was incubated with either DMSO (dotted) or 10 μ M DD2 (solid). Mixtures were loaded onto a size exclusion chromatography column, pre-equilibrated with running buffer containing either DMSO or 10 μ M DD2 respectively. Experimental methods are described in main paper.

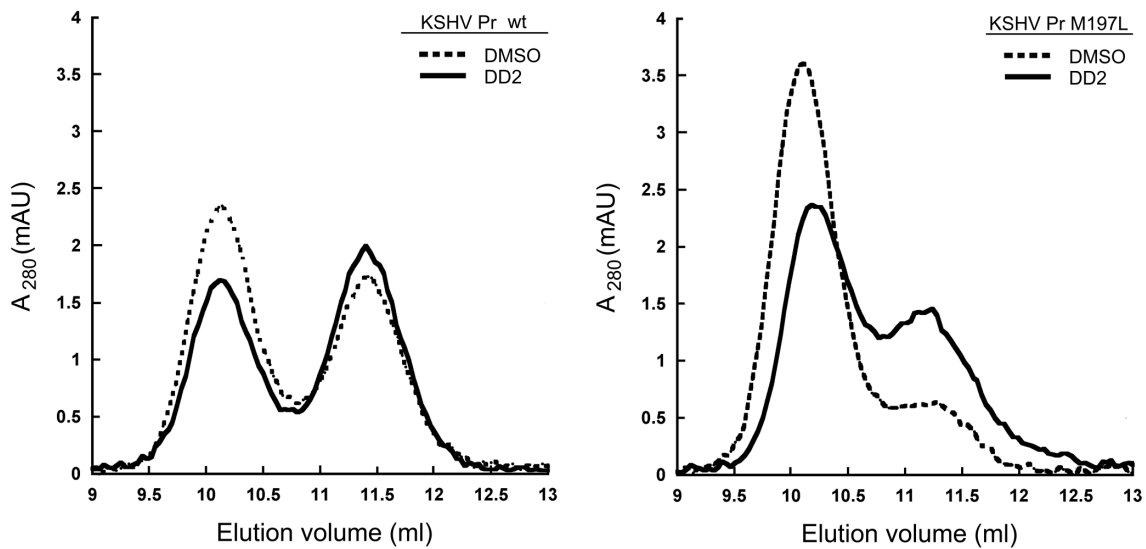


Figure 2-6

^1H - ^{15}N -HSQC titration data map the DD2 binding site to the dimer interface. (a) The overlaid ^1H - ^{15}N -HSQC spectra of the monomeric variant, KSHV Pr M197D (170 μM) in the absence (red) and presence (blue) of 170 μM DD2 is shown. The zoomed region highlights the Trp109 side-chain indole NH (boxed). The full ^1H - ^{15}N -HSQC spectra is included in **Fig. 2-7**. (b) Perturbed resonances from the titration study are mapped onto a monomeric unit of the KSHV Pr crystal structure. Residues are color coded based on the extent of peak intensity loss observed at the 1 molar equivalence titration point with DD2.

Figure 2-6

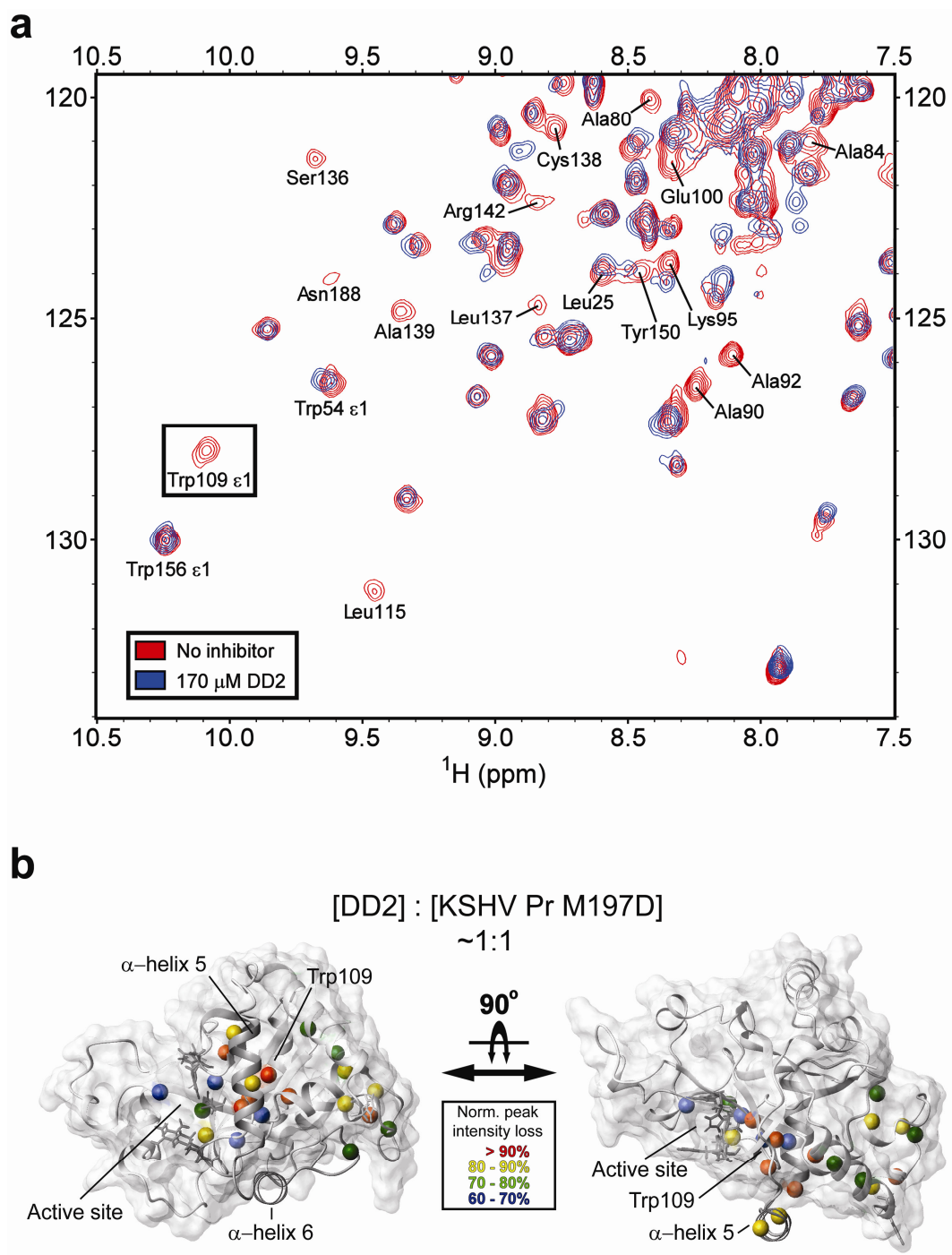


Figure 2-7

Full ^1H - ^{15}N -HSQC titration data for 170 μM DD2.

The overlaid ^1H - ^{15}N -HSQC spectra of the monomeric variant, KSHV Pr M197D (170 μM) in the absence (red) and presence (blue) of 170 μM DD2 is shown. The green box highlights the annotated region discussed in **Fig. 2-4a**. Experimental methods and data acquisition are described in main paper.

Figure 2-7

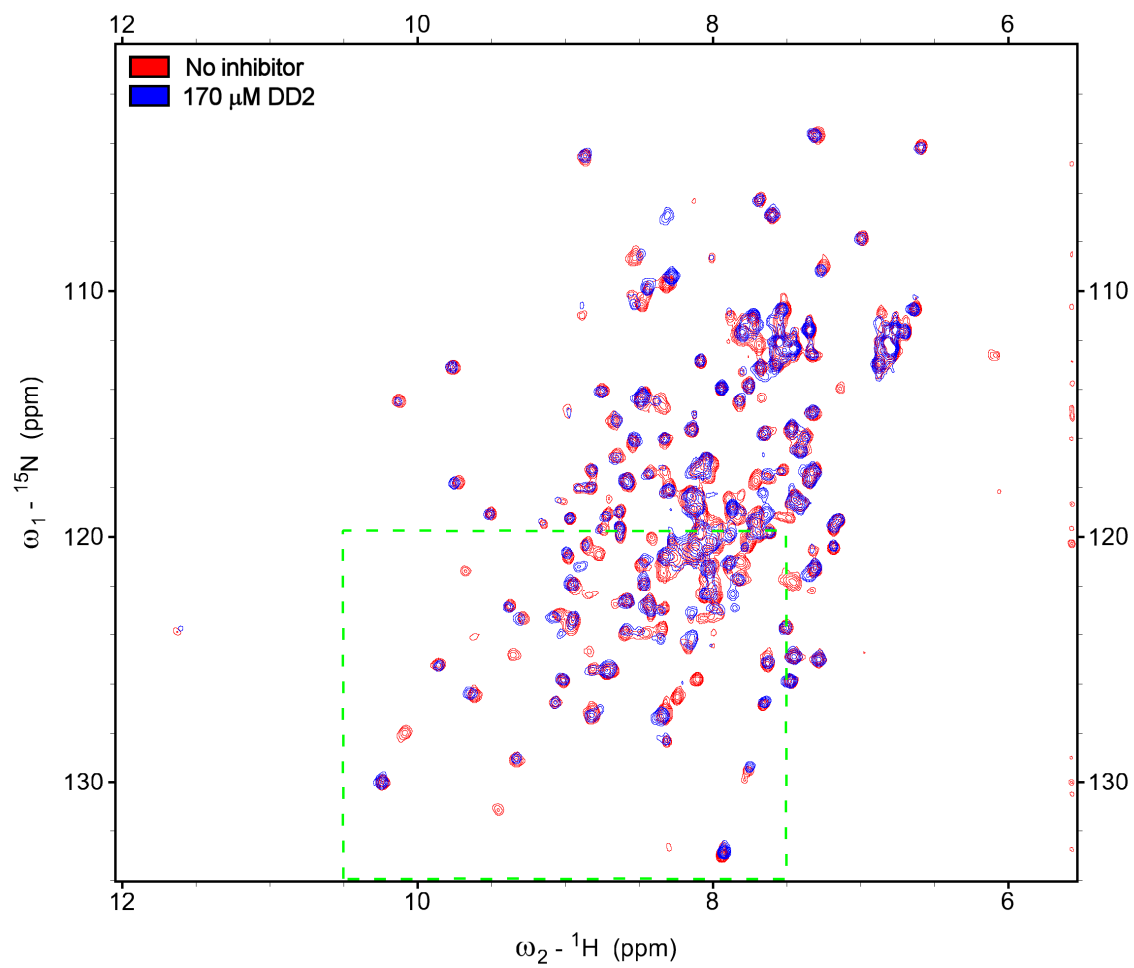


Figure 2-8

^1H - ^{15}N -HSQC titration data for 17 μM DD2. The overlaid ^1H - ^{15}N -HSQC spectra of the monomeric variant, KSHV Pr M197D (170 μM) in the absence (red) and presence (green) of 17 μM DD2 is shown. The blue box on the full data set (top) highlights the annotated zoomed region (bottom). The Trp109 side-chain indole NH experiences extensive conformational peak broadening. Experimental methods and data acquisition are described in main paper.

Figure 2-8

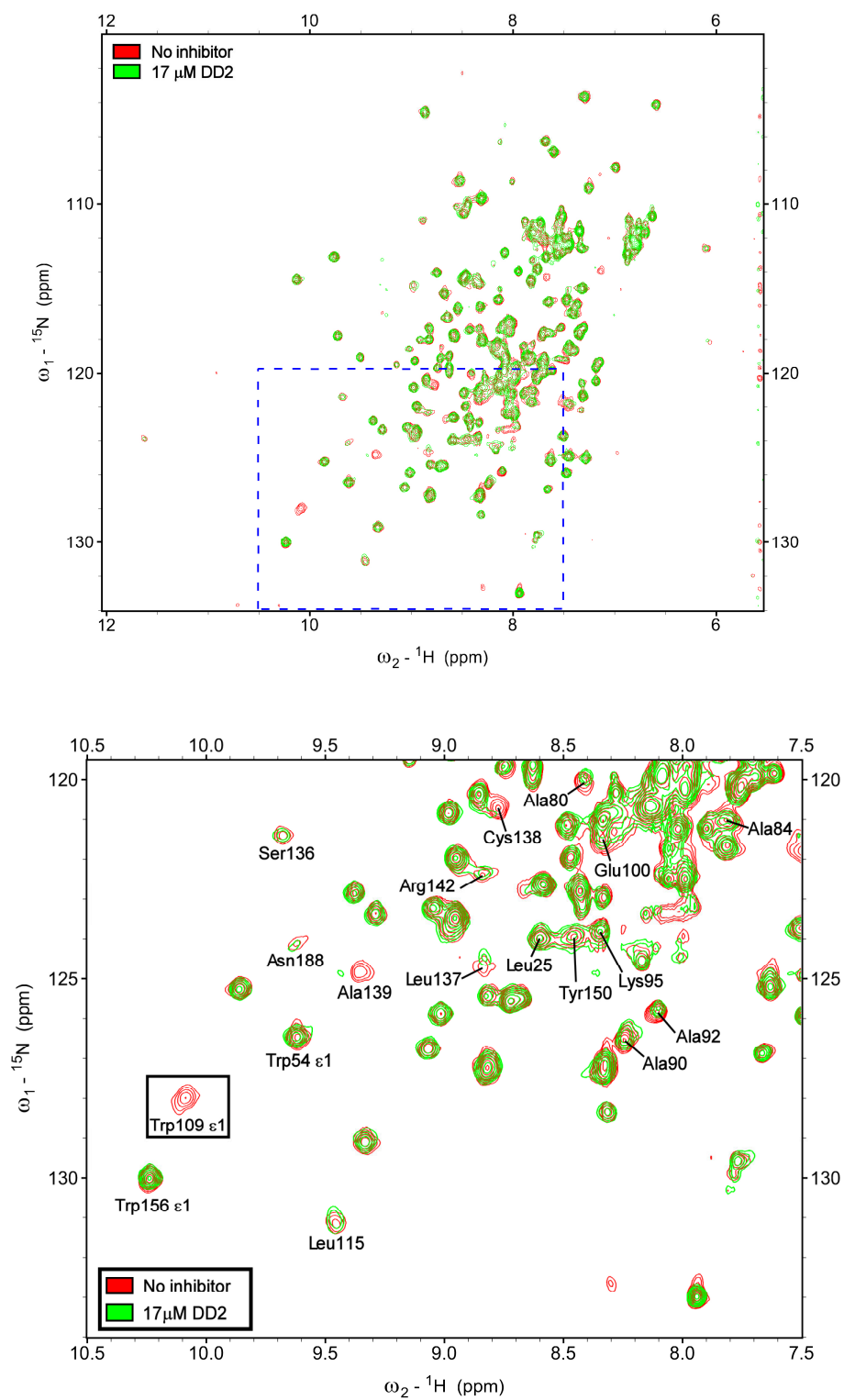
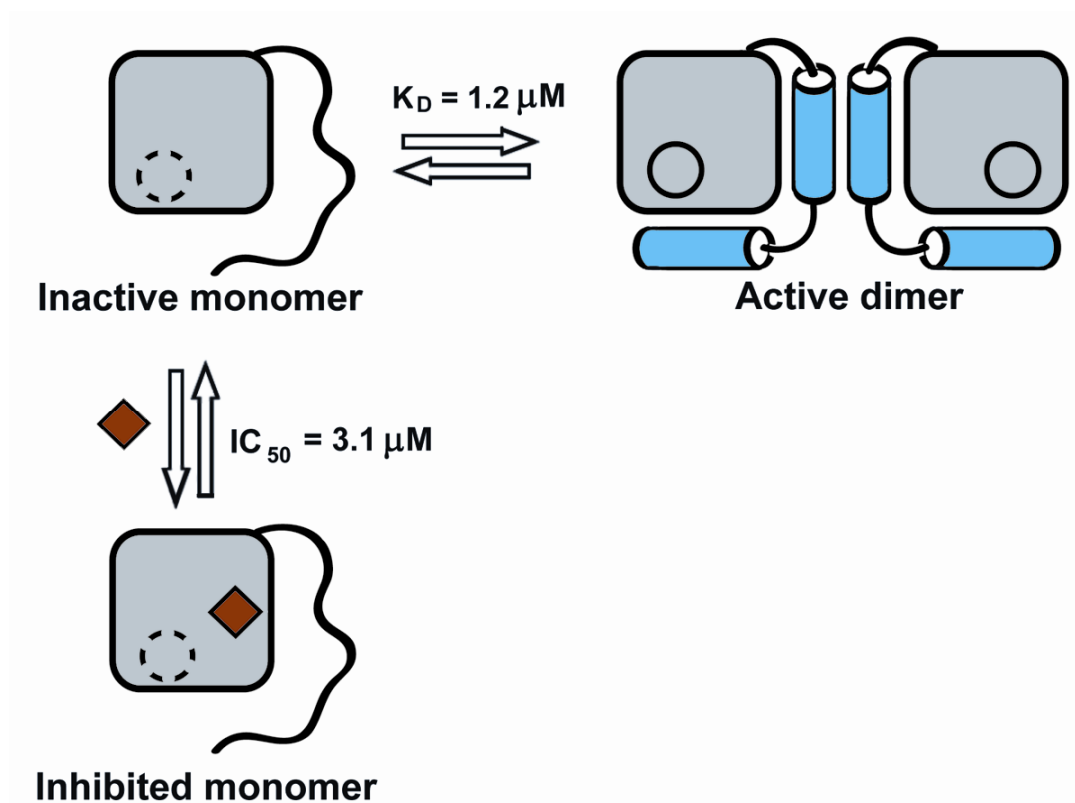


Figure 2-9

Monomer Trap model of inhibition by compound DD2. Inhibitor binding to a monomer of KSHV Pr directly competes with the process of dimerization, which is a required step in enzyme activation. When bound to interface residues, DD2 shifts the equilibrium towards a pre-existing folding intermediate, hence trapping the protease in an inactive monomeric state.



CHAPTER 3: Enzyme Inhibition by Allosteric Capture of an Inactive Conformation

/

Gregory M. Lee¹, Tina Shahian², Aida Baharuddin¹, Jonathan E. Gable³,
and Charles S. Craik¹

¹ Department of Pharmaceutical Chemistry University of California San
Francisco, CA 94158-2280 USA

² Graduate Group in Biochemistry and Molecular Biology University of
California San Francisco, CA, 94158-2280 USA

² Graduate Group in Biophysics University of California San Francisco,
CA, 94158-2280 USA

This chapter is reformatted from “Enzyme Inhibition by Allosteric Capture of an Inactive Conformation”, Journal of Molecular Biology, (2011)

ABSTRACT

All members of the human herpesvirus protease family are active as weakly associating dimers, but inactive as monomers. A small molecule allosteric inhibitor of Kaposi's sarcoma-associated herpesvirus protease (KSHV Pr) traps the enzyme in an inactive monomeric state where the C-terminal helices are unfolded and the hydrophobic dimer interface is exposed. NMR titration studies demonstrate that the inhibitor binds to KSHV Pr monomers with low μM affinity. A 2.0 Å resolution X-ray crystal structure of a C-terminal truncated KSHV Pr-inhibitor complex locates the binding pocket at the dimer interface and displays significant conformational perturbations at the active site, 15 Å from the allosteric site. NMR and CD data suggest that the small molecule inhibits human cytomegalovirus protease (HCMV Pr) via a similar mechanism. As all HHV proteases are functionally and structurally homologous, the inhibitor represents a class of compounds that may be developed into broad-spectrum therapeutics which allosterically regulate enzymatic activity by disrupting protein-protein interactions.

BACKGROUND

Proteins exhibit conformational selection that can have significant effects on their activity. In some cases, proteins exhibit intrinsic disorder as part of their regulatory mechanism.^{1,2} Processes of conformational selection, in the form of protein-protein interactions (PPIs), are governed by the internal motions of the individual subunits of the complex. Non-ideal interactions within these macromolecular complexes may result in misregulation of function, and, eventually to disease. Conversely, optimal binding between protein partners may actually enhance a pre-existing condition. To better understand these relationships, a recent upsurge of attention has been paid to linking protein dynamics and regulation of PPIs towards disease and drug discovery.³⁻⁶ As a result, PPIs have gained more traction as targets for therapeutics.^{7,8}

Until recently, the most successful mediators of PPIs had been antibody or peptide based.⁹ Though quite powerful, both modalities have their liabilities. A growing number of examples of preclinical compounds that target PPIs have focused on small molecules that mimic protein structural motifs, such as α -helices.^{10,11} Although a key feature of PPIs are large, relatively flat hydrophobic surfaces devoid of deep pockets or crevices, recent studies have indicated that these small molecule therapeutics may only need to bind a small subset of the interface residues, termed the “hot spot”.¹² Notably, bioinformatic analyses have indicated the presence of aromatic residues at these hot spots, with tryptophan the most commonly occurring.¹³

PPIs play a significant role in the activity of human herpesvirus (HHV) proteases. Two archetypal members of the HHV protease family include Kaposi’s sarcoma-associated herpesvirus protease (KSHV Pr) and human cytomegalovirus protease (HCMV Pr). As with

other structurally and functionally homologous HHV Pr family members, both KSHV Pr and HCMV Pr exist in equilibrium between an inactive monomeric and an active, weakly associating dimeric state. The proteolytically active dimer is critical for the viral lifecycle. The interface of all HHV Pr dimers consists of two α -helices (helix 5, one from each monomer), which buries an approximate 2500 Å² hydrophobic surface on each partner monomeric unit. Each monomer contains a non-canonical Ser-His-His catalytic triad and an accompanying substrate binding pocket located approximately 15-20 Å from the dimer interface (**Fig. 3-1a-b**).¹⁴

Previous structural studies performed on KSHV Pr suggested that the trigger for the concentration-dependent dimer formation is a disorder-to-order transition of the C-terminal residues.^{14,15} Notably, single point mutations of a key residue within helix 5 influence this equilibrium: Met197-to-Asp (M197D) results in an inactive obligate monomer,¹⁴ while Met197-to-Leu (M197L) stabilizes the dimer.¹⁶ NMR-based chemical shift perturbation mapping and hydrogen-deuterium exchange experiments performed on the KSHV Pr obligate monomer demonstrated that residues 191-230, which constitute the helices 5 and 6 in the dimer, are conformationally dynamic.¹⁴ An obligate monomeric version of KSHV Pr in which helix 6 was “stapled” to the core structure via an engineered disulfide bond displayed enhanced enzymatic activity in the oxidized state relative to the reduced state.¹⁴ This result suggested that the positioning of helix 6 is also critical for stabilizing the active dimeric conformation of KSHV Pr.

In light of these observations, we focused our efforts towards discovering small molecule ligands that allosterically regulate HHV Pr activity by disrupting dimerization. Since proteins and enzymes are able to sample multiple pre-existing conformational states,^{6,17} one such

inhibitory mechanism is to capture HHV proteases in their inactive monomeric forms. Regulating this conformational switch, which is believed to be conserved across all HHV proteases, represents an unexploited pathway for the development of potential broad-spectrum therapeutics against herpesviruses. In contrast to the successful antivirals used for AIDS treatment that target proteolytic activity of HIV protease, no active-site inhibitors that target HHV proteases have been successfully developed as clinical therapeutics. Successful disruption of the herpesvirus protease dimer offers the potential to resurrect a promising family of drug targets that were deemed undruggable due to the limited efficacy of active-site directed inhibitors.¹⁸⁻²⁰

To validate this approach, we previously demonstrated that addition of a 30-residue helical peptide abolished protease activity by disrupting KSHV Pr dimerization.¹⁶ Potential KSHV Pr inhibitors from small molecule helical mimetic libraries were then screened via a high-throughput fluorescence-based activity assay.²¹ One of the lead candidates, DD2 (**Fig. 3-1c**), resulted from chemical optimization of an initial screening hit, and exhibited an IC₅₀ value of $3.1 \pm 0.2 \mu\text{M}$ against KSHV Pr. DD2 is a diaryl-substituted 4-(pyridine-2-amido) benzoic acid. Initial ¹³C- and ¹⁵N-based NMR titration mapping studies indicated that DD2 disrupts dimerization by binding at or near Trp109, which is located in the center of the hydrophobic dimer interface.²¹ This led to a proposed “monomer trap” model of inhibition: DD2 alters the KSHV Pr monomer-dimer equilibrium by capturing a pre-existing inactive monomer and shifting the population of conformers from the active dimeric state.

In this study, we answer two key questions. (1) How does a small molecule alter the conformation of a dimeric enzyme in order to trap an inactive monomeric conformation? (2) Is this inhibitory mechanism applicable to other members of a family of related enzymes? In

particular, we use a C-terminal truncation variant of monomeric KSHV Pr to characterize HHV Pr-DD2 interactions via NMR spectroscopy and X-ray crystallography. By employing this truncated variant, we confirm that KSHV Pr-DD2 binding occurs, even in the absence of the conformationally dynamic C-terminus. We also report the first crystallographic structure of an allosterically inhibited HHV Pr monomer to date. Finally, using the structurally and functionally homologous human cytomegalovirus protease (HCMV Pr), we demonstrate that, in general, dimer dissociation is a viable allosteric route towards inhibiting HHV Pr activity.

RESULTS

Truncation of the C-terminal helices does not affect the core KSHV Pr structure.

Residues 191 – 230 constitute helices 5 and 6 in the KSHV Pr dimer, but are conformationally dynamic and only partially structured in the case of the KSHV Pr M197D obligate monomer.¹⁴ Truncation of the monomeric KSHV Pr sequence to its native autolysis site, S204, (henceforth, Δ , **Fig. 3-1a-b**) displayed no significant chemical shift perturbations with respect to the full-length obligate monomer in the ^{15}N - ^1H HSQC spectra.¹⁵ This suggested that the core structure of the KSHV Pr monomer (residues 1-191) remains intact, even with the absence of helix 6. Determining the minimal construct required for the correct fold of the monomeric protease core was deemed necessary for optimizing both NMR and crystallographic studies. Other constructs were therefore designed to remove portions of the C-terminal helices (**Fig. 3-1a-b**): KSHV Pr M197D Δ 209 (residues 1-209; Δ 209); KSHV Pr Δ 196 (residues 1-196; Δ 196); and KSHV Pr Δ 191 (residues 1-191; Δ 191). As with the Δ construct, size exclusion chromatogram elution profiles and ^{15}N - ^1H HSQC spectra indicate that the resulting truncations are expressed as monomers, with the core protease structure intact and well-folded (**Fig. 3-2**). Since DD2 binds to the obligate monomer,²¹ these newly created truncations can be used to simplify further small-molecule inhibitor binding studies.

Isoleucine δ 1-methyl groups act as KSHV Pr dimer interface binding probes.

Previous NMR studies of the KSHV Pr M197D monomer reported the hydrophobic dimer interface anchored by Trp109 as the DD2 binding “hot spot”.²¹ However, significant backbone amide peak broadening was observed in the ^{15}N - ^1H HSQC spectra during the

titration, precluding quantification of the binding effect. Subsequently, the non branched δ 1-methyl groups of isoleucine residues were used as NMR binding probes. Each monomeric unit of the KSHV Pr dimer structure (2pbk)²² contains ten isoleucine residues, which can be separated into five “zones” in relation to their distance from Trp109 (**Fig. 3-3a**). The ^{13}C - ^1H HSQC spectrum of selective [^{13}C - ^1H methyl] Ile-Leu-Val (ILV) labeled KSHV Pr M197D displays 10 relatively well-dispersed δ 1-methyl isoleucine resonances (**Fig. 3-4**). In order to assign the resonance peaks, Ile-to-Val mutations were performed on the M197D and Δ 196 constructs. As with the truncations, both ^{13}C - ^1H (**Fig. 3-5**) and ^{15}N - ^1H HSQC (data not shown) spectra of the Ile-to-Val mutants indicate no significant structural perturbation in the KSHV Pr core.

As expected, Ile44 and Ile105, both located within 5 Å of the KSHV Pr dimer interface, display the largest chemical shift resonance perturbations upon truncation of the C-terminal residues (**Fig. 3-4**). Ile71 is located within 10 Å of the KSHV Pr dimer interface and exhibits moderate resonance perturbations. Conversely, isoleucine residues located greater than 10 Å from the dimer interface exhibit little or no resonance perturbations. In addition, overlap of the Ile71-Ile206 and Ile105-Ile201 resonances are observed in the Δ 209 ^{13}C - ^1H HSQC spectrum, but not in the corresponding Δ 196 spectrum (**Fig. 3-4**). Although the Δ 191 and Δ 196 spectra exhibit no differences (data not shown), the Δ 191 construct displayed greater tendencies to aggregate in solution under the current NMR conditions. As a result, DD2 binding studies were performed using the Δ 196 construct, in comparison with the full-length M197D obligate monomer.

DD2 binds to KSHV Pr in the presence and absence of the dynamic C-terminus.

Addition of greater than five molar equivalents of DD2 to the ILV-labeled M197D obligate monomer induced significant chemical shift perturbations of the isoleucine residues located at the KSHV Pr dimer interface (**Fig. 3-3b**). Here, the methyl resonances of the isoleucine residues most proximal to the “hot spot” Trp109 (Ile44, Ile71, and Ile105) were the most affected. Not unexpectedly, resonances of the C-terminal isoleucines (Ile201, Ile206, and Ile222) are also perturbed, as these are the residues that would transiently interact with the KSHV Pr dimer interface in the absence of DD2. Because the Ile105 and Ile201 resonances of KSHV Pr M197D overlapped, the KSHV Pr M197D-I201V construct was also examined (**Fig. 3-6**). All isoleucine peaks in the M197D-I201V construct displayed similar resonances as those in the “wild-type” obligate monomer. Moreover, the absent Ile201 peak in the M197D-I201V construct allows for easier determination of the Ile105 chemical shift resonances. DD2 titration spectra acquired on the Δ 196 truncation (**Fig. 3-3c**) display the same general patterns as observed for the full-length KSHV Pr monomer analogs.

Ile44, Ile71, and Ile105 were chosen as NMR reporter probes due to their proximity of less than 10 Å to the “hot spot” Trp109. The Hill equation was used to perform a non-linear regression curvefit analysis of the δ 1-methyl group chemical shift resonances as a function of total ligand concentration (**Fig. 3-3d**). The apparent K_d values from these three reporter residues were then averaged to obtain an estimate of DD2 binding. The resulting NMR-based binding curves indicate that DD2 binds with equal affinity to the M197D ($K_{d,app} = 5.5 \pm 3.5$ μ M) and M197D-I201V ($K_{d,app} = 5.8 \pm 2.1$ μ M) constructs (**Fig. 3-3e**). DD2 appears to bind to the Δ 196 construct with lower affinity ($K_{d,app} = 13.0 \pm 2.0$ μ M). However, this observation may be a reflection of the presence (M197D or M197D-I201V variants) or absence (Δ 196

construct) of C-terminal residues transiently interacting with Trp109. Collectively, the NMR titration data clearly demonstrate that mutations or deletions of residues within the conformationally dynamic C-terminus have no significant effect towards DD2 binding affinity.

The crystal structure of the KSHV Pr Δ 196-DD2 complex.

In parallel to the NMR-based DD2 titration studies, a 2.0 Å resolution crystal structure of the KSHV Pr-DD2 complex was obtained (PDB accession code 3NJQ). To date, there have been no reported NMR or X-ray crystallographic structures of an allosterically inhibited HHV Pr monomer. In general, the majority of the published HHV Pr structures have either been in their respective apo or active-site inhibited dimeric forms, as illustrated by the apo (1FL1)²³ and covalently bound peptide phosphonate-inhibited (2PBK)²² dimeric KSHV Pr structures. Prior attempts to crystallize the full-length uninhibited KSHV Pr M197D obligate monomer proved fruitless, possibly due to the conformationally dynamic C-terminal residues disrupting the formation of a stable crystal lattice. Crystallization trials using the KSHV Pr M197D, Δ 209, and Δ 191 constructs yielded no appreciable crystals, either in the presence or absence of DD2. However, the Δ 196 construct in the presence of excess molar equivalents of DD2 yielded small cube-like crystals that were used to acquire a 2.0 Å resolution X-ray diffraction data set (**Tables 3-1 & 3-2**). Notably, no crystals were observed for the apo Δ 196 under similar reservoir conditions.

In contrast to the previously published structures of the full-length KSHV Pr dimers,^{22,23} the Δ 196-DD2 complex crystallizes as an asymmetric pair of KSHV Pr Δ 196 monomers

containing three DD2 molecules (**Fig. 3-7**). While the dimer interface of proteolytically active KSHV Pr consists of interfacial α -helices and a hydrophobic surface centered on Trp109, the Δ 196-DD2 complex forms a dimer on the distal side of the molecule with respect to Trp109. Both monomers in the asymmetric unit are conformationally similar with respect to one another and to residues 1-196 of the previously published KSHV Pr dimer structures (1FL1 and 2PBK), with overall RMS deviations less than 1.0 Å for backbone and heavy atom overlays (**Table 3-3**). Comparing a monomeric unit of the KSHV Pr dimer and the Δ 196-DD2 complex structures reveals two significant differences: the formation of an allosteric DD2 binding pocket and the conformational perturbation of the active site.

The “hot spot” Tryptophan 109 acts as a hinge to create the DD2 binding pocket.

One of the major differences in the backbone conformation between the “apo” and DD2-bound states is apparent in the α 1- α 2 loop (residues 87-99) and helix 2 (residues 100-110) (**Fig. 3-8**). In the case of the enzymatically active KSHV Pr dimer, the Trp109 indole ring adopts a “closed” conformation in each monomer, forming a relatively flat hydrophobic surface which interacts with the two interfacial helices. Dimerization is stabilized by the Met197 and Ile201 sidechains of the partner monomer, forming intermolecular hydrophobic interactions with Trp109 (**Fig. 3-8a-b**).^{21,22} Conversely, the Trp109 indole ring adopts an “open” conformation in each monomer of the Δ 196-DD2 complex, creating a hydrophobic cavity that acts as the DD2 binding pocket (**Fig. 3-8c-d**).

The DD2 binding pocket of KSHV Pr Δ 196.

The DD2 binding pocket is dominated by aliphatic residues located in several secondary structure motifs. Residues within the β 2- β 3 loop (residues 44-52), helix 1 (residues 73-91), helix 2 (residues 100-110), the β 6- β 7 loop (residues 139-148), and the C-terminus (residues 189-196) are involved (**Fig. 3-9 & 10**). With the exception of residues 189-196, the backbone conformation of the DD2 binding pockets are similar in the two asymmetric Δ 196-DD2 monomers. Minor fluctuations in the orientation of the Trp109 sidechain indole ring and in the loop located between helix 1 and helix 2 suggest that the binding pocket may be able to sample other conformational states, even in the presence of the small-molecule inhibitor.

Notably, the asymmetric dimer contains three DD2 poses. While monomer A (**Fig. 3-9**) contains only one DD2 molecule (pose 1) in the binding pocket, monomer B (**Fig. 3-10**) displays two DD2 molecules (poses 2 and 3). Inspection of the two monomers indicates that poses 1 and 2 are located within the DD2 binding pocket, albeit in slightly different rotations about their vertical axes. Pose 3 is located outside the hydrophobic cavity and appears to be a consequence of a crystal contact, acting as a “bridge” molecule between adjoining unit cells. The average B-factor values observed for the three DD2 molecules (31.0 \AA^2 , 29.0 \AA^2 , 33.6 \AA^2), as well as residues within close proximity ($\leq 5 \text{ \AA}$) to the inhibitor (33.4 \AA^2), are lower than the overall mean B-factor of the complex (46.4 \AA^2). The specific individual B-factors are listed in **Tables 3-1** and **Fig.5**. In addition, each of the DD2 molecules exhibit occupancies of 1.0 in the 2fo-fc difference maps. These results suggest that, upon DD2 binding, the sidechains of the hydrophobic binding pocket samples less conformational mobility relative to the rest of the structure.

Overall RMS deviation values of the three poses suggest that the individual DD2 structures are similar (**Table 3-4**). However, visual inspection of their structural overlays indicates that poses 1 and 2 are more closely related to each other than to pose 3 (**Fig. 3-11**). The DD2 benzyl and methylenyl-cyclohexyl “sidechain” groups adopt the same relative elevations and positions within the KSHV Pr binding pocket as the Met197 and Ile201 sidechains of the partner monomer in the active dimeric enzyme. This suggests that the DD2 “sidechains” mimic the $i \rightarrow i+4$ positioning inherent with sidechains of residues that adopt a helical conformation (**Fig. 3-9**). Moreover, the DD2 “sidechains” of both poses 1 and 2 are enveloped by the hydrophobic cavity formed upon the Trp109 indole ring adopting the “open” position (**Fig. 3-9 & 3-10**).

Further examination of the DD2 conformations may also explain the structure-activity relationships in the helical mimetic library used in the initial fluorescence-based activity screening. Of our original optimized mimetic library, only DD2 contained an amide group in the ortho position with respect to the nitrogen atom of the pyridinyl ring.²¹ The stacking positions of the cyclic DD2 “sidechain” groups prevent the amide proton and the pyridinyl nitrogen from interacting with the protease, either directly or via a water molecule (**Fig. 3-11**). Interatomic distances and “backbone” dihedrals measured from the crystallographic poses of DD2 suggest that the amide proton and pyridinyl nitrogen may form a weak intramolecular hydrogen bond (**Table 3-4**). Such interactions may help stabilize the conformation necessary for efficient binding to KSHV Pr. Further alterations to the DD2 “backbone”, such as the addition of polar functional groups, would be required to enhance solubility and, perhaps, increase efficacy towards the HHV proteases.

Loss of helix 6 disrupts the conformation of the KSHV Pr active site.

The loss of helix 6 results in a dramatic conformational perturbation of the KSHV Pr active site, located $\sim 15 - 20$ Å from the dimer interface (**Fig. 3-12**). The most noticeable change is observed for the conformation of β -strand 1 (residues 5-13), and is propagated through the β 1- α 0 loop (residues 14-27) and helix 0 (residues 27-33). In the case of the KSHV Pr dimer, β -strand 1 points outward from the structural core of the enzyme, allowing the β 1- α 0 loop and the following helices to adopt a conformation suitable for substrate binding and proteolytic cleavage (**Fig. 3-12a-b**). In the case of the Δ 196-DD2 complex, the C-terminal portion of β -strand 1 adopts a nearly orthogonal conformation with respect to its corresponding position in the KSHV Pr dimer. This results in a rotation of the β 1- β 0 loop into a position that occludes the substrate binding pocket and the catalytic triad (**Fig. 3-12c-d**).

Another striking difference in this conformational rearrangement is the positioning of Arg142 and Arg143 (**Fig. 3-12**). These two arginine residues are conserved among all members of the HHV Pr family, and are known to have important roles in stabilizing the structure of the oxyanion hole.²⁴ In the case of KSHV Pr, both the backbone amide and sidechain guanidino groups of Arg142 and Arg143 stabilize peptide substrate interactions within the active site via a series of intermolecular hydrogen bonds.²² The KSHV Pr dimer structure displays the Arg142 and Arg143 sidechains pointing inward towards the catalytic residues and forming a ridge of the substrate binding pocket (**Fig. 3-12a-b**). We term this the “closed” state in conjunction with the “closed” Trp109 indole ring. Alternatively, in the structure of the Δ 196-DD2 complex, the sidechains of both arginine residues point outward

towards the space originally occupied by helix 6 (**Fig. 3-12c-d**). We term this the “open” conformational state, analogous to the “open” Trp109 indole ring.

An examination of the average B-factor values indicates that the residues of the catalytic triad (33.6 \AA^2) are smaller than that of the overall structure (46.4 \AA^2), but those of the $\beta 1$ - $\alpha 0$ loop (56.6 \AA^2) are larger. In addition, the average B-factor values for residues of monomer A in the loop containing Arg142 and Arg143 are also significantly larger (59.1 \AA^2) than the overall average value. The individual B-factor values corresponding to these residues are listed in **Table 3-5**. This suggests a general allosteric mechanism of HHV Pr inhibition: that DD2 binding at the dimer interface enhances mobility of the oxyanion hole-stabilizing loop, allowing the active site to be conformationally destabilized. Notably, no significant differences in the average B-factor values are observed for the residues 138-149 of monomer B (35.2 \AA^2). However, this may reflect the presence of the bridging DD2 molecule in monomer B restricting conformational mobility of the Cys138-Val149 loop.

These observations point to the importance of a structured helix 5 in propagating conformational changes within KSHV Pr. Here, a DD2 molecule captures an inactive KSHV Pr conformation by binding to the hydrophobic patch in the area normally occupied by helix 5, disrupting interactions between the protease structural core and helices 5 and 6. If helix 5 was located at the dimer interface, helix 6 would be in a position to sterically force the sidechains of Arg142 and Arg143 inward towards the structural core of the enzyme, allowing the formation of the active site and oxyanion hole. The loss of helix 6 likely allows the loop containing Arg142 and Arg143 to sample multiple conformational states, effectively destabilizing both the oxyanion hole and the substrate binding pocket.

DD2 inhibits HCMV Protease by binding to the dimer interface.

As all eight HHV proteases are structurally and functionally homologous,²⁴ we speculated that DD2 acts upon human cytomegalovirus protease (HCMV Pr) in the same manner as on KSHV Pr. Using a fluorescence-based substrate cleavage kinetics assay previously described for KSHV Pr,²¹ the *in vitro* dissociation constant was re-determined for the HCMV Pr monomer-dimer equilibrium as $1.3 \pm 0.1 \mu\text{M}$. This value is nearly identical to that reported for KSHV Pr ($K_d = 1.7 \mu\text{M}$) under similar conditions,^{21,25} indicating that both HHV proteases are weakly associating dimers. Activity assays also indicate that DD2 exhibits four-fold weaker inhibition against HCMV Pr relative to KSHV Pr, with an IC_{50} value of $12.8 \pm 1.1 \mu\text{M}$. In addition, circular dichroism spectra of the wild-type HCMV Pr exhibit loss of helical content upon addition of excess molar equivalents DD2 (**Fig. 3-13**), suggesting that the C-terminal helices are unfolded.

To further probe DD2 interactions with HCMV Pr, HSQC spectra of selective [^{13}C - ^1H methyl] isoleucine labeled samples were acquired. Two HCMV Pr constructs homologous to the KSHV Pr monomers mentioned above were engineered. The first was an HCMV Pr obligate monomer (L222D), which exhibits an approximate 25-fold reduction in specific protease activity relative to the wild-type sequence (data not shown). The second was a HCMV Pr truncation ($\Delta 221$) that mimics the KSHV Pr $\Delta 196$ construct. In the case of the full-length HCMV Pr obligate monomer, two isoleucines (Ile61 and Ile96) are positioned at the dimer interface, while the third (Ile231) is located in the C-terminal region. Tyr128 was identified as the potential “hot spot” aromatic residue of HCMV Pr (**Fig. 3-14a**). ^{13}C - ^1H HSQC spectra acquired on the selectively labeled HCMV Pr L222D full length obligate (**Fig. 3-14b**) and HCMV Pr $\Delta 221$ truncated monomers (**Fig. 3-14c**) indicates that DD2 binds to the

dimer interface. Both Ile61 and Ile96 resonances are affected upon addition of DD2, with Ile61 exhibiting more extensive peak broadening. Importantly, as in the case of KSHV Pr, DD2 can bind to the C-terminal truncated HCMV Pr analog, but exhibits greater peak broadening and smaller chemical shift perturbations even at higher relative DD2 concentrations. Collectively, the fluorescence activity assay and the CD and NMR spectra suggest that DD2 binds to HCMV Pr in a structurally homologous pocket as KSHV Pr. The apparent weaker inhibition of HCMV Pr by DD2 may be the result of the smaller Tyr aromatic moiety creating a smaller hydrophobic pocket relative to KSHV Pr. However, with further chemical optimization of DD2, these results provide a promising pathway for developing broad-spectrum allosteric inhibitors for all eight HHV proteases.

DISCUSSION

From a drug-discovery standpoint, focusing on a conformationally dynamic target and capturing an inactive state in order to influence regulatory pathways is an appealing concept.^{4,6} In particular, regulating PPIs via allosteric mechanisms has recently gained traction. Allosterically targeting the subunit interface of dimeric complexes, such as the interdigitated β -sheets of HIV protease, has become an important goal due to increased incidents of resistance towards active-site therapeutics. Recent reports have noted the development of peptidic HIV protease dimer disruptors,^{26,27} including an alkylated tripeptide which “sequesters” a monomer.²⁸ Importantly, small molecule peptide mimetics have been shown to disrupt other PPIs. Perhaps the most well documented are the helical mimetics such as the Nutlins that inhibit p53/MDM2²⁹ interactions, and the multi-aryl compounds which disrupt calmodulin/smMLCK³⁰ and Bcl-x_L/Bak^{31,32} interactions. Multi-aryl and multi-cyclic compounds were also recently discovered to regulate CREB KID/CBP KIX domain^{33,34} and human survivin homodimer³⁵ interactions.

We have validated a methodology in which small molecules are used to allosterically inhibit an active enzyme by targeting a conformationally dynamic region. In the case of KSHV Pr, this conformationally dynamic region also governs the PPIs which influence the inactive monomer/active dimer equilibrium. Taken together, the NMR and X-ray crystallography data indicate a “monomer trap” model of KSHV Pr inhibition:²¹ that DD2 binds to and captures a pre-existing inactive monomer, thereby shifting the monomer-dimer equilibrium towards the inactive conformational state. Since HHV proteases are known to play critical roles in the late lytic stage of the viral lifecycle,²⁴ inhibiting protease function at this stage would be key to the development of novel therapeutics targeting herpesviruses. Although promising results

are observed *in vitro* for two of the eight members of the HHV protease family examined thus far, modifications to DD2 or the discovery of new helical mimetic scaffolds with improved pharmacokinetic and pharmacodynamic properties are necessary for further development. In particular, DD2 did not display an inhibitory effect in preliminary viral infectivity studies (data not shown) using a stably KSHV-infected SLK219 endothelial cell line.³⁶⁻³⁸ These results are explained by poor solubility and cell permeability of DD2 (**Table 6**), and we are currently exploring different chemical modifications to the DD2 scaffold in order to address these issues.

As the first structure of an allosterically inhibited HHV Pr monomer to date, our KSHV Pr Δ 196-DD2 complex provides valuable insights. First, conformational perturbations in the crystal structure of the inactive complex relative to the active KSHV Pr dimer suggest a reason why previous attempts at developing an active site inhibitor have failed. Specifically, the substrate binding pocket of the active site may be too shallow and too dynamic for a competitive inhibitor to bind. Second, the Δ 196-DD2 structure, focusing on the DD2 binding pocket, can be used as a template for *in silico* docking studies in future efforts to discover other allosteric KSHV Pr inhibitors, including those that exhibit more pharmacologically favorable characteristics than DD2. Third, and more importantly, although members of the HHV protease family have low sequence homology, they are structurally and functionally highly homologous. Inspection of the available HHV Pr structures (**Fig. 3-15**) reveals that all eight proteases have a potential hot spot aromatic residue at the dimer interface. This region could act as a target site for more potent allosteric, pan-specific inhibitors that trap the other HHV proteases in their respective inactive monomeric states. Allosteric inhibition as a method to regulate conformationally dynamic complexes such as protein-protein interactions

remains a mostly unexploited pathway. By examining KSHV Pr-DD2 interactions, we have utilized this route as a potential solution towards developing therapeutics that regulate high value, but previously intractable targets.

MATERIALS AND METHODS

Protease Truncation and Mutagenesis

Genes encoding the $\Delta 209$, $\Delta 196$, and $\Delta 191$ truncation constructs were based upon the KSHV Pr M197D-S204G^{14,16} sequences. Genes encoding all KSHV Pr M197D Ile \rightarrow Val single point mutations were synthesized using the unoptimized sequences of KSHV Pr M197D or KSHV Pr $\Delta 196$ as templates. Briefly, codons within the gene sequence representing isoleucine (ATA, ATC, or ATT) were changed to those encoding valine (GTA, GTC, or GTT). All gene sequences were designed at UCSF, and synthesized/purchased from GeneArt, Inc. Site-directed mutagenesis for the HCMV Pr L222D construct was performed using the QuickChange Site Directed Mutagenesis Kit (Stratagene). The HCMV Pr $\Delta L221$ truncated construct was based upon the wild-type HCMV Pr sequence using the pET11a expression vector (Novagen).

Primers (Integrated DNA Technologies, Inc.) encoding restriction sites were as follows:

KSHV Pr

NcoI

All Truncations:

5'-CCA TGG CAC AGG GCC TGT ACG TCG-3'

BamHI

$\Delta 191$: 5'-GGA TCC TTA ACT GAC GAA ATT TGG TGT GGA AAG GTC CTC-
3'

Δ196: 5'-GGA TCC TTA TAA GGT CTC CAG GGG ACT GAC GAA ATT TGG-
3'

Δ209: 5'-GGA TCC TTA GCG GTC CCG TAT GAA GCT GCC ATC-3'

HMCV Pr

L222D mutation

5'-GAC AGC TAC GGC CTG GAC GGC AAC AGC GTG GAC GC-3'

Δ221:

NdeI: 5'- GGT TCA TAT GCA TCA CCA TCA CCA TCA CAT GAC-3'

BamHI: 5'- AAT TGG ATC CTT ACA GGC CGT AGC TGT CTG AGC-3'

Protein Expression and Purification

All KSHV Pr protein samples were expressed in M9 minimal media (NMR) or Luria Broth (X-ray crystallography) and purified as previously described.^{15,21,22} Soluble HCMV Pr was expressed and purified as described previously³⁹ with the following modifications. Following overnight expression at 16 °C cells were pelleted and lysed by sonication, 0.5-second pulse/1-second recovery for 5 minutes, followed by 3-second pulse/3-second recovery for 2 minutes. After centrifugation at 30,000 g for 45 minutes, soluble fractions were passed over a 1 ml HisTrap FF column (GE Healthcare LifeSciences) using the following buffers: Wash/binding (50 mM NaP_i, 300 mM NaCl, 25 mM imidazole, 5 mM β-mercaptoethanol, pH 8.0); elution (50 mM NaP_i, 300 mM NaCl, 300 mM imidazole, 5 mM β-mercaptoethanol). Eluted His-tagged proteins were buffer exchanged into 25 mM NaP_i, 150 mM NaCl, 5 mM β-

mercaptoethanol and further purified over a Superdex75 (26/60) size exclusion chromatography column (GE Healthcare LifeSciences).

Starting protein concentrations for all assays described below were measured using a Nanodrop 2000c UV spectrophotometer (Thermo Scientific). Selective [^{13}C - ^1H methyl] isotopic labeling of the isoleucine, leucine, and valine residues was achieved by adding 100 mg/L [dimethyl- $^{13}\text{C}_2$]- α -ketoisovaleric acid (Cambridge Isotope Laboratories) and 50 mg/L [methyl- $^{13}\text{C}_1$]- α -ketobutyric acid (Sigma) to otherwise unlabeled M9 minimal media 1 hr prior to IPTG induction.⁴⁰

Calculation of Protein Sample Concentrations

Starting protein concentrations for all assays described below were measured using a Nanodrop 2000c UV spectrophotometer (Thermo Scientific) at 280 nm using the following extinction coefficients: KSHV Pr M197D and KSHV Pr M197D-I201V, $\epsilon = 23,950 \text{ M}^{-1} \text{ cm}^{-1}$; KSHV Pr $\Delta 209$, $\Delta 196$, $\Delta 191$, and all $\Delta 196 \text{ Ile} \rightarrow \text{Val}$ mutants, $\epsilon = 22,460 \text{ M}^{-1} \text{ cm}^{-1}$; HCMV Pr wild-type and HCMV Pr L222D, $\epsilon = 28,420 \text{ M}^{-1} \text{ cm}^{-1}$; HCMV Pr $\Delta 221$, $\epsilon = 23,950 \text{ M}^{-1} \text{ cm}^{-1}$.

Protease Kinetic Analysis

Kinetic proteolysis assays were performed on HCMV Pr variants using the same methodology as previously described for KSHV Pr studies.²¹ Monomer-dimer K_d (N=3) and IC_{50} (N=4) values reported herein represent the average and standard deviation.

Circular Dichroism Analysis

Protease was allowed to equilibrate with or without DD2 for 1 h at room temperature in buffer solution (25 mM sodium phosphate buffer, 75 mM NaCl, 1 mM β -mercaptoethanol, 0.8% dioxane, pH 8). Spectra were obtained using a 2 mm path length cuvette on a Jasco J-715 spectropolarimeter with a final protein concentration of $\sim 3 \mu\text{M}$. Data were acquired at a constant temperature of 25 °C with the following parameters: accumulations 3, scan rate 50 nm/min, data pitch 0.1 nm, response 4 s, bandwidth 20 nm, and standard sensitivity. Buffer with and without DD2 were used to acquire background spectra. Final CD data spectra are reported as mean residue ellipticity ($\text{deg} \cdot \text{cm}^2 \cdot \text{dmol}^{-1} \cdot \text{residue}^{-1}$). Fractional helicity (f_H) values were estimated from the 222 nm band:⁴¹

$$\theta_{222,\text{max}} = (-44000 + 250T) \left(1 - \frac{2.5}{N}\right) \quad (1),$$

where $\theta_{222,\text{max}}$ is the calculated mean residue ellipticity value for a theoretical 100% helical polypeptide of N residues, collected at temperature T (°C). At 25 °C: KSHV Pr (N = 229 residues), $\theta_{222,\text{max}} = -37,338 \text{ deg cm}^2 \text{ dmol}^{-1} \text{ residue}^{-1}$; HCMV Pr (N = 262 residues), $\theta_{222,\text{max}} = -37,390 \text{ deg cm}^2 \text{ dmol}^{-1} \text{ residue}^{-1}$.

NMR Data Acquisition and Analysis

All spectra were acquired on cryoprobe-equipped Bruker Avance 500 MHz or 800 MHz NMR spectrometers at 12 °C or 27 °C. Typical NMR samples used for the ^{13}C - ^1H HSQC titration studies consisted of $\sim 0.01 - 0.02 \text{ mM}$ selective [^{13}C - ^1H methyl] ILV labeled protein in 0.45 mL buffer. Sample preparation, including buffer conditions and DD2 titrations, and spectral acquisition parameters were as previously described.²¹ Each titration study contained

at least one repeat acquisition point. All data were processed using NMRPIPE⁴² and analyzed using SPARKY⁴³.

Calculation of NMR-based apparent K_d values

Chemical shift data for the δ 1-methyl groups of Ile44, Ile71, and Ile105 were converted to frequency values. Chemical shift perturbation values versus resonances corresponding to the apo protein are expressed as combined ^{13}C - ^1H frequency perturbations ($\Delta\omega_{obs}$):

$$\Delta\omega_{obs} = \sqrt{(\Delta\delta_H * \text{specfreq}_H)^2 + (\Delta\delta_C * \text{specfreq}_C)^2} \quad (2),$$

where $\Delta\delta_H$ and $\Delta\delta_C$ correspond to the ^1H and ^{13}C chemical shift perturbation versus the apo protein, respectively. specfreq_H and specfreq_C correspond to the spectral frequencies of ^1H and ^{13}C , respectively.

Titration data point from the ^{13}C - ^1H HSQC spectra were fit to a modified Hill Equation⁴⁴ using Matlab (The Mathworks, Inc).

$$\Delta\omega_{obs} = \frac{\Delta\omega_{max} * [L]_T^N}{K_d + [L]_T^N} \quad (3),$$

where $\Delta\omega_{max}$ is the maximum frequency perturbation, corresponding to a fully saturated ligand-bound state. $[L]_T$ is the total ligand concentration, and N is the Hill coefficient. Estimated values for $\Delta\omega_{max}$, N , and K_d were calculated from a non-linear regression fitting of Equation 2, using a grid search methodology to minimize χ^2 errors. Final estimated apparent K_d values and errors reported in this paper are averages and standard deviations calculated for Ile44, Ile71, and Ile105. Estimated experimental errors were based upon repeat data points acquired during the NMR titrations and were propagated throughout the calculations.

X-Ray Crystallography Data Acquisition and Structure Determination

KSHV Pr \square 196 stock solutions used for X-ray crystallography consisted of 25 mM Tris (pH 8.0), 150 mM KCl, 0.1 mM EDTA, and 2 mM DTT. Crystals were grown at 25 °C with the hanging drop vapor diffusion method, with DD2 in greater than five-fold molar excess with respect to \square 196. The reservoir solution consisted of 2 M $(\text{NH}_4)_2\text{SO}_4$, 0.2 M NaCl, 0.05 M sodium cacodylate (pH 7.0), 0.1 M urea, and 0.1 M anhydrous sodium acetate. Following one day of incubation, 1 μL of 14 M β -mercaptoethanol was added to the reservoir. After 14-21 days, crystals appeared as a small cube measuring $0.03 \times 0.05 \times 0.05 \text{ mm}^3$. A 2.0 Å-resolution X-ray diffraction data set was collected at the Lawrence-Berkeley National Laboratory Advanced Light Source Beamline 8.3.1, using a crystal flash-cooled to 100 K in mother liquor with 20% glycerol as the cryoprotectant.

Diffraction images were processed using DENZO and SCALEPACK from the HKL-2000 suite.⁴⁵ The resulting structure was solved by molecular replacement using PHASER⁴⁶ using the phosphonate-inhibited KSHV Pr dimer (2pbk)²² with residues 196 – 230 deleted as the template search model. The structure model resulted in as a dimer in an asymmetric unit (R-factor = 45.6%, R_{free} = 49.5%), and was subjected to multiple rounds of restrained refinement and isotropic B-factor minimization with REFMAC⁴⁷ and COOT⁴⁸.

All structural figures and animations within this paper and the supplementary materials were created using PYMOL 1.2 (Schrödinger, LLC). Morph calculations were performed using the Yale Morph Server (<http://www.molmovdb.org/>).

DD2 Solubility Measurements

Test compounds were serially diluted from 10,000 μM to 625 μM in DMSO and placed in columns 1-5 and 7-11 of a 96-well polypropylene plate (Costar 3365). Columns 6 and 12 were filled with DMSO as the background. From each well, 5 μL was transferred into the 96-well disposable UV-Star plate (Greiner Bio-One). Acetonitrile (97.5 μL) and pH 7.4 PBS buffer (97.5 μL) were added to each well, and the plate was agitated for 30 min using an IKA microtiter plate shaker. The UV spectra from 200–500 nm was measured for all wells and subtracted from the DMSO background. Correlations between concentrations and absorbance at 260, 280, and 300 nm were determined as slopes. Then, 5 μL from each well of the polypropylene plate was added to a MultiScreen Solubility Filter Plate (Millipore) and diluted with 195 μL of PBS. The plate was agitated for 2 hrs and filtered into a 96-well disposable UV-Star plate, and the UV absorbance at 260, 280, and 300 nm was measured. The aqueous solubility (A_{max} filtrate/slope) was determined for all three wavelengths, and values are given as the means with 95% confidence intervals.

DD2 Cell Permeability Measurements

All liquid-handling steps for the PAMPA assay were performed on a Biomek FX Laboratory Automation Workstation (Beckman-Coulter) and analyzed by pION's (London, UK) PAMPA Evolution 96 Command Software. The PAMPA Evolution 96 Permeability Assay Kit includes the Acceptor Sink Buffer (ASB), Double-Sink Lipid Solution, and a PAMPA sandwich plate, preloaded with magnetic disks. For each experiment, 4 μL of lipid was transferred onto the support membrane in the acceptor well, followed by addition of 200 μL of ASB (pH 7.4). Then, 180 μL of diluted test compound (50 μM in system buffer at pH 7.4 starting from a 10 mM DMSO solution) was added to the donor wells. The PAMPA sandwich plate was assembled and placed on the Gut-Box and stirred for 30 min. The

distribution of the compounds in the donor and acceptor buffers (100 μ L aliquot) was determined by measuring the UV spectra from 200 to 500 nm using the SpectraMax reader (Molecular Devices). The permeability coefficient was determined using the maximum absorbance from 200 to 500 nm:⁴⁹

$$P_e = \frac{2.3 V_D}{[A(t - t_{lag})]} \log_{10} \left\{ \left[\frac{1}{(1-R)} \right] \left[\frac{C_D(t)}{C_D(0)} \right] \right\} \quad (4),$$

where V_D is the donor well volume (cm^3); A is the filter area (cm^2); $C_D(0)$ is the sample concentration in the donor well at time 0 (mole/cm^3); $C_D(t)$ is the sample concentration in the donor well at time t (mole/cm^3); t is the interval of time (sec); t_{LAG} is the lag time needed to reach steady state conditions (sec); and R is the membrane retention (related to the membrane/water partition coefficient). Standards used were verapamil ($P_e = 1505 \times 10^{-6}$ cm/s) as a high permeability standard, carbamazepine ($P_e = 150 \times 10^{-6}$ cm/s) as medium permeability standard and ranitidine ($P_e = 2.3 \times 10^{-6}$ cm/s) as low permeability standard. The compounds were measured in triplicate, and values are given as the mean values with 95% confidence intervals.

PDB Accession Numbers

Structural coordinates for the KSHV Pr Δ 196-DD2 complex have been deposited at the Brookhaven Protein Data Bank with accession number **3NJQ**.

ACKNOWLEDGMENTS

This work was funded in part by grants from the National Institutes of Health (grant 1R01-A1067423) and the HIV Accessory and Regulatory Complex Center (grant P50-GM082250).

This research was also supported by a grant from the National Institutes of Health, University of California San Francisco-Gladstone Institute of Virology & Immunology Center for AIDS Research (P30-A122763 to G.M.L.). We thank Prof. Don Ganem, Prof. R. Kip Guy, Dr. Leggy Arnold, and Mr. Ernest Lam for technical support. We also thank Prof. John D. Gross and Dr. Ana Lazic for helpful discussions of this manuscript.

REFERENCES

1. Dyson, H. J. & Wright, P. E. (2005). Intrinsically unstructured proteins and their functions. *Nat Rev Mol Cell Biol* **6**, 197-208.
2. Boehr, D. D., Nussinov, R. & Wright, P. E. (2009). The role of dynamic conformational ensembles in biomolecular recognition. *Nat Chem Biol* **5**, 789-96.
3. Zinzalla, G. & Thurston, D. E. (2009). Targeting protein-protein interactions for therapeutic intervention: a challenge for the future. *Future Med Chem* **1**, 65-93.
4. Metallo, S. J. (2010). Intrinsically disordered proteins are potential drug targets. *Curr Opin Chem Biol* **14**, 481-488.
5. Kar, G., Keskin, O., Gursoy, A. & Nussinov, R. (2010). Allostery and population shift in drug discovery. *Curr Opin Pharmacol* **10**, 715-22.
6. Lee, G. M. & Craik, C. S. (2009). Trapping moving targets with small molecules. *Science* **324**, 213-5.
7. Arkin, M. R. & Wells, J. A. (2004). Small-molecule inhibitors of protein-protein interactions: progressing towards the dream. *Nat Rev Drug Discov* **3**, 301-17.
8. Berg, T. (2008). Small-molecule inhibitors of protein-protein interactions. *Curr Opin Drug Discov Devel* **11**, 666-74.
9. Yin, H. & Hamilton, A. D. (2005). Strategies for targeting protein-protein interactions with synthetic agents. *Angew Chem Int Ed Engl* **44**, 4130-63.
10. Hershberger, S. J., Lee, S. G. & Chmielewski, J. (2007). Scaffolds for blocking protein-protein interactions. *Curr Top Med Chem* **7**, 928-42.

11. Ross, N. T., Katt, W. P. & Hamilton, A. D. (2010). Synthetic mimetics of protein secondary structure domains. *Philos Transact A Math Phys Eng Sci* **368**, 989-1008.
12. Clackson, T. & Wells, J. A. (1995). A hot spot of binding energy in a hormone-receptor interface. *Science* **267**, 383-6.
13. Ma, B. & Nussinov, R. (2007). Trp/Met/Phe hot spots in protein-protein interactions: potential targets in drug design. *Curr Top Med Chem* **7**, 999-1005.
14. Nomura, A. M., Marnett, A. B., Shimba, N., Dotsch, V. & Craik, C. S. (2005). Induced structure of a helical switch as a mechanism to regulate enzymatic activity. *Nat Struct Mol Biol* **12**, 1019-20.
15. Nomura, A. M., Marnett, A. B., Shimba, N., Dotsch, V. & Craik, C. S. (2006). One functional switch mediates reversible and irreversible inactivation of a herpesvirus protease. *Biochemistry* **45**, 3572-9.
16. Shimba, N., Nomura, A. M., Marnett, A. B. & Craik, C. S. (2004). Herpesvirus protease inhibition by dimer disruption. *J Virol* **78**, 6657-65.
17. del Sol, A., Tsai, C.-J., Ma, B. & Nussinov, R. (2009). The Origin of Allosteric Functional Modulation: Multiple Pre-existing Pathways. *Structure* **17**, 1042-1050.
18. Ogilvie, W., Bailey, M., Poupart, M. A., Abraham, A., Bhavsar, A., Bonneau, P., Bordeleau, J., Bousquet, Y., Chabot, C., Duceppe, J. S., Fazal, G., Goulet, S., Grand-Maitre, C., Guse, I., Halmos, T., Lavallee, P., Leach, M., Malenfant, E., O'Meara, J., Plante, R., Plouffe, C., Poirier, M., Soucy, F., Yoakim, C. & Deziel, R. (1997). Peptidomimetic inhibitors of the human cytomegalovirus protease. *J Med Chem* **40**, 4113-35.

19. Borthwick, A. D., Crame, A. J., Ertl, P. F., Exall, A. M., Haley, T. M., Hart, G. J., Mason, A. M., Pennell, A. M., Singh, O. M., Weingarten, G. G. & Woolven, J. M. (2002). Design and synthesis of pyrrolidine-5,5-trans-lactams (5-oxohexahydropyrrolo[3,2-b]pyrroles) as novel mechanism-based inhibitors of human cytomegalovirus protease. 2. Potency and chirality. *J Med Chem* **45**, 1-18.
20. Gopalsamy, A., Lim, K., Ellingboe, J. W., Mitsner, B., Nikitenko, A., Upeslakis, J., Mansour, T. S., Olson, M. W., Bebernitz, G. A., Grinberg, D., Feld, B., Moy, F. J. & O'Connell, J. (2004). Design and syntheses of 1,6-naphthalene derivatives as selective HCMV protease inhibitors. *J Med Chem* **47**, 1893-9.
21. Shahian, T., Lee, G. M., Lazic, A., Arnold, L. A., Velusamy, P., Roels, C. M., Guy, R. K. & Craik, C. S. (2009). Inhibition of a viral enzyme by a small-molecule dimer disruptor. *Nat Chem Biol* **5**, 640-6.
22. Lazic, A., Goetz, D. H., Nomura, A. M., Marnett, A. B. & Craik, C. S. (2007). Substrate Modulation of Enzyme Activity in the Herpesvirus Protease Family. *J Mol Biol* **373**, 913-923.
23. Reiling, K. K., Pray, T. R., Craik, C. S. & Stroud, R. M. (2000). Functional consequences of the Kaposi's sarcoma-associated herpesvirus protease structure: regulation of activity and dimerization by conserved structural elements. *Biochemistry* **39**, 12796-803.
24. Tong, L. (2002). Viral proteases. *Chem Rev* **102**, 4609-26.
25. Pray, T. R., Reiling, K. K., Demirjian, B. G. & Craik, C. S. (2002). Conformational change coupling the dimerization and activation of KSHV protease. *Biochemistry* **41**, 1474-82.

26. Hwang, Y. S. & Chmielewski, J. (2005). Development of low molecular weight HIV-1 protease dimerization inhibitors. *J Med Chem* **48**, 2239-42.
27. Frutos, S., Rodriguez-Mias, R. A., Madurga, S., Collinet, B., Reboud-Ravaux, M., Ludevid, D. & Giralt, E. (2007). Disruption of the HIV-1 protease dimer with interface peptides: structural studies using NMR spectroscopy combined with [2-(13)C]-Trp selective labeling. *Biopolymers* **88**, 164-73.
28. Bannwarth, L., Rose, T., Dufau, L., Vanderesse, R., Dumond, J., Jamart-Gregoire, B., Pannecouque, C., De Clercq, E. & Reboud-Ravaux, M. (2009). Dimer disruption and monomer sequestration by alkyl tripeptides are successful strategies for inhibiting wild-type and multidrug-resistant mutated HIV-1 proteases. *Biochemistry* **48**, 379-87.
29. Hu, C. Q. & Hu, Y. Z. (2008). Small molecule inhibitors of the p53-MDM2. *Curr Med Chem* **15**, 1720-30.
30. Orner, B. P., Ernst, J. T. & Hamilton, A. D. (2001). Toward proteomimetics: terphenyl derivatives as structural and functional mimics of extended regions of an alpha-helix. *J Am Chem Soc* **123**, 5382-3.
31. Kutzki, O., Park, H. S., Ernst, J. T., Orner, B. P., Yin, H. & Hamilton, A. D. (2002). Development of a potent Bcl-x(L) antagonist based on alpha-helix mimicry. *J Am Chem Soc* **124**, 11838-9.
32. Petros, A. M., Dinges, J., Augeri, D. J., Baumeister, S. A., Betebenner, D. A., Bures, M. G., Elmore, S. W., Hajduk, P. J., Joseph, M. K., Landis, S. K., Nettesheim, D. G., Rosenberg, S. H., Shen, W., Thomas, S., Wang, X., Zanze, I., Zhang, H. & Fesik, S. W. (2006). Discovery of a potent inhibitor of the antiapoptotic protein Bcl-xL from NMR and parallel synthesis. *J Med Chem* **49**, 656-63.

33. Best, J. L., Amezcu, C. A., Mayr, B., Flechner, L., Murawsky, C. M., Emerson, B., Zor, T., Gardner, K. H. & Montminy, M. (2004). Identification of small-molecule antagonists that inhibit an activator: coactivator interaction. *Proc Natl Acad Sci USA* **101**, 17622-7.
34. Bates, C. A., Pomerantz, W. C. & Mapp, A. K. (2011). Transcriptional tools: Small molecules for modulating CBP KIX-dependent transcriptional activators. *Biopolymers* **95**, 17-23.
35. Wendt, M. D., Sun, C., Kunzer, A., Sauer, D., Sarris, K., Hoff, E., Yu, L., Nettesheim, D. G., Chen, J., Jin, S., Comess, K. M., Fan, Y., Anderson, S. N., Isaac, B., Olejniczak, E. T., Hajduk, P. J., Rosenberg, S. H. & Elmore, S. W. (2007). Discovery of a novel small molecule binding site of human survivin. *Bioorg Med Chem Lett* **17**, 3122-9.
36. Bechtel, J. T., Liang, Y., Hvidding, J. & Ganem, D. (2003). Host range of Kaposi's sarcoma-associated herpesvirus in cultured cells. *J Virol* **77**, 6474-81.
37. Vieira, J. & O'Hearn, P. M. (2004). Use of the red fluorescent protein as a marker of Kaposi's sarcoma-associated herpesvirus lytic gene expression. *Virology* **325**, 225-40.
38. Chandriani, S. & Ganem, D. (2010). Array-based transcript profiling and limiting-dilution reverse transcription-PCR analysis identify additional latent genes in Kaposi's sarcoma-associated herpesvirus. *J Virol* **84**, 5565-73.
39. Brignole, E. J. & Gibson, W. (2007). Enzymatic activities of human cytomegalovirus maturational protease assemblin and its precursor (pPR, pUL80a) are comparable: [corrected] maximal activity of pPR requires self-interaction through its scaffolding domain. *J Virol* **81**, 4091-103.

40. Goto, N. K., Gardner, K. H., Mueller, G. A., Willis, R. C. & Kay, L. E. (1999). A robust and cost-effective method for the production of Val, Leu, Ile (δ^1) methyl-protonated ^{15}N -, ^{13}C -, ^2H -labeled proteins. *J Biomol NMR* **13**, 369-74.
41. Wallimann, P., Kennedy, R. J. & Kemp, D. S. (1999). Large Circular Dichroism Ellipticities for N-Templated Helical Polypeptides Are Inconsistent with Currently Accepted Helicity Algorithms. *Angew Chem Int Ed Engl* **38**, 1290-1292.
42. Delaglio, F., Grzesiek, S., Vuister, G. W., Zhu, G., Pfeifer, J. & Bax, A. (1995). NMRPipe: a multidimensional spectral processing system based on UNIX pipes. *J. Biomol. NMR* **6**, 277-93.
43. Goddard, T. D. & Kneller, D. G. (1999). Sparky 3. University of California, San Francisco.
44. Ramstad, T., Hadden, C. E., Martin, G. E., Speaker, S. M., Teagarden, D. L. & Thamann, T. J. (2005). Determination by NMR of the binding constant for the molecular complex between alprostadil and alpha-cyclodextrin. Implications for a freeze-dried formulation. *Int J Pharm* **296**, 55-63.
45. Otwinowski, Z., Minor, W. & Carter, C. W., Jr. (1997). Processing of X-ray diffraction data collected in oscillation mode. *Meth Enzymol* **276**, 307-326.
46. McCoy, A. J., Grosse-Kunstleve, R. W., Adams, P. D., Winn, M. D., Storoni, L. C. & Read, R. J. (2007). Phaser crystallographic software. *J Appl Crystallogr* **40**, 658-674.
47. Skubak, P., Murshudov, G. N. & Pannu, N. S. (2004). Direct incorporation of experimental phase information in model refinement. *Acta Crystallogr D Biol Crystallogr* **60**, 2196-201.

48. Emsley, P., Lohkamp, B., Scott, W. G. & Cowtan, K. (2010). Features and development of Coot. *Acta Crystallogr D Biol Crystallogr* **66**, 486-501.
49. Avdeef, A. (2001). Physicochemical profiling (solubility, permeability and charge state). *Curr Top Med Chem* **1**, 277-351.
50. Laskowski, R. A., MacArthur, M. W., Moss, D. S. & Thornton, J. M. (1993). PROCHECK: a program to check the stereochemical quality of protein structures. *J Appl Crystallog* **26**, 283-291.

Table 3-1

TABLE 1: SUMMARY OF CRYSTALLOGRAPHIC INFORMATION, 3NJQ

| | | |
|---|-------------------|-------------|
| <u>Data collection and processing</u> | | |
| Number of crystals used | 1 | |
| Wavelength (Å) | 1 | |
| Space group | I 222 | |
| Unit cell parameters | | |
| a, b, c (Å) | 69.3, 95.9, 119.2 | |
| α, β, γ (°) | 90, 90, 90 | |
| Matthews coefficient (Å ³ /Da) | 2.32 | |
| Solvent content (%) | 46.47 | |
| Molecules per asymmetric unit | 2 | |
| Beamline | ALS 8.3.1 | |
| <u>Diffraction Data</u> | | |
| Resolution range (Å) | 50 – 2.0 | (2.1 – 2.0) |
| Unique reflections | 27221 | (1200) |
| $R(I)_{\text{sym}}$ (%) ^a | 6.3 | (31.1) |
| Completeness (%) | 99.9 | (70.1) |
| Redundancy | 4.1 | (2.0) |
| $I/\sigma(I)$ | 30.5 | (3.3) |
| <u>Refinement</u> | | |
| Resolution range (Å) | 48 – 2.0 | |
| Reflections used in refinement (work / free) | 25855 / 1366 | |
| Final R values for all reflections (work ^b / free ^c) (%) | 20.3 / 24.8 | |
| Protein residues | 377 | |
| Inhibitor | 3 | |
| Water molecules | 106 | |
| <u>RMS Deviations</u> | | |
| Bonds (Å) | 0.019 | |
| Angles (°) | 1.979 | |
| <u>Ramachandran parameters^d</u> | | |
| Residues in most favored regions | 90.0% | |
| Residues in additional allowed regions | 8.7% | |
| Residues in generously allowed regions | 0.6% | |
| <u>Mean B-factor (Å²)</u> | | |
| Protein | 46.4 | |
| Inhibitors | | |
| 3NJQ A 197 | 31.0 | |
| 3NJQ B 198 | 29.0 | |
| 3NJQ B 199 (bridging molecule) | 33.6 | |
| Water molecules | 27.0 | |

Numbers in parentheses represent the highest resolution shell.

^a $R_{\text{sym}} = (\sum |I - \langle I \rangle|) / \sum I$, where $\langle I \rangle$ is the average intensity of multiple measurements.

^b $R_{\text{work}} = (\sum |F_{\text{obs}} - F_{\text{calc}}|) / \sum |F_{\text{obs}}|$

^c $R_{\text{free}} = R_{\text{work}}$ based on ~ 1000 (at least 10%) of reflections excluded from refinement

^d Calculated using Procheck⁵⁰

Table 3-2**AVERAGE B-VALUES: KSHV PR Δ 196-DD2**

| KSHV Pr Δ 196-DD2 complex | Monomer A (\AA^2) | Monomer B (\AA^2) |
|----------------------------------|------------------------------|------------------------------|
| Backbone heavy atoms | 49.1 | 40.2 |
| Sidechain heavy atoms | 52.8 | 43.7 |
| All heavy atoms | 50.9 | 41.9 |

Table 3-3**STRUCTURAL COMPARISON OF KSHV PR CONSTRUCTS**

| Overlay (residues 1-196) | ^a RMSD Backbone Atoms (Å) | ^a RMSD Heavy Atoms(Å) |
|---------------------------|---|-------------------------------------|
| 2PBK (A) vs. Δ196-DD2 (A) | 0.77 | 0.89 |
| 2PBK (A) vs. Δ196-DD2 (B) | 0.77 | 0.95 |
| 1FL1 (B) vs. Δ196-DD2 (A) | 0.60 | 0.74 |
| 1FL1 (B) vs. Δ196-DD2 (B) | 0.60 | 0.77 |
| Δ196-DD2 monomer A vs B | 0.52 | 0.61 |

^aRMSD calculations performed using Pymol 1.2 (Schrödinger, LLC).

2PBK = peptide-phosphonate inhibited KSHV Pr dimer¹

1FL1 = apo KSHV Pr dimer²

3NJQ = KSHV Pr Δ196-DD2 complex, **this study**.

Table 3-4

AVERAGE ^aSIDECHAIN B-VALUES OF RESIDUES:

| $\leq 5 \text{ \AA}$ to DD2 ^b Poses 1 & 2 (inhibitors) | | | $\leq 5 \text{ \AA}$ to DD2 ^b Pose 3 (bridging molecule) | | |
|--|---------------------------------|---------------------------------|--|---------------------------------|---------------------------------|
| Residue | Monomer A (\AA^2) | Monomer B (\AA^2) | Residue | Monomer A (\AA^2) | Monomer B (\AA^2) |
| Phe 76 | 26.3 | 28.4 | Glu 45 | n/a | 31.4 |
| Leu 79 | 30.0 | 36.2 | Leu 47 | n/a | 34.4 |
| Ala 80 | 26.7 | 28.8 | Trp 109 | n/a | 24.7 |
| Leu 83 | 29.2 | 29.8 | Leu 110 | n/a | 23.4 |
| Val 89 | 28.5 | 34.4 | Ala 139 | n/a | 30.4 |
| Ala 90 | 26.3 | 27.3 | Leu 140 | n/a | 30.9 |
| Trp 109 | 28.6 | 24.7 | Arg 144 | n/a | 47.3 |
| Leu 110 | 25.0 | 23.4 | | | |
| Ala 139 | 36.5 | 30.4 | | | |
| Leu140 | 48.7 | 30.9 | | | |
| Phe 189 | 32.6 | 33.7 | | | |
| Pro 192 | 44.9 | 37.2 | | | |
| Leu 193 | 50.7 | 39.3 | | | |
| Glu 194 | ^c | 53.1 | | | |
| ^d Average | 34.2 | 32.6 | ^d Average | n/a | 32.0 |
| Stdev. | 9.5 | 8.1 | Stdev. | n/a | 9.5 |
| ^e Overall | 33.4 | | ^e Overall | 32.0 | |
| Average | | | Average | | |
| Stdev. | 8.8 | | Stdev. | 9.5 | |

^a Includes C α atom.

^b Pose 1 = 3NJQ A 197; Pose 2 = 3NJQ B 198; Pose 3 = 3NJQ B 199

^c Electron density maps of Glu194 – Leu 196 not observed for 3NJQ monomer A.

^d Average and standard deviation of the individual monomers.

^e Overall average and standard deviation of the dimer.

Table 3-5

STRUCTURAL COMPARISON OF KSHV PR-BOUND DD2 POSES

| DD2 Overlay | ^a RMSD (Å) all atoms | ^a RMSD (Å) all hv atoms | ^a RMSD (Å) ^b backbone | ^a RMSD (Å) ^b backbone+ ^c sidechain 1 | ^a RMSD (Å) ^b backbone+ ^d sidechain 2 |
|---------------------------|------------------------------------|---------------------------------------|--|---|---|
| ^e pose 1 vs. 2 | 1.91 | 1.12 | 0.51 | 0.86 | 1.03 |
| ^e pose 1 vs. 3 | 1.99 | 0.53 | 0.34 | 0.85 | 0.36 |
| ^e pose 2 vs. 3 | 3.12 | 2.43 | 0.67 | 1.74 | 0.98 |

^a RMSD calculations performed using Pymol 1.2 (Schrödinger, LLC).

^b DD2 backbone = 4-(pyridine-2-amido) benzoic acid.

^c Sidechain 1 = methylenyl cyclohexyl group

^d Sidechain 2 = benzyl group

^e pose 1 = 3NJQ A 197; pose 2 = 3NJQ B 198; pose 3 = 3NJQ B 199

| DD2 pose # (Monomer ID) | ^f Amide H-pyridine N distance (Å) | ^f Amide N-pyridine N dihedral angle (°) |
|----------------------------|---|---|
| pose 1 (A 197) | 2.1 Å | -7.0° |
| pose 2 (B 198) | 2.2 Å | -4.9° |
| pose 3 (B 199) | 2.2 Å | -9.7° |

^f Measurements performed using Pymol 1.2 (Schrödinger, LLC).

Table 3- 6

AVERAGE ^aSIDECHAIN B-VALUES OF THE ACTIVE-SITE RESIDUES

| Residue | Catalytic Triad | |
|---------|-----------------------------|-----------------------------|
| | Monomer A (Å ²) | Monomer B (Å ²) |
| His 46 | 32.3 | 36.1 |
| Ser 114 | 35.8 | 31.8 |
| His 134 | 32.8 | 32.9 |
| Average | 33.3 | 34.0 |
| Stdev. | 2.1 | 2.8 |

| β1-α0 loop (residues 14-27) | | | β6-β7 loop (residues 139-149) | | |
|--------------------------------|--------------------------------|--------------------------------|----------------------------------|--------------------------------|--------------------------------|
| Residue | Monomer A (Å ²) | Monomer B (Å ²) | Residue | Monomer A (Å ²) | Monomer B (Å ²) |
| Val 14 | 43.8 | 35.7 | Cys 138 | 34.1 | 31.6 |
| Ser 15 | 52.9 | 48.4 | Ala 139 | 36.5 | 30.4 |
| Cys 16 | 52.9 | 53.2 | Leu 140 | 48.7 | 30.9 |
| Pro 17 | 45.9 | 61.2 | Gly 141 | 54.9 | 34.6 |
| Lys 18 | 52.3 | 77.7 | ^b Arg 142 | 59.4 | 36.0 |
| Leu 19 | 61.7 | 81.0 | ^b Arg 143 | 75.6 | 41.0 |
| Glu 20 | 86.6 | 66.8 | Arg 144 | 84.4 | 47.3 |
| Gln 21 | 73.8 | 54.1 | Gly 145 | 63.3 | 32.4 |
| Glu 22 | 58.3 | 41.9 | Thr 146 | 60.4 | 26.6 |
| Leu 23 | 64.4 | 47.0 | Val 147 | 45.9 | 27.1 |
| Tyr 24 | 55.7 | 33.8 | Ala 148 | 38.0 | 26.0 |
| Leu 25 | 54.9 | 41.7 | Val 149 | 40.5 | 30.2 |
| Asp 26 | 75.5 | 50.2 | | | |
| Pro 27 | 64.0 | 42.7 | | | |
| ^c Average | 61.0 | 52.3 | ^c Average | 59.1 | 35.2 |
| Stdev. | 12.1 | 15.1 | Stdev. | 17.1 | 8.3 |
| ^d Overall | 56.6 | | ^d Overall | 47.3 | |
| Average | | | Average | | |
| Stdev. | 14.3 | | Stdev. | 18.0 | |

^a Includes Cα atom. ^b Oxyanion hole-stabilizing residues.

^c Average and standard deviation of the individual monomers.

^d Overall average and standard deviation of the dimer.

Table 3-7**DD2 SOLUBILITY AND CELL PERMEABILITY**

| | ^a Solubility (μM) | ^b Permeability (10 ⁻⁶ cm s ⁻¹) | ^c Retention (%) |
|-----|------------------------------|--|----------------------------|
| DD2 | 0.49 | 296 | 91 |

^a Solubility in PBS buffer (pH 7.4) containing 1% DMSO

^{b,c} Permeability/retention across an artificial membrane (PAMPA), pH 7.4

Figure 3-1

Domain diagram of KSHV Pr. (a) Linear domain diagram of KSHV Pr displaying the positions of the catalytic residues (cyan) and the conformationally dynamic C-terminus (gray). C-terminal truncations are indicated by yellow or blue asterisks. (b) The dimer interface of a KSHV Pr monomer (2pbk). The partner monomer is omitted for clarity. The active site (cyan), the inhibitor-binding “hot spot” Trp109 (red), and truncation sites (yellow and blue balls) are indicated as in Figure 1a. (c) The chemical structure of DD2, an optimized analog of a first generation lead inhibitor of KSHV Pr.²¹

Figure 3-1

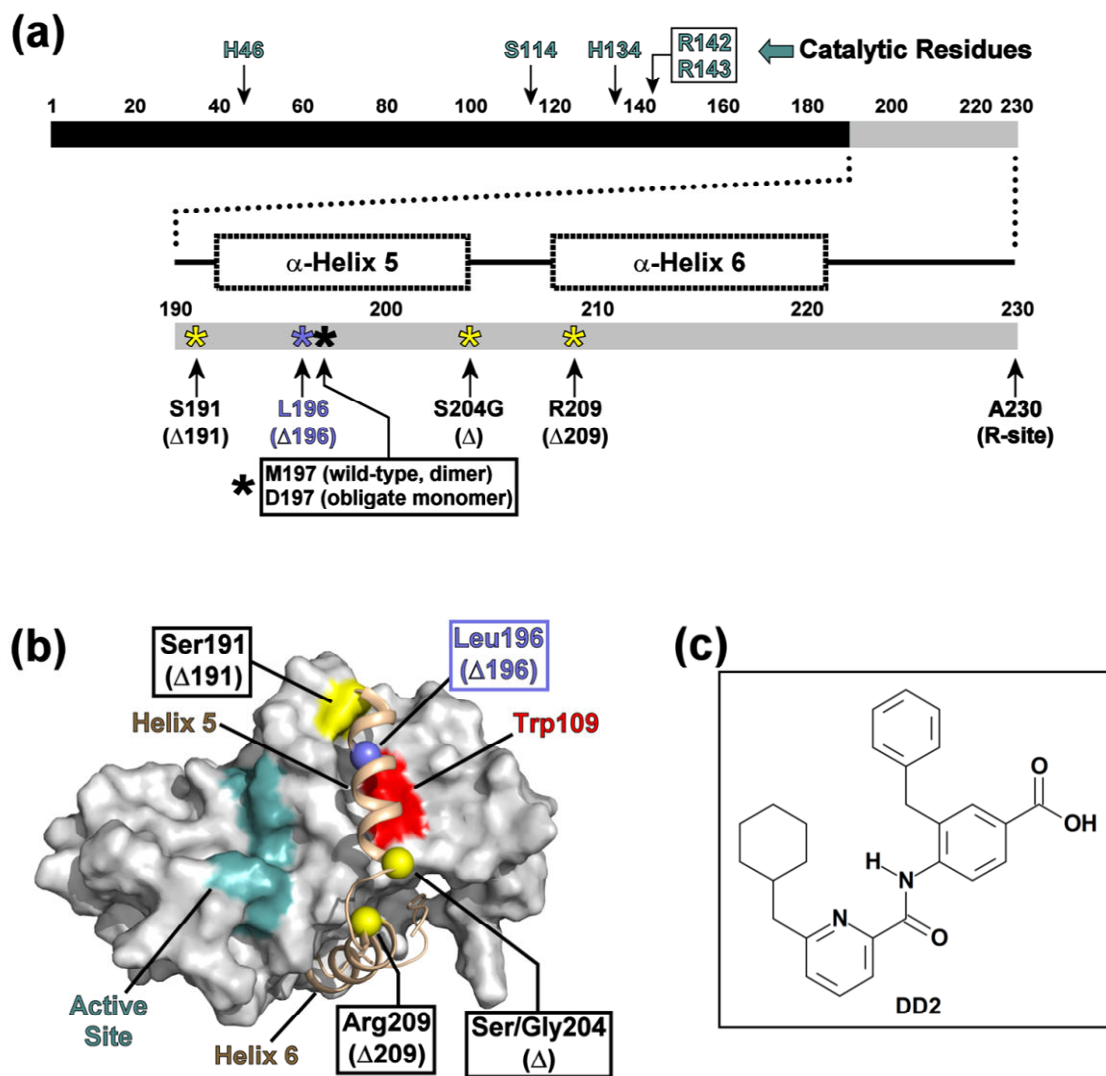


Figure 3-2

The ^{15}N - ^1H HSQC spectra of KSHV Pr truncations. (a) Size exclusion chromatograms of the KSHV Pr truncations ($\Delta 09$, blue; $\Delta 96$, red; $\Delta 91$ green) indicate that each elute as monomers. Wild-type KSHV Pr dimer (dashed black) and the obligate M197D monomer (solid black) are presented as references. The peaks eluting less than 150 mL indicate unidentified oligomeric species. Overlays of the ^{15}N - ^1H HSQC spectra of uniformly ^{15}N -labeled KSHV Pr M197D and $\Delta 09$ (b), $\Delta 96$ (c), and $\Delta 91$ (d) indicate no significant structural perturbations of the core protein backbone upon truncation of the conformationally dynamic C-terminal residues.

Figure 3-2

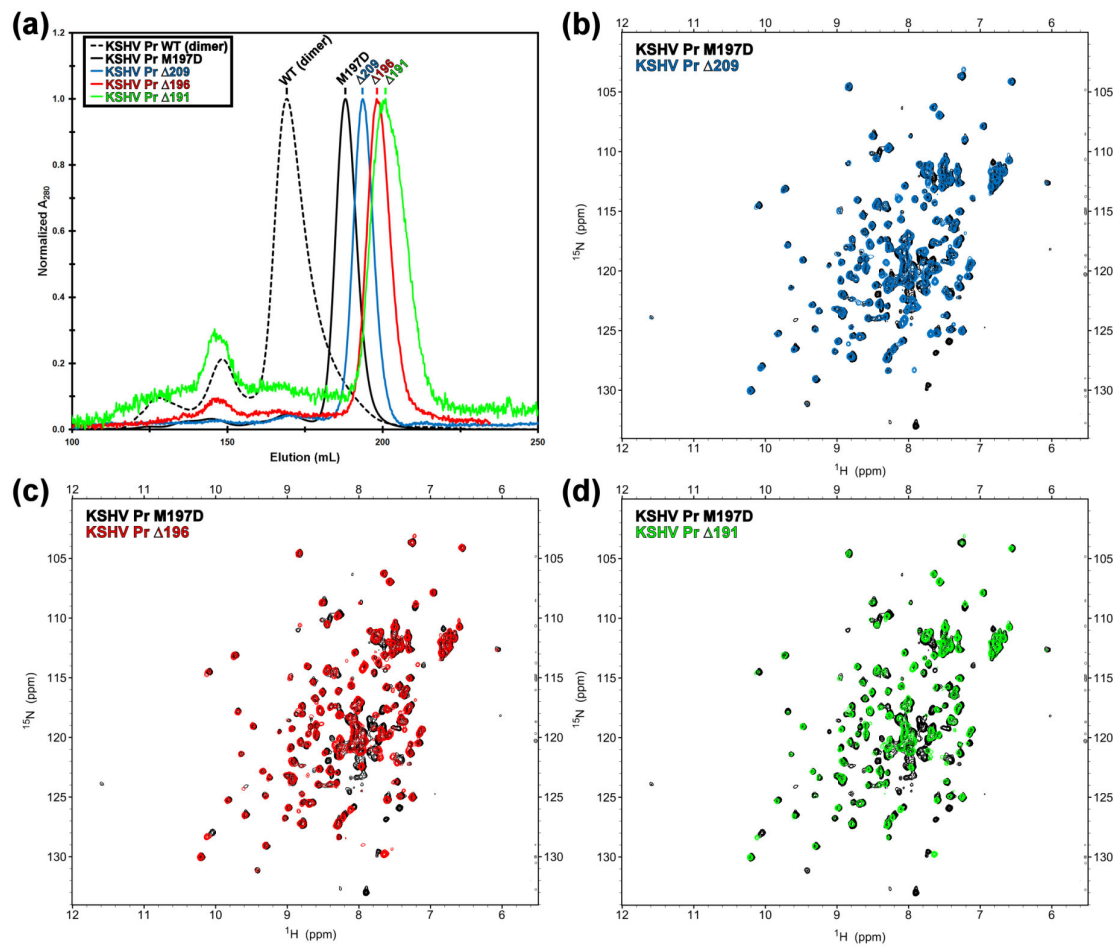


Figure 3-3

KSHV Pr-DD2 titration. (a) The distribution of isoleucine δ 1-methyl groups on a full length KSHV Pr monomer structure, based upon 2pbk. The view is a 90 degree rotation about the horizontal axis, relative to that in Figure 1b. Isoleucines separate into five zones with respect to distance from Trp109 as indicated by colored balls. The ^{13}C - ^1H HSQC titration spectra of the KSHV Pr M197D (b) and Δ 196 (c) constructs with DD2, focusing on the isoleucine δ 1-methyl region. The spectral overlays display apo (black) and > 5 molar equivalents DD2 (red). Ile44 (solid blue box), Ile105 (dotted blue box), and Ile71 (solid black box) are used as the binding probes. (d) The binding curves (M197D, solid black; Δ 196, dashed red) represent the average apparent K_d values calculated for the three Ile probes, and are summarized as a bar chart (e). HSQC titration spectra and binding curves for the M197D-I201V construct are displayed in Figure S4.

Figure 3-3

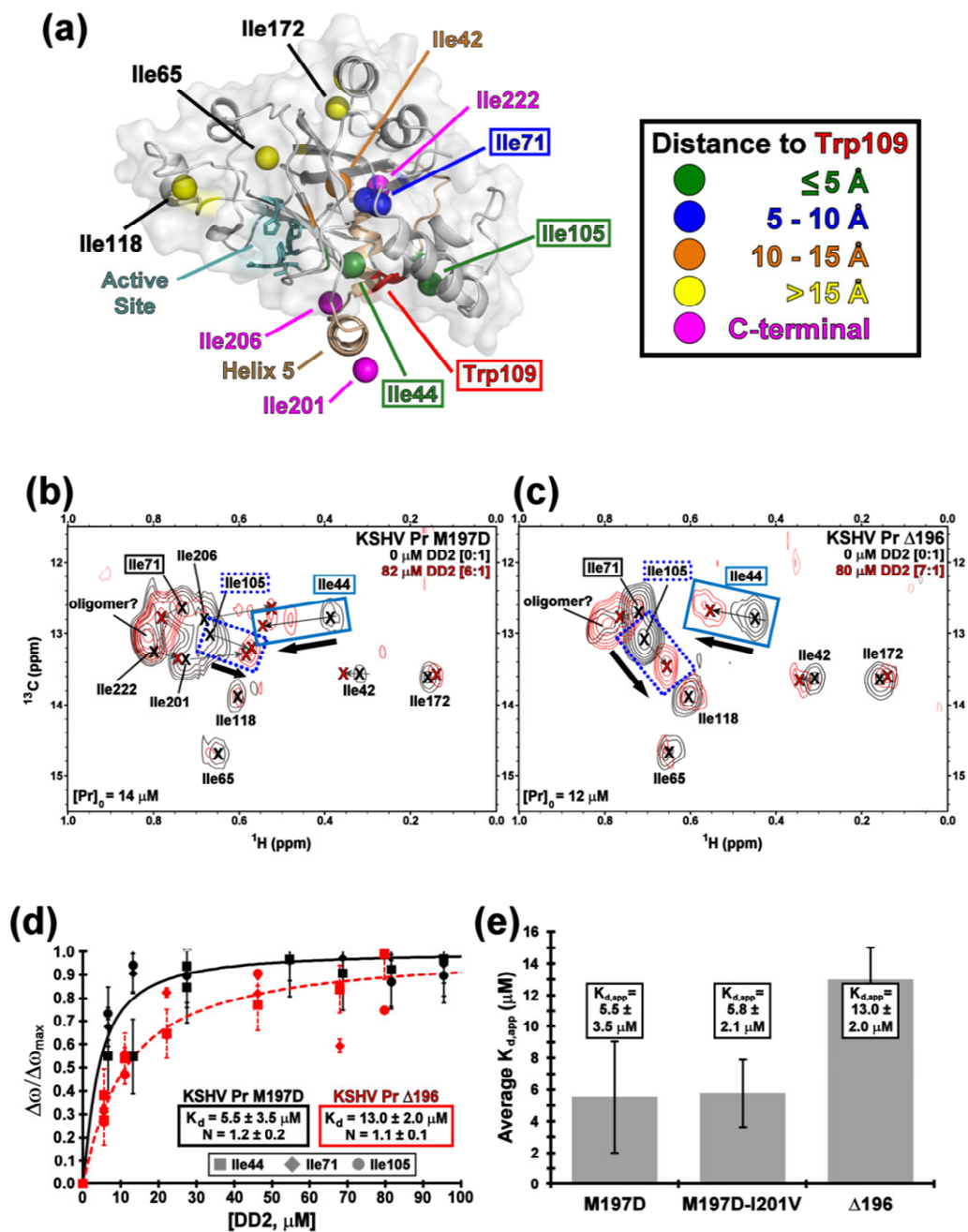


Figure 3-4

^{13}C - ^1H HSQC spectra of KSHV Pr truncations. The ^{13}C - ^1H HSQC spectra focusing on the isoleucine δ 1-methyl resonances of selective [^{13}C - ^1H methyl] ILV labeled KSHV Pr M197D (black) superimposed with those of Δ 209 (**a**, red) and Δ 196 (**b**, red). No significant spectral differences are observed between the Δ 196 and Δ 191 constructs (not shown). (**c**) Combined chemical shift perturbations between the full-length monomer and truncated KSHV Pr constructs > 0.01 ppm (dotted line) clearly identify the interfacial (Ile44 and Ile105) and C-terminal (Ile201, Ile206, and Ile222) residues. Asterisks indicate no isoleucine residue present in the selected truncation.

Figure 3-4

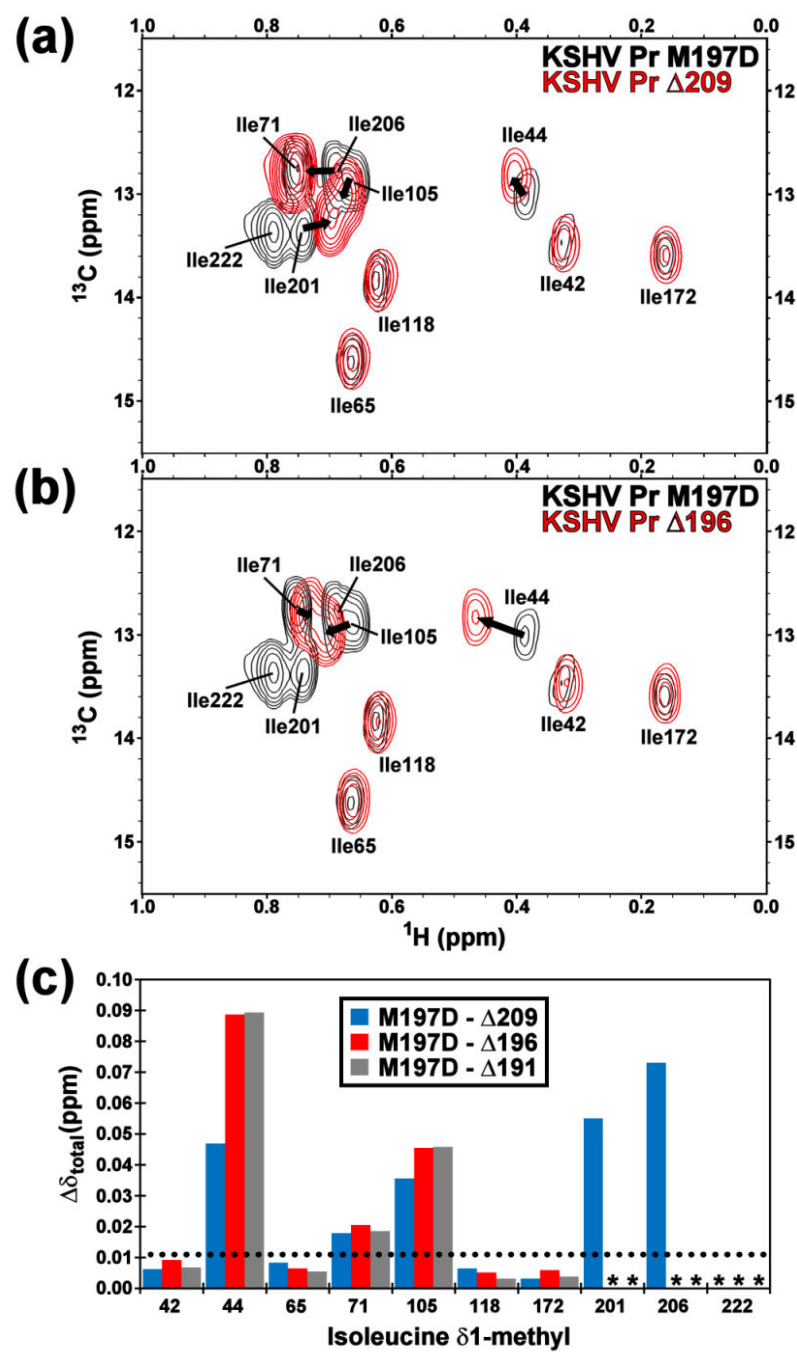


Figure 3-5

The ^{13}C - ^1H HSQC spectra of the Ile-to-Val mutants. Significant aggregation of the KSHV Pr obligate monomer at high protein concentrations precluded the acquisition of triple-resonance experiments typically used to assign resonances. Therefore, Ile-to-Val mutations were performed to assign the Ile $\delta 1$ -methyl groups. Overlays of the ^{13}C - ^1H HSQC spectra of these mutants (**a-h**, as indicated) suggest no significant structural perturbations relative to the “wild-type” constructs. Missing resonances (boxed) indicate the identity of the Ile-to-Val mutation. The Ile222 peak was identified by comparing the spectra of full-length KSHV Pr M197D and the $\Delta 209$ construct (**Fig. 3-4**). The Ile206 peak was identified through a process of elimination. The respective ^{15}N - ^1H HSQC spectra (not shown) display no significant resonance perturbations relative to the full-length KSHV Pr M197D construct.

Figure 3-5

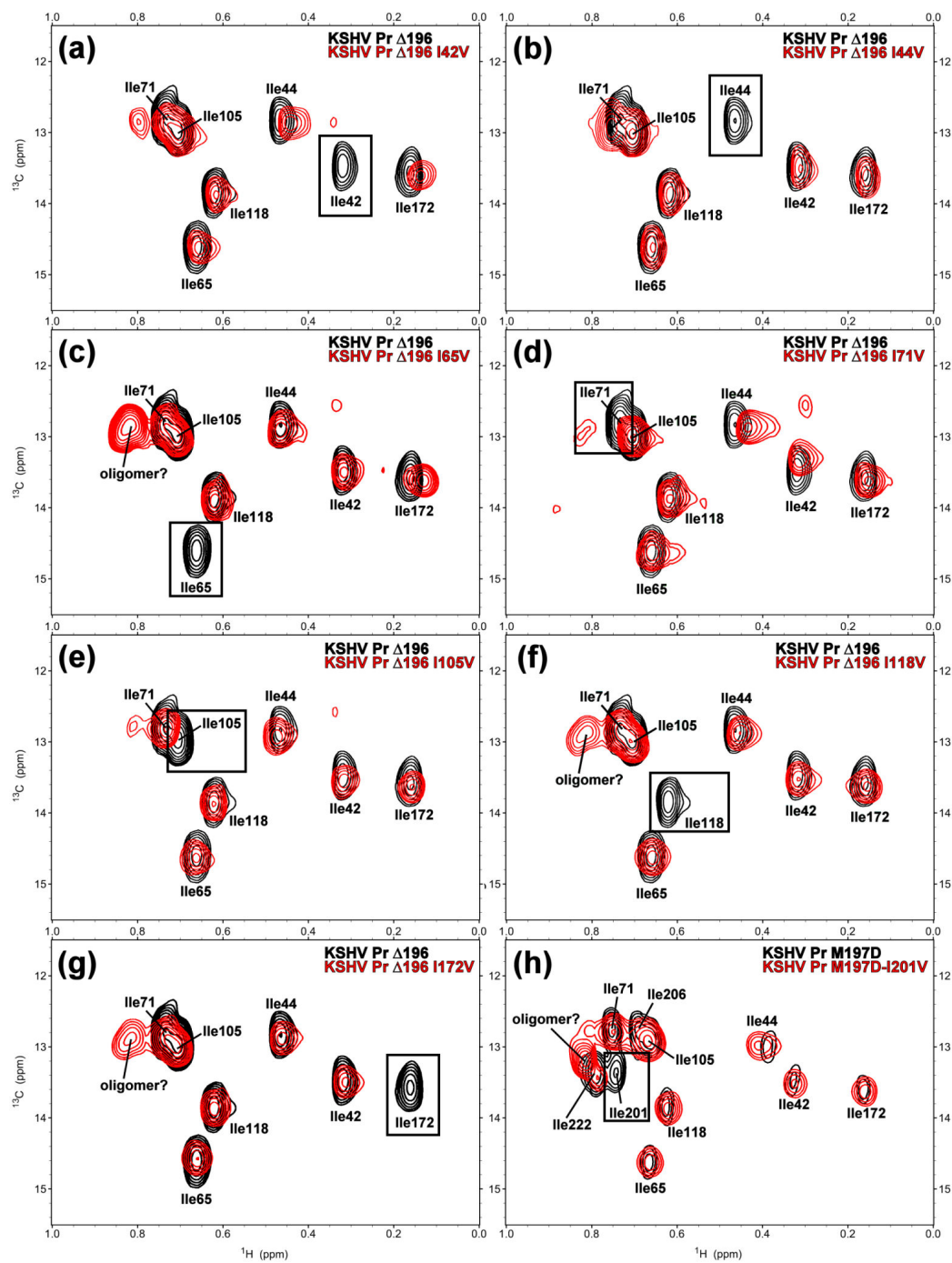


Figure 3-6

DD2 titration of KSHV Pr M197D-I201V. (a) The ^{13}C - ^1H HSQC titration spectra of the KSHV Pr M197D-I201V construct with DD2. The spectral overlays display apo (black) and > 5 molar equivalents DD2 (red), and are focused on the isoleucine $\delta 1$ -methyl region. Ile44 (solid blue box), Ile105 (dotted blue box), and Ile71 (solid black box) are used as the binding probes. (b) The binding curve represents the average of the Hill equation-derived apparent K_d values calculated for the three probes (symbols as indicated). Comparisons with the M197D and $\Delta 196$ constructs are illustrated in **Figure 3-3**.

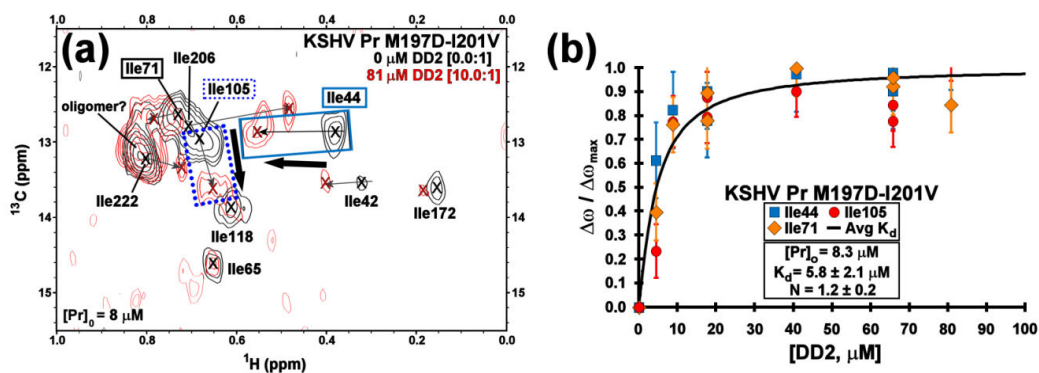


Figure 3-7

Structural comparison of the “apo” and DD2-inhibited KSHV Pr monomers. (a) The dimer structure of peptide-phosphonate inhibited KSHV Pr (2PBK). The catalytic residues (cyan) are located $\sim 15 - 20$ Å from the dimer interface. The interfacial helix 5 and the following helix 6 (monomer A, red; monomer B, green) are displayed. Helix 1 of monomer A (blue) and monomer B (orange) also form a portion of the dimer interface and are aligned in an anti-parallel orientation with respect to each other. (b) The structure of the KSHV Pr $\Delta 196$ -DD2 complex (3NJQ) crystallizes as an asymmetric dimer, with dimerization occurring on the opposite face with respect to 2PBK. DD2 molecules bind to the hydrophobic surface normally occupied by helix 5. Monomer A of the complex contains one DD2 molecule (pose 1, green carbons), while monomer B contains two DD2 molecules (pose 2, magenta carbons; pose 3, cyan carbons). The truncated C-terminal residues of the $\Delta 196$ constructs (red, monomer A; green, monomer B) are also indicated. Helix 1 of monomer A (blue) and monomer B (orange) are oriented end-on-end with respect to each other. Below each structure are cartoon representations of the monomeric units, with the wedges representing the active site, and stars the DD2 molecules.

Figure 3-7

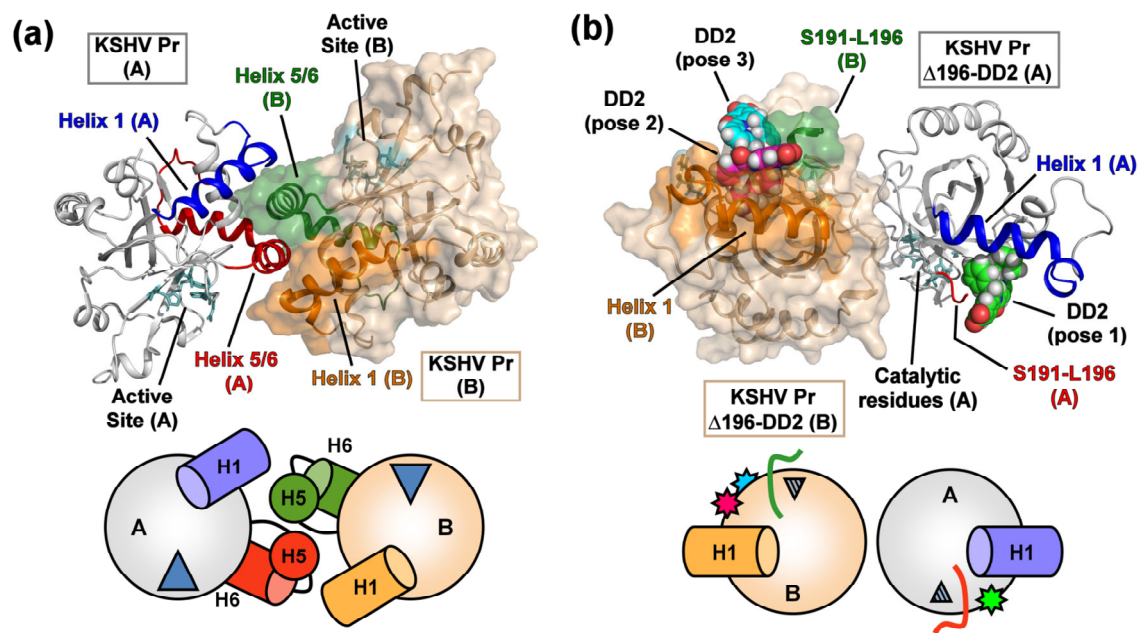


Figure 3-8

Comparison of the apo and DD2-bound KSHV Pr crystal structures. (a) The dimer interface of KSHV Pr (2PBK) consists of two helices from each monomeric unit (helix 5, tan, monomer A; light blue, monomer B), which stabilize the active site (cyan) via the C-terminal helix 6 and occlude the Trp109 (red). (b) The Met197 and Ile201 sidechains from helix 5 of monomer B (orange) form hydrophobic interactions with Trp109 of monomer A. Both $\Delta 196$ -DD2 monomer A (c) and monomer B (Fig. 3-10) exhibit independent DD2 binding pockets in which the Trp109 sidechain indole ring (red) adopts an “open” form (d).

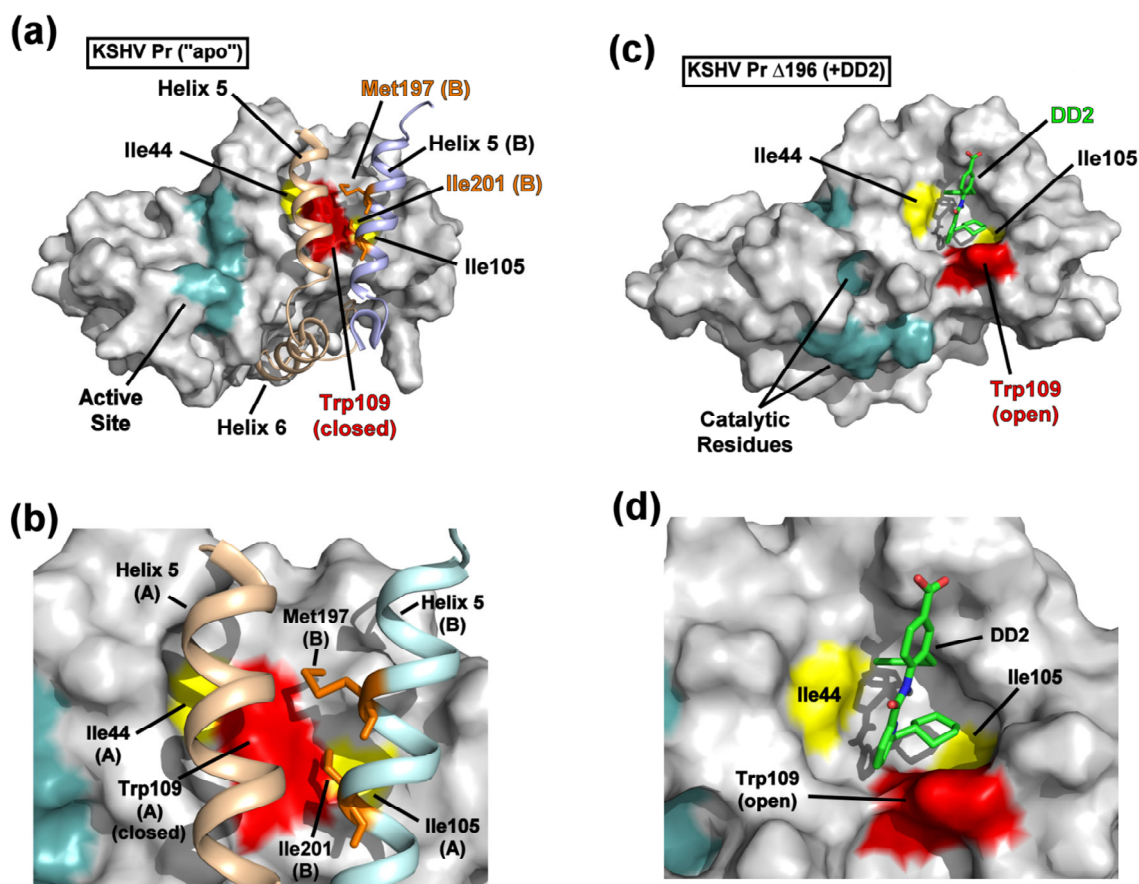
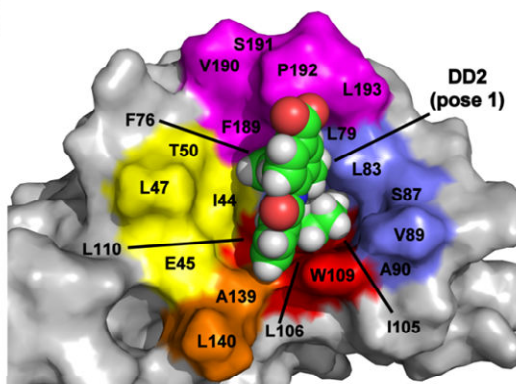


Figure 3-9

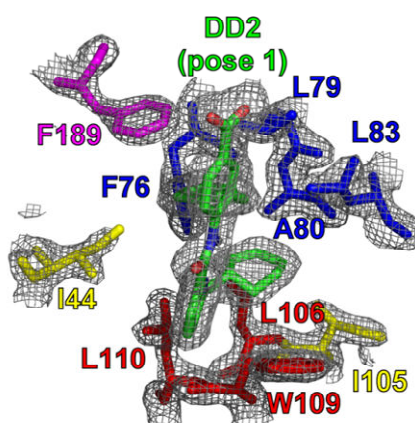
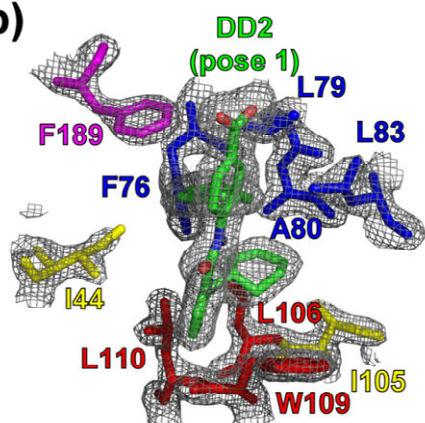
The DD2 binding pocket. (a) The hydrophobic DD2 binding pocket is composed of aliphatic residues from the β 2- β 3 loop (yellow), helix 1 and the α 1- α 2 loop (blue), helix 2 (red), the β 6- β 7 loop (orange), and the C-terminus (magenta). DD2 (green carbons) is shown as a space-filling model. (b) Stereoview of DD2 (green) within the Δ 196 binding pocket of monomer A, in relation to the “hot spot” Trp109 (red) and the Ile44 and Ile105 reporter groups (yellow). Also displayed are buried aliphatic residues of helix 1 (blue), helix 2 (red), and the C-terminus (magenta) that compose the binding pocket. The mesh represents the $2F_o - F_c$ 1σ electron density map. (c) **Figure 3-5b** with the protein backbone ribbons displayed. Comparable views of monomer B are displayed in **Figure 3-10**.

Figure 3-9

(a)



(b)



(c)

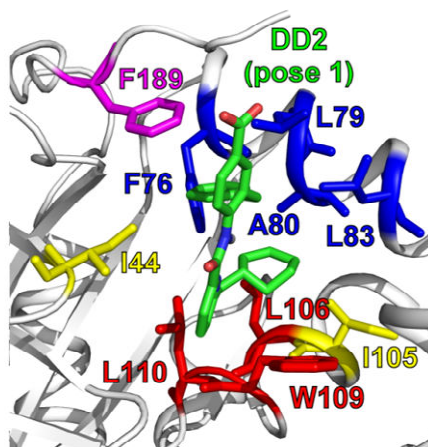
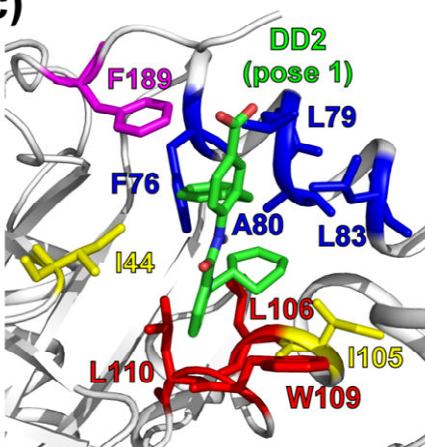


Figure 3-10

The alternate conformation of the KSHV Pr Δ 196-DD2 complex. (a) Monomer B of the KSHV Pr Δ 196-DD2 complex contains two DD2 molecules (pose 2, green carbons; pose 3, cyan carbons). Pose 3 is located outside the binding pocket and may act as a “bridging” molecule between crystallographic unit cells. (b) The hydrophobic DD2 binding pocket is composed of aliphatic residues from the β 2- β 3 loop (yellow), helix 1 and the α 1- α 2 loop (blue), helix 2 (red), the β 6- β 7 loop (orange), and the C-terminus (magenta). Pose 2 (green carbons) and pose 3 (cyan carbons) of DD2 are shown as space filling models. (c) Stereoview of DD2 poses 2 (green) and 3 (cyan) within the Δ 196 binding pocket of monomer B, in relation to the “hot spot” Trp109 (red) and the Ile44 and Ile105 reporter groups (yellow). Also displayed are the buried aliphatic residues of helix 1 (blue), helix 2 (red), and the C-terminus (magenta) that compose the binding pocket. The mesh represents the $2F_o - F_c$ 1σ electron density map. (d) **Figure 3-10c** with the protein backbone ribbons displayed. These figures are comparable to **Figures 3-8** and **3-9**.

Figure 3-10

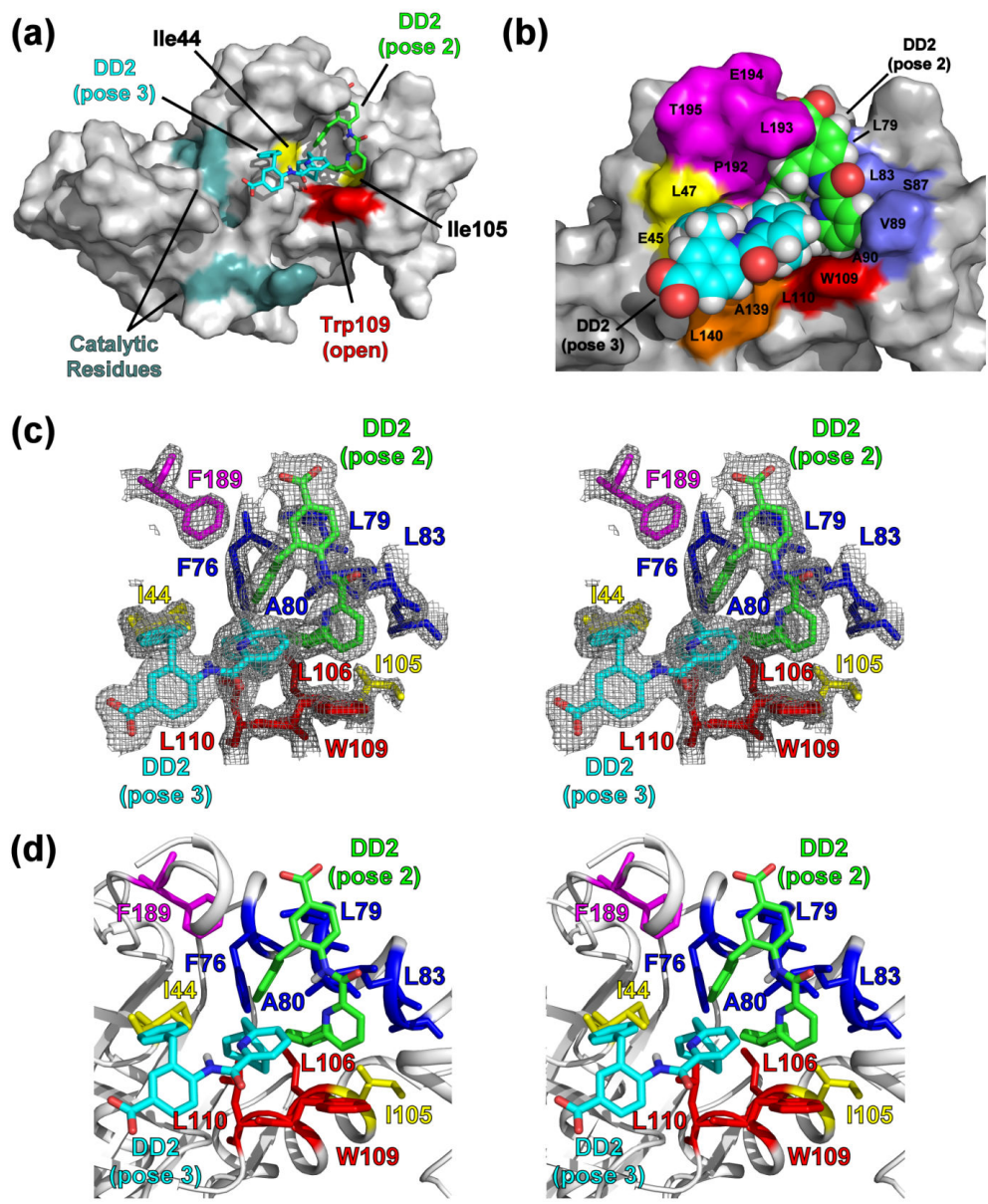


Figure 3-11

The poses of KSHV Pr-bound DD2. (a) A stereoview of the superimposed DD2 crystal structures (pose 1, green carbons; pose 2, magenta carbons; pose 3, cyan carbons) exhibit distinct conformers. Shown are the $2F_o - F_c$ 1σ electron density stereo-images of the three poses of the DD2 bound to the $\Delta 196$ construct: pose 1 (**b**, green) in monomer A; pose 2 (**c**, magenta) and pose 3 (**d**, cyan) in monomer B. The structures of the $\Delta 196$ construct are omitted for clarity.

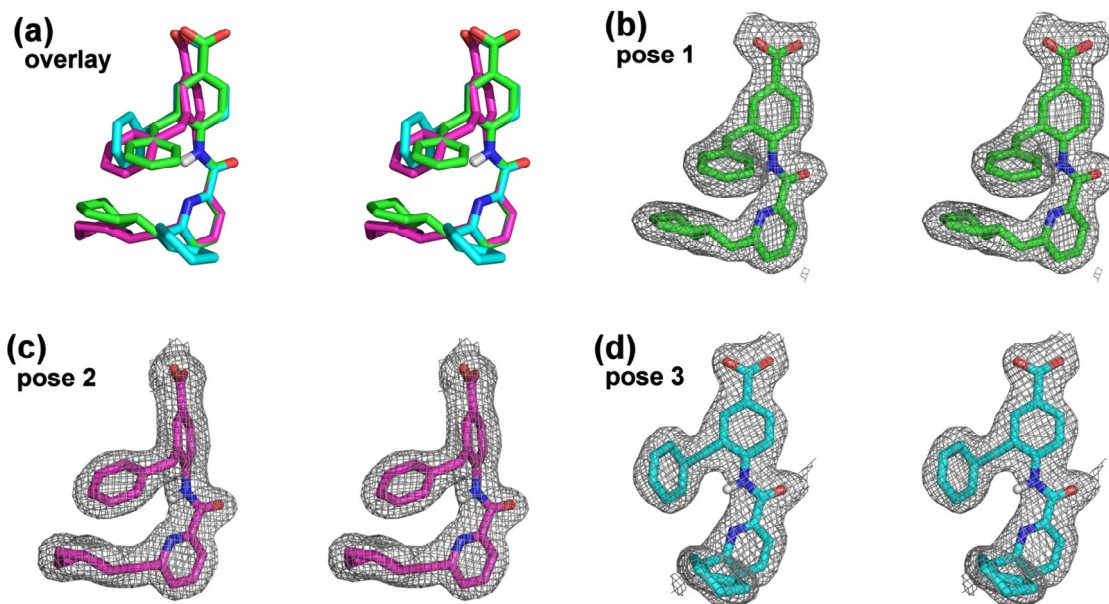


Figure 3-12

Structural perturbation of the KSHV Pr active site upon DD2 binding. (a-b) The active site of the 2PBK represents an “apo” state of KSHV Pr. The catalytic triad (H46, H134, and S114, cyan) and the conserved oxyanion hole-stabilizing arginine residues (R142 and R143, red) are displayed as sticks. Also highlighted are the positions of β -strand 1 and α -helix 0 (yellow), the β 1/ α 0 loop (dark green), and the β 6/ β 7 loop (orange). Residues 197-230 are omitted for clarity. (c-d) The conformation of the “apo” state active site residues displays clear differences relative to the Δ 196-DD2 complex (3NJQ). The Arg142 and Arg143 sidechains (red) adopt a “closed” conformation in the apo state, but an “open” conformation while in complex with DD2. In the DD2-bound state, the β 1/ α 0 loop (dark green) occludes the catalytic triad (cyan) and disrupts the substrate binding pocket.

Figure 3-12

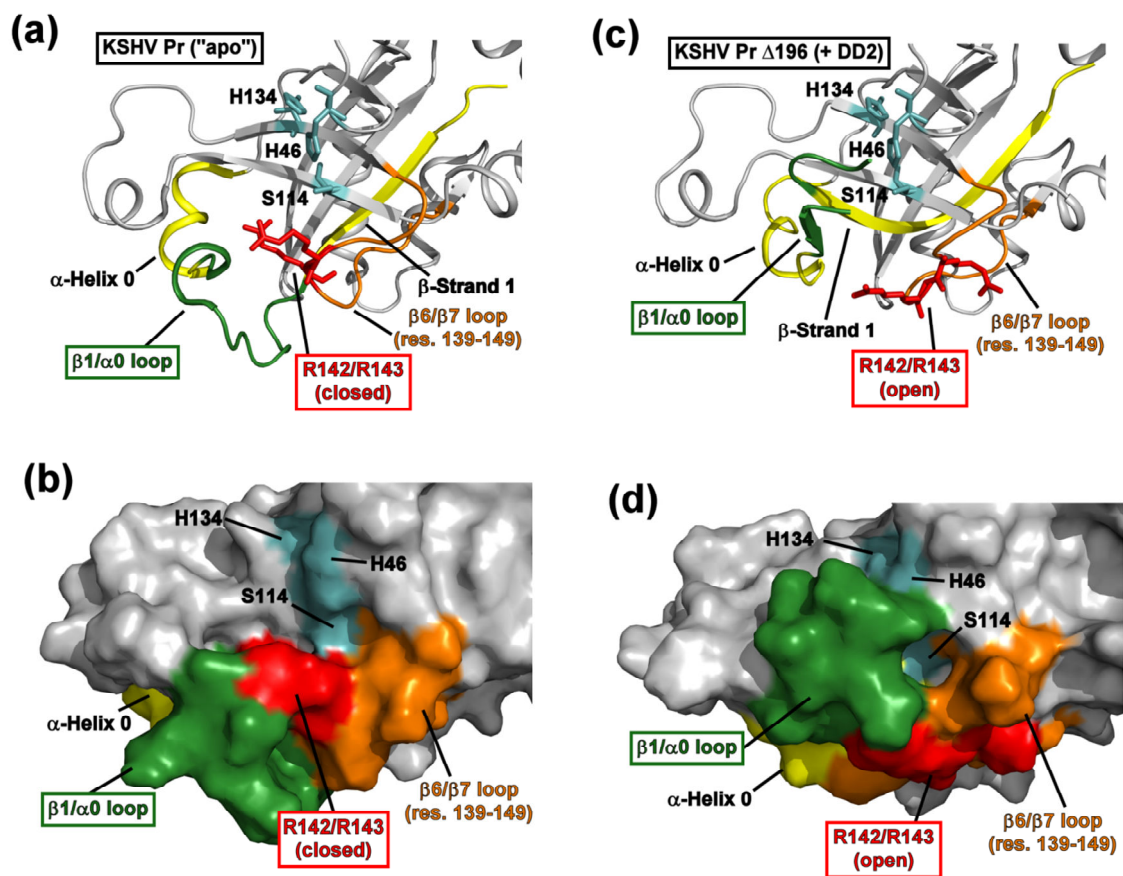


Figure 3-13

CD spectra of DD2 titrations with KSHV Pr and HCMV Pr. The circular dichroism spectra of $\sim 3 \mu\text{M}$ (a) KSHV Pr and (b) HCMV Pr in the presence of $0 \mu\text{M}$ (black), $30 \mu\text{M}$ (red), and $80 \mu\text{M}$ (blue) DD2. Estimated fractional helicity (f_H) values derived from the mean residue ellipticity of the 222 nm band are listed in the insets, and indicate loss of helical content with increasing molar equivalents of DD2. Loss of helicity is a strong indication of HHV protease dimer disruption.

Figure 3-13

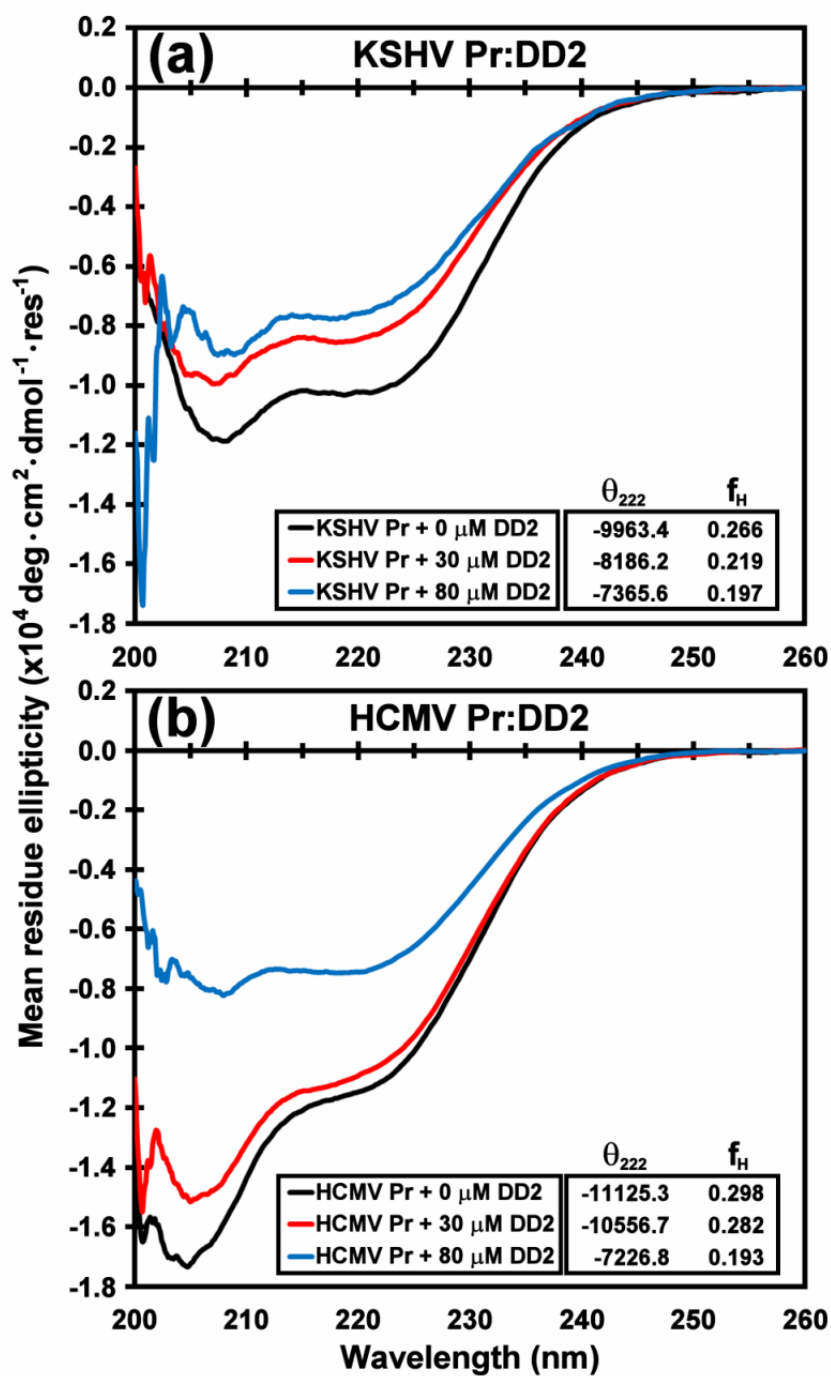


Figure 3-14

HCMV Pr-DD2 titration data. (a) The three isoleucine $\delta 1$ -methyl groups in human CMV Pr are localized at the dimer interface, and color-coded with respect to distance to Tyr128, as indicated. Helix 5 (tan), the active site (cyan), and Tyr128 (red) are also displayed. Tyr128 is homologous to Trp109 of KSHV Pr. The ^{13}C - ^1H HSQC spectra of selective [^{13}C - ^1H methyl] isoleucine labeled CMV Pr L222D obligate monomer (b), and $\Delta 221$ truncation (c) in the presence of 0 (black) and 16 molar equivalents DD2 (red) indicates DD2 binds at the dimer interface. Both Ile61 and Ile96 are putatively assigned; Ile231 was assigned by the loss of the resonance in the $\Delta 221$ truncation.

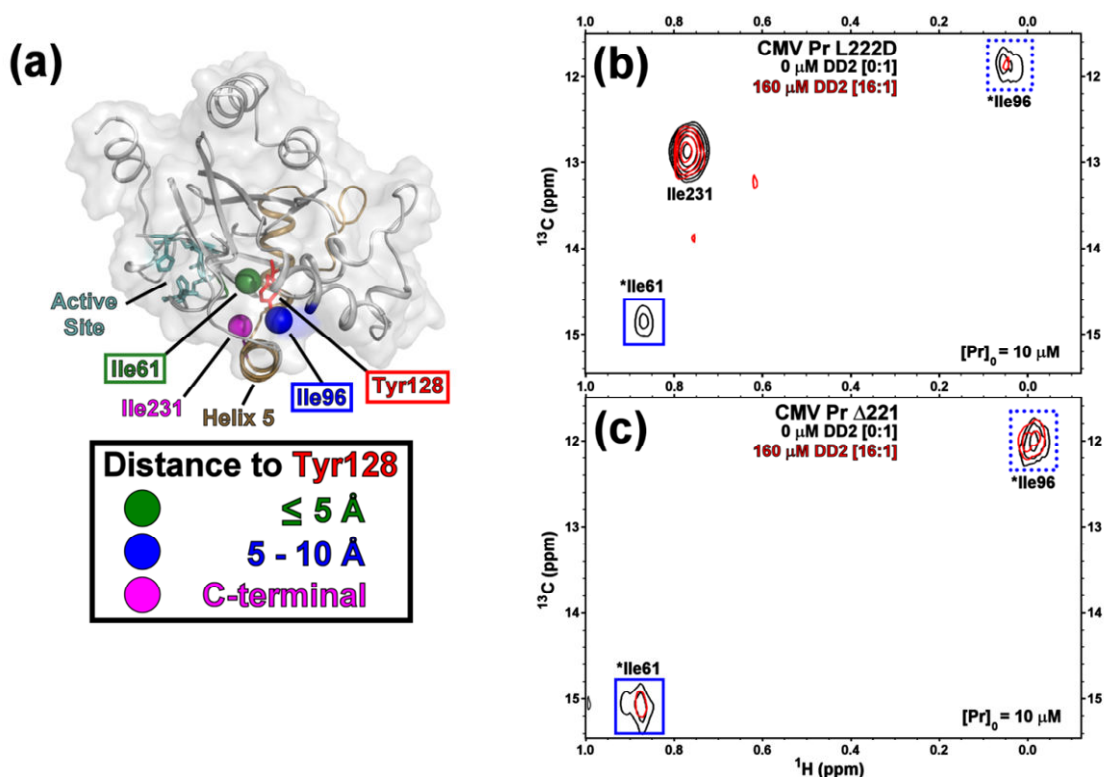
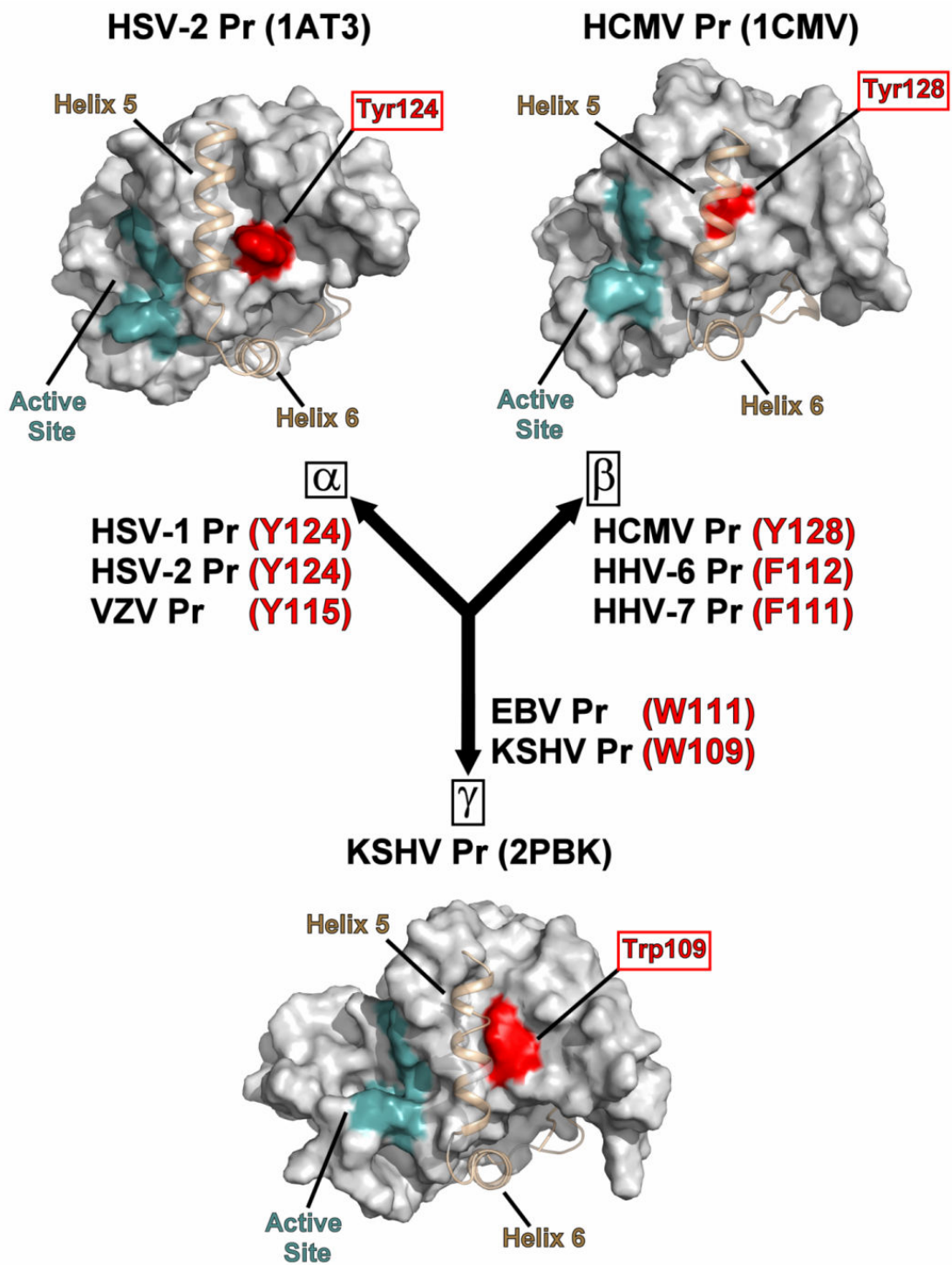


Figure 3-15

Structural homology of the HHV protease “hot spots”. Representative X-ray crystallographic structures of the three structurally homologous HHV protease subfamilies (HSV-2 Pr, 1AT3; HCMV Pr, 1CMV; KSHV Pr, 2PBK), with the active site (cyan) and interfacial helix 5 and following helix 6 (tan) as indicated. “Hot spot” aromatic residues (red) are located at the center of the hydrophobic dimer interface and are potential target sites for small-molecule inhibitors that disrupt protein-protein interactions. α -subfamily HHV proteases: **HSV-1** = herpes simplex virus-1/; **HSV-2** = herpes simplex virus-2; **VZV** = Varicella Zoster virus. β -subfamily HHV proteases: **HCMV** = human cytomegalovirus; **HHV-6** = human herpesvirus-6; **HHV-7** = human herpesvirus-7. γ -subfamily HHV proteases: **KSHV** = Kaposi’s sarcoma-associated herpesvirus; **EBV** = Epstein-Barr virus.

Figure 3-15



CHAPTER 4: A Screening Strategy for Trapping the Inactive Conformer of a Dimeric Enzyme with a Small Molecule Inhibitor

Tina Shahian¹, David Smithson³, R. Kiplin Guy³, Charles S. Craik²

¹Graduate Group in Biochemistry and Molecular Biology, University of California, San Francisco, 600 16th St., Genentech Hall, San Francisco, CA 94143, USA

²Department of Pharmaceutical Chemistry, University of California, San Francisco, 600 16th St., Genentech Hall, San Francisco, CA 94143, USA

³ Department of Chemical Biology and Therapeutics, St. Jude Children's Research Hospital, 262 Danny Thomas Place, Memphis, TN 38105, USA

Portions of this chapter will be published in a volume of Methods in Molecular Biology entitled "Rational Drug Design".

ABSTRACT

Kaposi's sarcoma-associated herpesvirus (KSHV) is the etiological agent of Kaposi's sarcoma (KS), the most common cancer in AIDS patients. All herpesviruses express a conserved dimeric serine protease that is required for generating infectious virions, and is therefore of pharmaceutical interest. Given the past challenges of developing drug-like active-site inhibitors to this class of proteases, small-molecules targeting allosteric sites are of great value. In light of evidence supporting a strong structural linkage between the dimer interface and the protease active-site, we have focused our efforts on the dimer interface for identifying dimer disrupting inhibitors. Here, we describe the high throughput screening component of a methodology for identifying small molecule dimerization inhibitors of KSHV protease. This methodology can be applicable to other systems where a protein/protein interaction is linked to the activity of interest, and *in vitro* assays to monitor function are in place.

BACKGROUND

Herpesviruses make up one of the most prevalent viral families including eight human types that cause a variety of devastating illnesses. The standard course of treatment for common herpesviral infections is a class of broad-acting viral DNA replication inhibitors, which exhibit undesirable toxicity, poor oral bioavailability, and in some cases inadequate efficacy. Efforts by pharmaceutical companies to target the active-site of the essential dimeric serine protease of human herpesviruses (HHV) have yet to yield a drug-like candidate.¹⁻⁶ Given the evidence supporting a conformational linkage between protease dimerization and activation, we have focused our efforts on identifying molecules that target the dimer interface.⁷⁻¹² In the case of KSHV protease (KSHV Pr) the dimer interface covers approximately 2500 Å², and includes the α -helix 5 of each monomer as the major constituent (**Fig. 4-1**).¹³ *In vitro* studies with KSHV Pr and other HHV proteases have shown the dimer interface to be very sensitive to genetic perturbation, where single point mutations often lead to a loss of dimerization and activity¹¹. Furthermore the dimerization affinity is weak; with a reported K_D of 1.7 μ M for KSHV Pr¹⁰. These characteristics define the dimer interface as a suitable candidate for dimerization inhibitors. We first tested this approach by inserting the key interfacial α -helix 5 residues on the internally-stabilized α -helix of a small protein.¹⁴ The resulting macromolecule disrupted the KSHV Pr dimer and inhibited enzyme activity, proving that targeting the dimer interface is a viable route for identifying novel inhibitors. In order to identify small molecule dimer disruptors of KSHV Pr, a workflow was developed that begins with high throughput screening (focus of this chapter), and continues with experiments that assess dimerization, mode of binding, and broad specificity against other HHV proteases (*See chapters 1 & 2, Fig. 4-2*).^{15,16} A high throughput screening (HTS) fluorogenic activity assay

was initially developed to be performed in a 96-well plate format. The substrate used is an optimized hexa-peptide attached to 7-amino-4-carbamoylmethyl coumarin (ACC), where cleavage at the scissile bond releases the ACC group resulting in increased fluorescence.^{7,12} We successfully used this assay to identify the small molecule inhibitor DD2 (**Fig. 4-3**), which binds a novel allosteric pocket at the dimer interface of KSHV Pr, and traps it in an inactive monomeric state.¹⁶ The identification and characterization of inhibitor DD2 are described in Chapters 1 and 2. The HTS assay was then adapted to a 384-well format for a research collaboration with Dr. R. Kiplin Guy at the HTS Core Facility at St. Jude Children's Research Hospital (SJCRH) in Memphis, TN. The results section of this chapter provides a summary of our screening efforts in the Guy laboratory. The detailed steps for performing the original HTS assay in a 96-well format are included in the Materials and Methods section.

RESULTS

HTS assay adaptation to 384-well format

In order to screen the small-molecule libraries available at the HTS Core Facility at SJCRH our existing 96-well fluorogenic activity assay was adapted to a 384 well format. The reaction volume was reduced from 100 μ l to 25 μ l. The volumes of the protease, control compounds, and substrate were 19 μ l, 1 μ l, and 5 μ l. The final concentrations of all components were kept as described in the Materials and Methods section. The allosteric inhibitor DD2 (described in Chapters 1 and 2) at a final concentration of 30 μ M was used as the positive control, and DMSO was used as the negative control. The endpoint fluorescence value obtained with the DMSO treated reaction is referred to as the “high signal control, and that obtained with the DD2 treated reaction is referred to as the “low signal” control. First we optimized our assay conditions in order to maximize the Z' -factor, which is a measure of assay quality (*see Note 1*). High and Low signal control assays were ran in parallel on a 384-well plate, with at least one entire column allocated to each. In each round, factors such as temperature and reaction time were varied. In this manner our Z' -factor was improved from an initial value of ~ 0.3 to over 0.8. The screening conditions that yielded the highest Z' -factor are included in the materials and methods. Next a plate uniformity test was carried out to ensure experimental measurements are not affected solely by their position on the assay plate. Uniformity issues can arise when, for example, the temperature inside the plate reader is not uniformly distributed. For this experiment 0 μ M, 10 μ M, and 30 μ M DD2 were used to obtain final assay readouts of High (H), Medium (M), and Low (L) fluorescence signals, respectively. On separate 384-well plates, H/M/L, M/L/H, and L/H/M experiments were set up, one condition per column, repeating across the plate (*for an example of setup in 96-well*

plate see Fig. 4-4). This process was repeated on three separate days, totaling nine plates. The raw data was transferred onto an excel spreadsheet template provided by SJCRH. According to the data, no signal drift is observed when comparing the final fluorescent readouts across the rows or columns. In addition the Z'-factors are consistently above 0.9 (**Fig. 4-5**).

Setup at the HTS Core Facility, SJCRH

The Bioactive library we screened comprised of roughly 3500 small molecules with some previously reported biological/pharmacological activity. At the HTS Core Facility, all the screening steps took place on a temperature-controlled deck, where plates were moved between stations by a robotic arm. In total 11 plates and 3520 compounds were screened. Minor adjustments were made to the protocol to accommodate the low-volume Pin tool liquid handler. The protease and substrate were both dispensed using the Matrix WellMate (Thermo Scientific) in volumes of 20 μ l and 5 μ l respectively. A low-volume Pin-tool delivered the control and test compounds, in volumes of 75 nl and 25nl respectively. In total 11 plates and 3520 compounds were screened.

Summary of screening results

Screening data analysis was performed with the help of David Smithson, a graduate student in the Guy laboratory. The 4224 raw data points on all 11 plates are shown on a scatter plot (**Fig. 4-6**). The green and red circles correspond to the positive and negative controls, respectively. As expected the majority of library compounds were inactive, shown as black circles, and overlap with the negative DMSO control. Compounds that showed inhibitory activity are indicated in blue. From a total of 3520 compounds screened, 3444 were inactive

and 76 were active, which translates to a hit rate of 2.2%. A hit was defined as compounds that yielded an endpoint fluorescent value below the lower limit (3rd standard deviation) of the high signal control. The Z' and Z factors remained around 0.5 for all eleven plates, which was determined to be sufficient for identifying true hits (**Fig. 4-7**).

Initial hit characterization of hit hexachlorophene

The screening hits were cherry-picked from the parent stock plates by a robot and used for further analysis. A 3-fold dilution series of each compound was prepared and the screening assay was repeated to assess the concentration dependence of inhibition. Only two compounds showed concentration dependence based on their IC₅₀ plots. The best hit was hexachlorophene (also known as Nabac, **Fig. 4-8**), which was originally used as a topical antiseptic before being withdrawn by the FDA in 1973 due to evidence of carcinogenicity. Hexachlorophene exhibited a sigmoidal dose-response curve with a calculated IC₅₀ of 3 μM (**Fig. 4-8**). The atypical IC₅₀ curves of four other hits are displayed on the same plot as a comparison. In order to ensure hexachlorophene does not absorb light at the emission wavelength of the KSHV Pr substrate, a full absorbance spectrum was obtained. No absorbance is observed in the emission regions of ACC, at 480 nm (**Fig. 4-8**).

Initial hit characterization of hit cholanolic acid

The second screening hit was cholanolic acid (**Fig. 4-9**), which is a Cholesterol derivative and a natural mammalian detergent involved in fat metabolism. Cholanolic acid had an IC₅₀ of 4 μM and showed no absorbance between 300-800 nm. However, under the assay conditions

used, its inhibitory activity peaked at 60%, possibly due to poor solubility. For this reason, we chose to follow through with hexachlorophene.

Hexachlorophene shows evidence of non-specific aggregation

In order to avoid false-positive hits due to non-specific aggregation mechanisms, including a small amount of non-ionic detergent in screening assays is recommended. However KSHV Pr does not tolerate detergents and even trace amounts inhibit activity. Therefore, we substituted an unrelated serine protease Granzyme B, which unlike KSHV Pr, tolerates detergents in assays for biochemical activity. In a spectrophotometric activity assay monitoring Granzyme B activity hexachlorophene inhibited Granzyme B, and its inhibitory effect was diminished with increasing detergent, Triton X-100 (**Fig. 4-10**). Hexachlorophene also showed evidence of particle formation when analyzed by dynamic light scattering. Collectively, this data suggests that hexachlorophene acts by a non-specific mechanism, and was therefore not a suitable inhibitor for further study.

DISCUSSION

HHV proteases, including KSHV Pr, offer an attractive drug target for the treatment of herpesviral diseases. However, this class of proteases is considered undruggable due the shallow nature of their active-sites. We have developed a methodology to identify and characterize small molecule inhibitors that target the critical dimer interface of KSHV Pr. This process begins with HTS, which was optimized and validated in this chapter. In collaboration with the HTS Core Facility at SJCRH, we screened a ~3000-member Bioactives library of small molecules. The KHSV Pr assay performed well under HTS setting and we obtained two hits, hexachlorophene and cholanic acid. In follow up experiments neither compound was an ideal candidate, either due to non-specific aggregation properties or insufficient activity.

Additional screening efforts are needed to identify inhibitors with desirable characteristics. We identified 13 structural analogues of hexachlorophene that were commercially available. Only one analogue, bithionol, demonstrated inhibition, but later it was found to act via non-specific mechanisms as well (data not shown).

Even though we did not identify promising inhibitors during our first round of screening, we were successful in validating our assay for future HTS efforts. The previous studies that characterized the KSHV Pr dimer disruptor DD2, combined with this validated HTS assay lay the groundwork for identifying novel inhibitors that target KHSV Pr, and potentially other members of the HHV protease family.

MATERIALS AND METHODS

Consumables and equipment

1. dimethyl sulfoxide (DMSO), 2-mercaptoethanol, and ethylenediaminetetraacetic acid (EDTA).
2. Round-bottom polypropylene 96-well assay plate, and plate sealing tape.
3. A 25 ml reagent reservoir, multichannel pipets (12-channel), and disposable tips for 10 and 200 μ l volumes.
4. Fluorescence microplate reader, table-top centrifuge with microplate rotors, and a small incubator.

Buffer stocks

1. Prepare all aqueous solutions in MilliQ water followed by gentle shaking or mixing to ensure all solids have dissolved and all components have thoroughly mixed. Filter all 1 L stocks into sterile 1 L bottles. Store all reagent stocks at room temperature.
2. Prepare a 10 ml stock of 0.5M EDTA by dissolving 2.9 g EDTA into 10 ml of water.
3. Prepare a 1 L stock of 1 M K_2HPO_4 by dissolving 141.9 g K_2HPO_4 into 1 L of water.
4. Prepare a 1 L stock of 1 M KH_2PO_4 by dissolving 136.09 g KH_2PO_4 into 1 L of water.
5. Prepare 1 L stock of 3 M KCl by dissolving 223.6 g KCl into 1 L of water.

Assay buffer

1. The assay buffer consists of 25 mM potassium phosphate pH 8, 150 mM KCl, 0.1 mM EDTA, and 1 mM 2-mercaptoethanol.
2. Prepare a 100 ml stock of assay buffer by mixing 2.4 ml of 1 M K₂HPO₄, 0.15 ml of 1 M KH₂PO₄, 5 ml of 3 M KCl, 20 µl of 0.5 M EDTA, and 92.48 ml water. Adjust pH to 8.0 using HCl and NaOH. Before use add 7 µl of 2-mercaptoethanol.

Protease expression and purification

Recombinant KSHV Pr is expressed in *Escherichia coli* and purified as reported previously.¹⁶ 80 µM aliquots of purified protease are flash frozen in storage buffer (same as assay buffer described in section 3.2) and stored at -20 °C. The total amount of protein required will vary depending on the assay and the number of plates being screened.

Protease substrate synthesis and purification

The protease substrate is an optimized hexa-peptide with the fluorogenic reporter group 7-amino-4-carbamoyl-methylcoumarin (ACC), which allows for monitoring enzyme activity spectroscopically. The peptide sequence is Ac-Pro-Val-Tyr-tBug-Gln-Ala-ACC with an observed K_M of 8.5 ± 0.8 µM for KSHV Pr. Substrate is synthesized using standard Fmoc chemistry and purified as reported previously.^{7,12} Substrate stocks of 10 mM in 100% DMSO are stored at -20 °C. The total amount of substrate required will vary depending on the assay and the number of plates being screened. (Ac = acetyl group, tBug = t-butyl glycine).

Test compounds

Compound libraries are generally provided in ready-to-use format, dissolved in 100% DMSO and plated in either 96-well or 384-well plates. An additional dilution step with 100% DMSO or plate reformatting may be necessary depending on the screening assay conditions. In order to avoid screening artifacts resulting from compound aggregation or precipitation, a final screening concentration between 10-30 μ M is recommended. Our compound library was in a ready-to-use format at a concentration of 1mM in a 96-well plate. Compound libraries are stored at -20 °C.

Control compound

Positive and negative controls are an important measure of assay performance and should ideally be included in every row (or column) of the assay plate. In assays, where timing is of particular importance, such as a protease assay, these controls allow for accurate calculation of % inhibition in each row (or column), as well as comparison of data across all rows (or columns). DMSO serves as the negative control and is used in the place of test compound. An ideal positive control may be a known active compound, such as a protease inhibitor in our case. Previously characterized small molecule KSHV Pr inhibitor DD2 serves as the positive control in our screen. The total amount of control compound required will vary depending on the assay and the number of plates being screened.

Screening protocol in 96-well plate

Prior to performing a high-throughput screen, it is critical to evaluate the quality of the screening assay by calculating a Z' -factor (*see Note 1*). High-throughput screening is typically performed in small assay volumes, therefore small fluctuations in liquid handling

may affect the final readout. For this reason working with professionally calibrated pipettes is highly recommended. The following is a step-by-step protocol for manually performing a screen in one 96-well plate. The ability to screen multiple plates at once depends on the assay conditions and access to liquid handlers.

Summary of assay conditions

1. The protease assay is carried out in a final volume of 100 μl per well. It is composed of 98 μl of KSHV Pr in assay buffer, 1 μl of test compound or DMSO, and 1 μl of the protease substrate. These proportions ensure that the final concentration of protease is minimally changed upon substrate addition.
2. In order to account for volume loss due to pipeting, add an extra 20% to all calculated reagent volumes. For example, to calculate the total volume of protease substrate required for 40 wells use the equation: $[40 \text{ wells} + (0.2 \times 40 \text{ wells})] \times 1 \mu\text{l} = 9.5 \text{ ml}$.
3. KSHV Pr is used at a final concentration of 2 μM . We selected a concentration close to the reported *in vitro* K_D of 1.7 μM , in order to identify compounds that effectively compete with protease dimerization.
4. Test compounds are used at a final concentration of 10 μM . This concentration is typical for high throughput screening and helps avoid precipitation and aggregation.

5. Positive control compound DD2 is used at a final concentration of 30 μM . This concentration is ten fold over the DD2 IC₅₀ of inhibition for KSHV Pr at 1.7 μM .
6. Protease substrate is used at a final concentration of 100 μM , which is roughly 10 fold above its reported K_M of $8.5 \pm 0.8 \mu\text{M}$ for KSHV Pr. This concentration ensures that substrate binding is not the rate-limiting step in the screening assay.
7. Both the protease substrate and test compounds are dissolved in 100% DMSO. Therefore the final assay concentration of DMSO is 1% (v/v), which is well below the previously determined 5% DMSO tolerance of the assay (*see Note 2*).

Setup of 96-well plate

1. Column 1 is designated for the positive control. The components are 98 μl of assay buffer, 1 μl of DD2, and 1 μl of protease substrate (**Fig. 4-11**).
2. Column 2 is designated for the negative control. The components are 98 μl of protease in assay buffer, 1 μl of DMSO, and 1 μl of protease substrate.
3. Columns 3-12 are designated for the test compounds. The components are 98 μl of protease in assay buffer, 1 μl of test compound, and 1 μl of protease substrate.

Dispensing KSHV Pr to assay plate

1. Retrieve a frozen 80 μM vial of KSHV Pr from the freezer and thaw quickly by placing inside a 37 °C water bath. Once the protease is thawed, store the vial on ice.

2. Transfer 10.5 ml of assay buffer into clean 50-ml conical tube.
3. Add 275 μ l of KSHV Pr from the thawed stock and mix. Label this conical tube “KSHV Pr”.
4. Carefully pour the entire mixture into a clean reagent reservoir labeled “KSHV Pr”.
5. Retrieve a clean 96-well plate, label it “Assay Plate”, and place on work bench at room temperature.
6. Load a 200 μ l-volume multichannel pipette with eight clean tips, place inside “KSHV Pr” reservoir, and load 98 μ l. Inspect all eight channels by eye to make sure the pipette is functioning properly. If large air bubbles are trapped inside the tip, empty all channels back into the “KSHV Pr” reservoir and try again.
7. Dispense contents into column 3, and then repeat until all remaining columns 4-12 receive KSHV Pr.

Dispensing test compounds to assay plate

1. Retrieve compound library from the -20 °C freezer and thaw at room temperature. Do not remove the plate seal.

2. Spin down plate in a table-top centrifuge at $3000 \times g$ for 1 minute. After centrifugation remove the seal, label the plate “Compound Plate”, and place it on the work bench at room temperature.
3. Load a 10 μ l-volume multichannel pipette with eight clean tips, place inside column 1 of “Compound Plate”, and load 1 μ l.
4. Dispense contents into column 3 of “Assay Plate”, such that compounds from wells A1-H1 of “Compound Plate” are transferred to wells A3-H3 of the “Assay Plate”.
5. Repeat steps 3-4 to transfer from columns 2-10 of “Compound Plate” to the corresponding columns 4-12 on the “Assay Plate”.
6. Columns 11-12 of the “Compound Plate” may be screened in a separate 96-well assay plate.

Dispensing the negative control to assay plate

1. Load a 200 μ l-volume multichannel pipette with eight clean tips, place inside “KSHV Pr” reservoir, and load 98 μ l.
2. Dispense contents into column 2 of “Assay Plate”.
3. In a fresh reagent reservoir, labeled “DMSO”, add 20 ml of DMSO.

4. Load a 10 μ l-volume multichannel pipette with eight clean tips, place inside the “DMSO” reservoir and load 1 μ l.
5. Dispense contents into column 2 of “Assay Plate”.

Dispensing the positive control to assay plate

1. Add 20 ml of assay buffer into a clean reagent reservoir labeled “Assay Buffer”.
 2. Load a 200 μ l-volume multichannel pipette with eight clean tips, place inside the “Assay Buffer” reagent reservoir, and load 98 μ l.
 3. Dispense contents into column 1 of “Assay Plate”.
-
1. 4- Retrieve 3 mM stock of DD2 from -20 °C freezer and thaw at room temperature.
 2. 5- In a fresh 96-well plate, labeled “DD2 Plate”, aliquot 5 μ l of DD2 into each well of column 1.
 6. Load a 10 μ l-volume multichannel pipette with eight clean tips, place inside column 1 of “DD2 Plate” and load 1 μ l.
 7. Dispense contents into column 1 of “Assay Plate”.

Incubation of assay plate

1. Load a 200 μ l-volume multichannel pipet with eight clean tips and set to 50 μ l.
2. Place tips midway inside column 1 of “Assay Plate”, load and empty three times to mix contents.
3. Repeat steps 1-2 for columns 2-12.
4. Cover the plate using a sealing tape and spin down in a table-top centrifuge at 3000 \times g for 1 minute.
5. Place plate inside 30 $^{\circ}$ C incubator for 30 minutes.

Addition of protease substrate to assay plate

- 1- Spin down “Assay Plate” in a table-top centrifuge at 3000 \times g for 1 minute.
Gently remove the plate seal.
- 2- Retrieve 10 mM stock of protease substrate from -20 $^{\circ}$ C freezer and thaw at room temperature.
- 3- In a fresh 96-well plate, labeled “Substrate Plate”, aliquot 15 μ l of substrate into each well of row A.

6. Load a 10 μl -volume multichannel pipette with twelve clean tips, place inside row A of “Substrate Plate” and load 1 μl .
7. Dispense contents into row A of “Assay Plate”.
8. Load a 200 μl -volume multichannel pipette with twelve clean tips and set to 50 μl .
9. Place tips midway inside row A of “Assay Plate”, load and empty three times to mix contents.
10. Repeat steps 4-7 for rows B-H of “Assay Plate”.

Incubation of assay plate

1. Cover the plate using a new sealing tape and spin down in a table-top centrifuge at $3000 \times g$ for 1 minute.
2. Place plate inside 30 °C incubator for 60 minutes. We have confirmed experimentally that the observed rate of substrate hydrolysis is linear during this time period.

Stopping the enzyme reaction

1. Spin down “Assay Plate” in a table-top centrifuge at $3000 \times g$ for 1 minute.
2. Place “Assay Plate” on the work bench at room temperature. Carefully remove the sealing tape.

3. Load a 200 μ l-volume multichannel pipette with twelve clean tips, place inside the “DMSO” reservoir, and load 100 μ l.
4. Dispense contents into row A of “Assay Plate”.
5. Load a 200 μ l-volume multichannel pipette with twelve clean tips and set to 100 μ l.
6. Place tips midway inside row A of “Assay Plate”, load and empty three times to mix contents.
7. Repeat steps 2-5 for rows B-H of “Assay Plate”.
8. Cover the plate with a new sealing tape.

Reading the assay plate in fluorescence plate reader

- 1- Spin down “Assay Plate” in a table-top centrifuge at $3000 \times g$ for 1 minute. Gently remove the plate seal.
- 2- Place in microplate reader and measure the endpoint fluorescence with the excitation and emission wavelengths set to 380 nm and 460 nm, respectively.

Data processing

- 1- For each row corrected endpoint fluorescence using the equation: $EF - C^P$

EF is the endpoint fluorescence of the experimental and negative control wells. C^P is the endpoint fluorescence of the positive control well.

2- For each row calculate the % inhibition using the equation: $1 - (T^{EF} / N^{EF})$

T^{EF} is the corrected endpoint fluorescence of the experimental well with test compound. N^{EF} is the corrected endpoint fluorescence of the negative control well.

3- Compounds that showed inhibition over 50% were considered true hits in our screen.

4- If possible repeat the screen and determine the average % inhibition from triplicate data set.

5- Follow up experiments will rule out false positives and determine if hits act as dimer disruptors (*see* **Notes 3-6**)

NOTES

1. The Z'-factor is the measure of assay quality and is vital to identifying true hits in a high throughput screen¹⁷. The value is typically calculated from the endpoint readouts of the positive and negative control experiments, which in our screen correspond to the “low” and “high” signals respectively. The resulting numerical values range between 0 and 1, where numbers closest to 1 are favorable. The method of calculating the Z'-factor has been reported previously. Z'-factor optimization is achieved by varying the assay conditions such that the separation between the “low” and “high” signal is increased. We optimized the Z'-factor for the KSHV Pr assay by increasing the assay incubation temperature, the reaction incubation time, and including centrifugations steps. The data from an actual screen may be used in a similar manner to determine a Z-factor . The equations are as follows:

$$\text{Z-prime factor} = 1 - \frac{3(\sigma_p + \sigma_n)}{|\mu_p - \mu_n|} \qquad \text{Z-factor} = 1 - \frac{3(\sigma_s + \sigma_c)}{|\mu_s - \mu_c|}.$$

σ = standard deviation, μ = mean, p = positive control, n = negative control, s = sample, c = control.

2. DMSO exhibits an inhibitory affect in most assays, therefore its final concentration should be kept to a minimum. However, library compounds and protease substrates are generally dissolved in 100% DMSO stocks, and often require some DMSO to remain dissolved in aqueous buffer. For this reason it is important to determine the DMSO tolerance of screening assays. This is done by performing the basic assay in the presence of increasing

concentration of DMSO until an inhibitory condition is reached. The DMSO tolerance for the KSHV Pr assay is 5% (v/v).

3. Some compounds form aggregates that interact with proteins in a non-specific manner^{18,19}. Aggregate forming compounds may result in a false-positive inhibitory effect when screened as part of large libraries. Including a small amount of detergent, such as 0.01% Triton X-100 (v/v), will eliminate aggregation-based hits in most cases¹⁹. In the case of assays like the KSHV Pr assay that don't tolerate detergents, including 1mg/ml BSA eliminates non-specific interactions. Ideally detergents are included in the initial screen. However, since the library we screened was small, we counter screened our hits in the presence of BSA.

4. Some compounds may exhibit fluorescent properties in the wavelengths monitored by the assay. For example a compound that absorbs light in the same region as our ACC substrate, may interfere with the final assay readout. Therefore, it's important to monitor the absorptions and emission properties of all screening hits at the wavelengths used to make read measurements.

5. A true inhibitor has a sigmoidal dose response curve with a hill slope value that is around 1. The concentration of inhibitor that achieves 50% inhibition is the IC_{50} . Dose response curves are obtained by repeating the screening assay with increasing concentrations of compound, ranging from 0 to 100 μ M. Generally a 3-fold dilution of compound is used (100 μ M, 33.3 μ M, 11.1 μ M, etc.). Percent inhibition values are then plotted as a function of inhibitor concentration.

6. Since the goal of the screen is to identify dimer disruptors, secondary assays that monitor dimerization must be available. We used two independent but complementary methods to determine whether our hit DD2 was a dimer disruptor^{7,16}. The first was an FPLC assay and the second was a 2D-NMR approach using protease containing a reporter at the dimer interface. Both methods were carried out as described previously.

ACKNOWLEDGMENTS

This work¹⁶ was supported by NIH grants T32 GM07810, AIO67423 (C.S.C.), and by the American Lebanese and Syrian Associated Charities and St Jude Children's Research Hospital (R.K.G.).

REFERENCES

1. Borthwick, A.D. et al. Design and synthesis of pyrrolidine-5,5-trans-lactams (5-oxohexahydropyrrolo[3,2-b]pyrroles) as novel mechanism-based inhibitors of human cytomegalovirus protease. 2. Potency and chirality. *J Med Chem* **45**, 1-18 (2002).
2. Borthwick, A.D. et al. Pyrrolidine-5,5-trans-lactams as novel mechanism-based inhibitors of human cytomegalovirus protease. Part 3: potency and plasma stability. *Bioorg Med Chem Lett* **12**, 1719-22 (2002).
3. Borthwick, A.D. et al. Design and synthesis of monocyclic beta-lactams as mechanism-based inhibitors of human cytomegalovirus protease. *Bioorg Med Chem Lett* **8**, 365-70 (1998).
4. Gopalsamy, A. et al. Design and syntheses of 1,6-naphthalene derivatives as selective HCMV protease inhibitors. *J Med Chem* **47**, 1893-9 (2004).
5. Ogilvie, W. et al. Peptidomimetic inhibitors of the human cytomegalovirus protease. *J Med Chem* **40**, 4113-35 (1997).
6. Waxman, L. & Darke, P.L. The herpesvirus proteases as targets for antiviral chemotherapy. *Antivir Chem Chemother* **11**, 1-22 (2000).
7. Marnett, A.B., Nomura, A.M., Shimba, N., Ortiz de Montellano, P.R. & Craik, C.S. Communication between the active sites and dimer interface of a herpesvirus protease revealed by a transition-state inhibitor. *Proc Natl Acad Sci U S A* **101**, 6870-5 (2004).
8. Nomura, A.M., Marnett, A.B., Shimba, N., Dotsch, V. & Craik, C.S. Induced structure of a helical switch as a mechanism to regulate enzymatic activity. *Nat Struct Mol Biol* **12**, 1019-20 (2005).

9. Nomura, A.M., Marnett, A.B., Shimba, N., Dotsch, V. & Craik, C.S. One functional switch mediates reversible and irreversible inactivation of a herpesvirus protease. *Biochemistry* **45**, 3572-9 (2006).
10. Pray, T.R., Nomura, A.M., Pennington, M.W. & Craik, C.S. Auto-inactivation by cleavage within the dimer interface of Kaposi's sarcoma-associated herpesvirus protease. *J Mol Biol* **289**, 197-203 (1999).
11. Pray, T.R., Reiling, K.K., Demirjian, B.G. & Craik, C.S. Conformational change coupling the dimerization and activation of KSHV protease. *Biochemistry* **41**, 1474-82 (2002).
12. Lazic, A., Goetz, D.H., Nomura, A.M., Marnett, A.B. & Craik, C.S. Substrate modulation of enzyme activity in the herpesvirus protease family. *J Mol Biol* **373**, 913-23 (2007).
13. Reiling, K.K., Pray, T.R., Craik, C.S. & Stroud, R.M. Functional consequences of the Kaposi's sarcoma-associated herpesvirus protease structure: regulation of activity and dimerization by conserved structural elements. *Biochemistry* **39**, 12796-803 (2000).
14. Shimba, N., Nomura, A.M., Marnett, A.B. & Craik, C.S. Herpesvirus protease inhibition by dimer disruption. *J Virol* **78**, 6657-65 (2004).
15. Lee, G.M. & Craik, C.S. Trapping moving targets with small molecules. *Science* **324**, 213-5 (2009).
16. Shahian, T. et al. Inhibition of a Viral Enzyme by a Small Molecule Dimer Disruptor. *Nature Chemical Biology* **5**, 640-646 (2009).

17. Zhang, J.H., Chung, T.D. & Oldenburg, K.R. A Simple Statistical Parameter for Use in Evaluation and Validation of High Throughput Screening Assays. *J Biomol Screen* **4**, 67-73 (1999).
18. Feng, B.Y., Shelat, A., Doman, T.N., Guy, R.K. & Shoichet, B.K. High-throughput assays for promiscuous inhibitors. *Nat Chem Biol* **1**, 146-8 (2005).
19. Feng, B.Y. & Shoichet, B.K. A detergent-based assay for the detection of promiscuous inhibitors. *Nat Protoc* **1**, 550-3 (2006).

Figure 4-1

Structure of KSHV Pr dimer. The top and side views of the dimeric crystal structure are shown. The active-site catalytic residues are in orange. The interfacial α -helix 5 moieties and the two independent catalytic triads are highlighted in black.

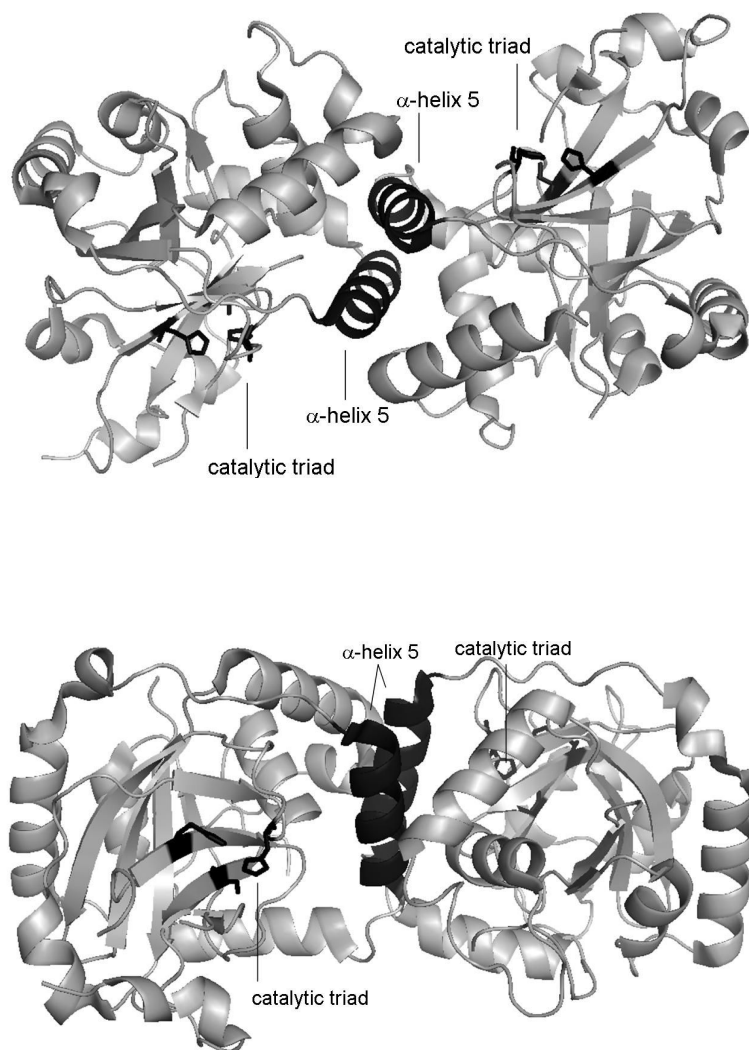


Figure 4-2

The workflow for identifying dimer disruptors of HHV proteases. Inhibitors of KSHV Pr activity are identified by high throughput screening (HTS) of small molecule libraries. Hits are further characterized for mode of inhibition and dimer disruption through 2D-NMR assays that have been described previously. Lead compounds are then tested for efficacy against other HHV proteases. This method will focus on the HTS assay (dotted box).

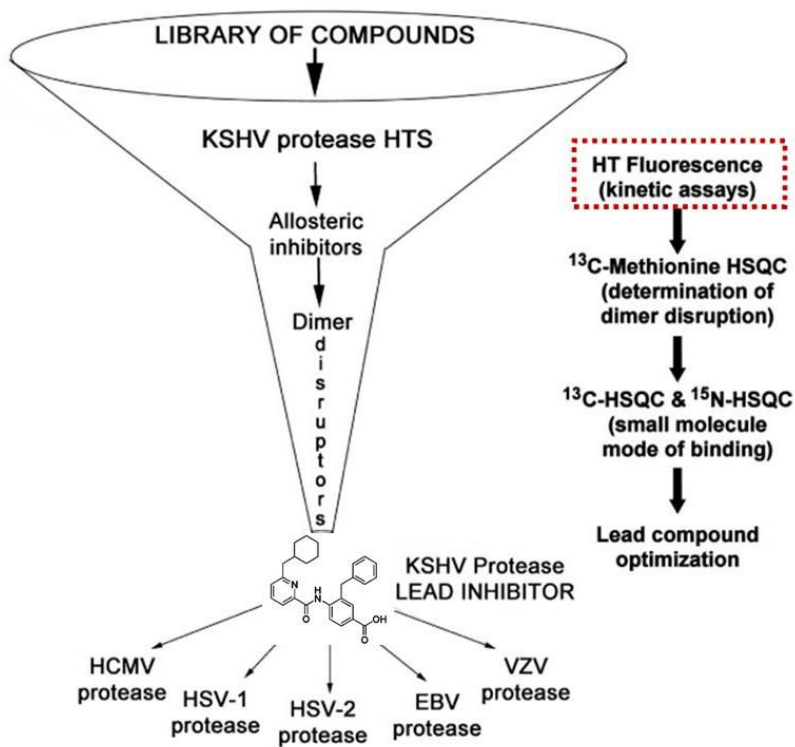


Figure 4-3

The structure of DD2.

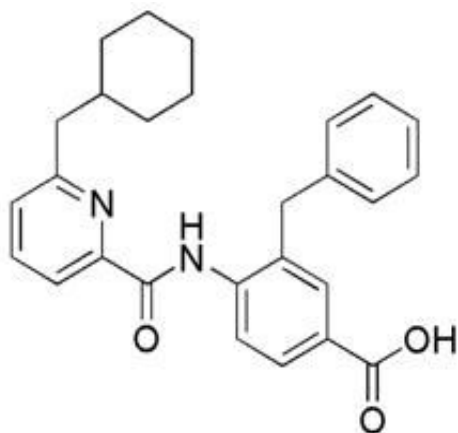


Figure 4-4

Plate uniformity layout for H/M/L. The assay layout for one plate uniformity experiment is shown in 96-well format. Assays resulting in final readouts of high (H) signal, medium (M) signal, and low (L) signal are plated as demonstrated below. The M/L/H, and L/H/M experiment plates are set up in a similar fashion.

| Row | C1 | C2 | C3 | C4 | C5 | C6 | C7 | C8 | C9 | C10 | C11 | C12 |
|-----|----|----|----|----|----|----|----|----|----|-----|-----|-----|
| 1 | H | M | L | H | M | L | H | M | L | H | M | L |
| 2 | H | M | L | H | M | L | H | M | L | H | M | L |
| 3 | H | M | L | H | M | L | H | M | L | H | M | L |
| 4 | H | M | L | H | M | L | H | M | L | H | M | L |
| 5 | H | M | L | H | M | L | H | M | L | H | M | L |
| 6 | H | M | L | H | M | L | H | M | L | H | M | L |
| 7 | H | M | L | H | M | L | H | M | L | H | M | L |
| 8 | H | M | L | H | M | L | H | M | L | H | M | L |

Figure 4-5

Sample plate uniformity data analysis. The data for one plate uniformity experiment is shown. Data points are plotted either from the row (top plot) or column (bottom plot) orientations. The plotted values of high (green), medium (purple), and low (navy) signals are linear in both orientations, confirming the lack of a drift effect.

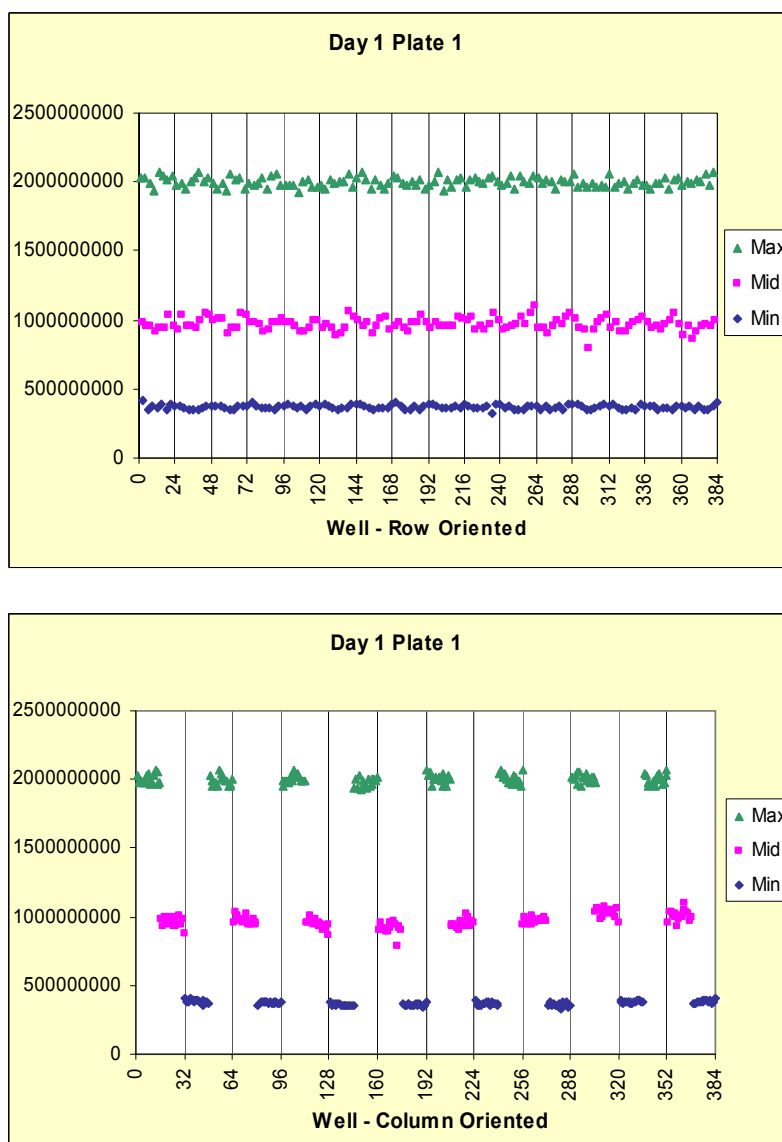


Figure 4-6

Scatter plot of screening data. The endpoint fluorescence value of each experimental well from all 11 plates is used to calculate the percentage inhibitory activity. The results are plotted with percent activity on the y axis, and compound on the x axis. DD2 positive control (green circles), DMSO negative control (red circles), inactive compounds (black circles), active compounds (blue circles), 95th activity quantile (orange line), 99th activity quantile (purple line).

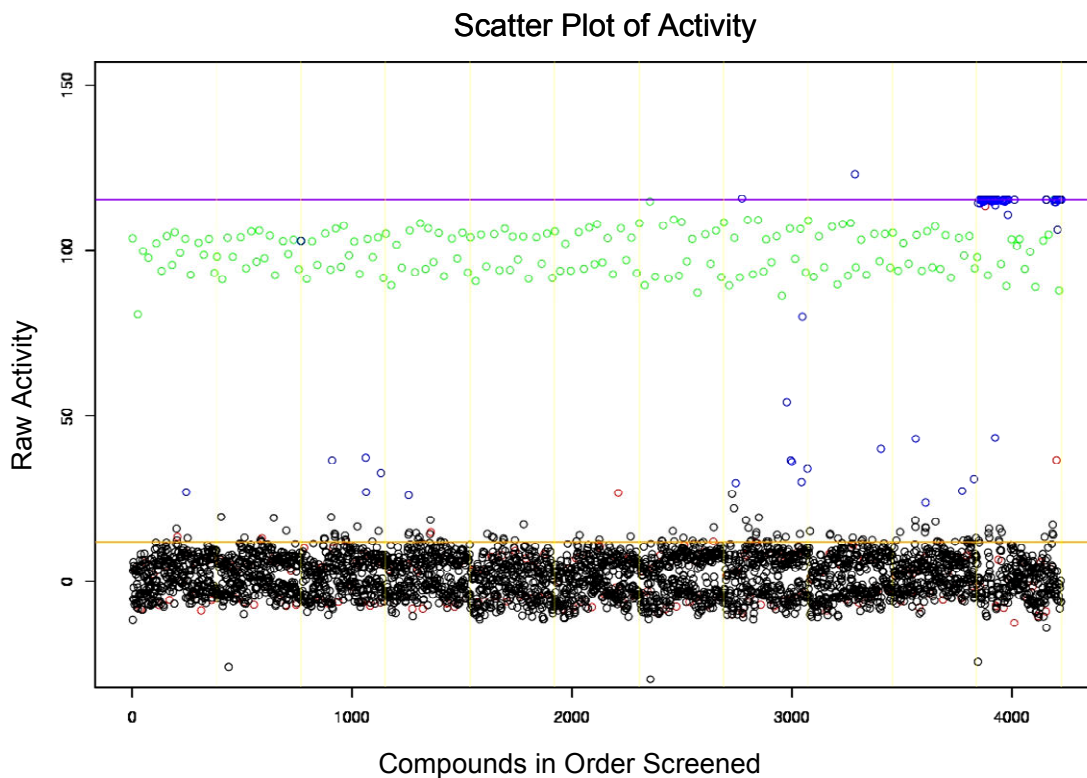


Figure 4-7

HTS assay quality data. The calculated Z' and Z factors are for each of 11 plates are shown on a scatter plot. The red lines mark the outlier cutoff.

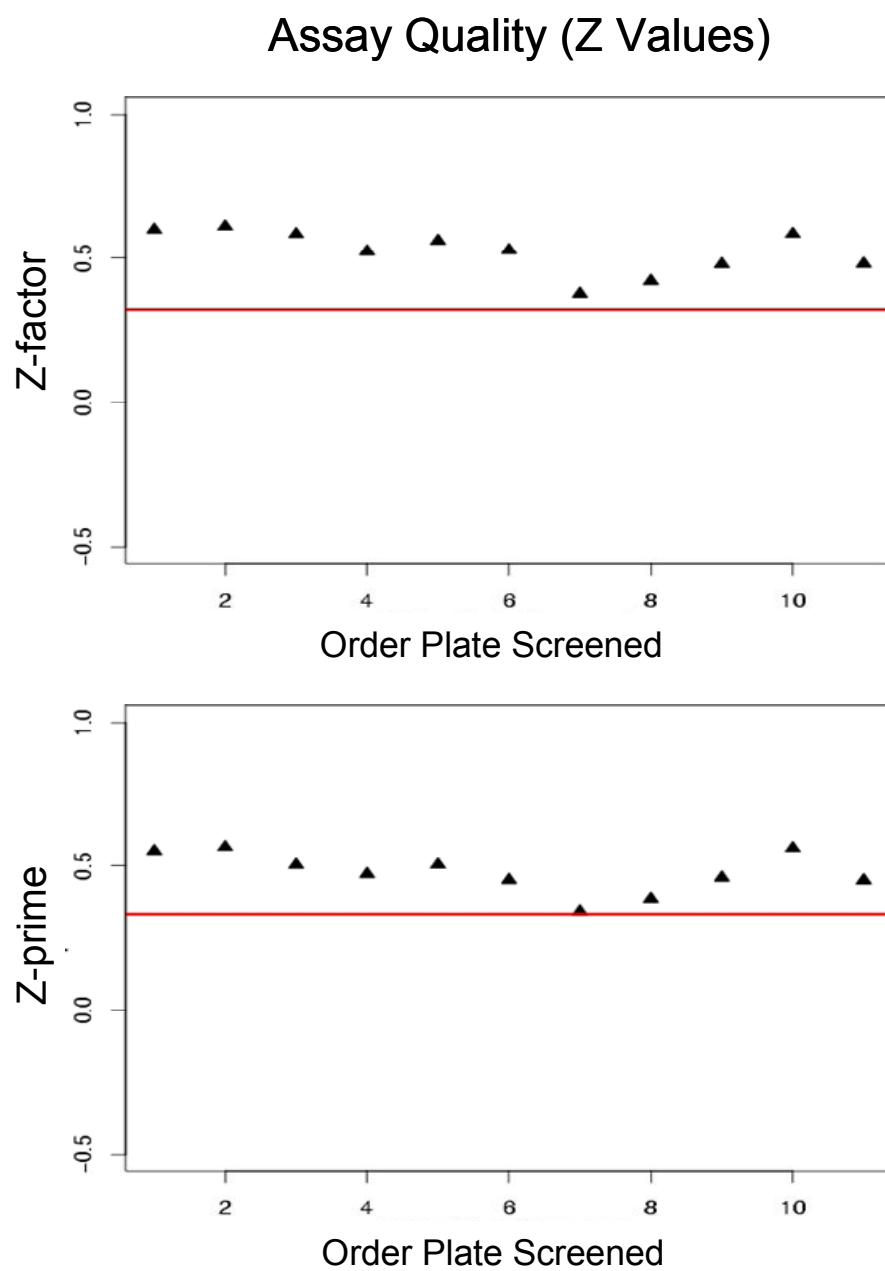


Figure 4-8

The structure and analysis of hexachlorophene. (a) The structure of hexachlorophene. (b) Dose response curves for hexachlorophene (red) and four other compounds. (c) Absorbance scan of hexachlorophene over 300-800 nm.

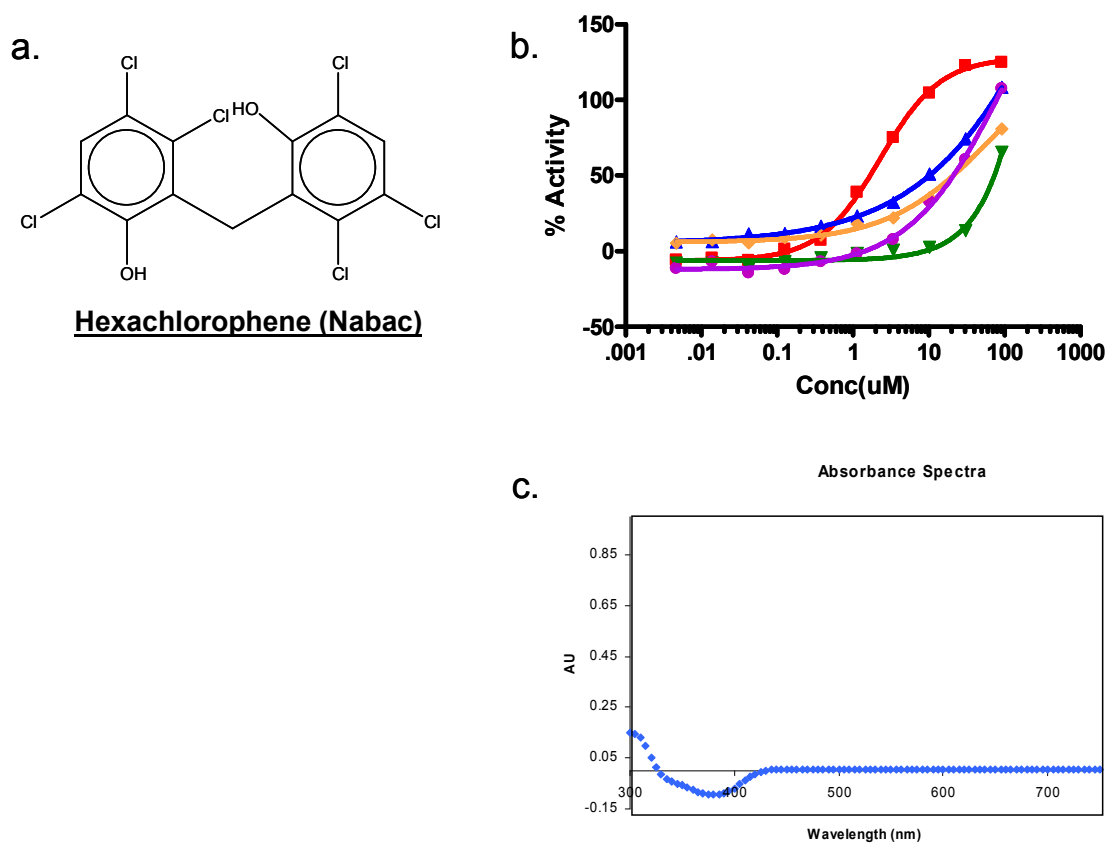


Figure 4-9

The structure and analysis of cholanic acid. (a) The structure of cholanic acid. (b) Dose response curves for cholanic acid (red) and four other compounds. (c) Absorbance scan of cholanic acid over 300-800 nm.

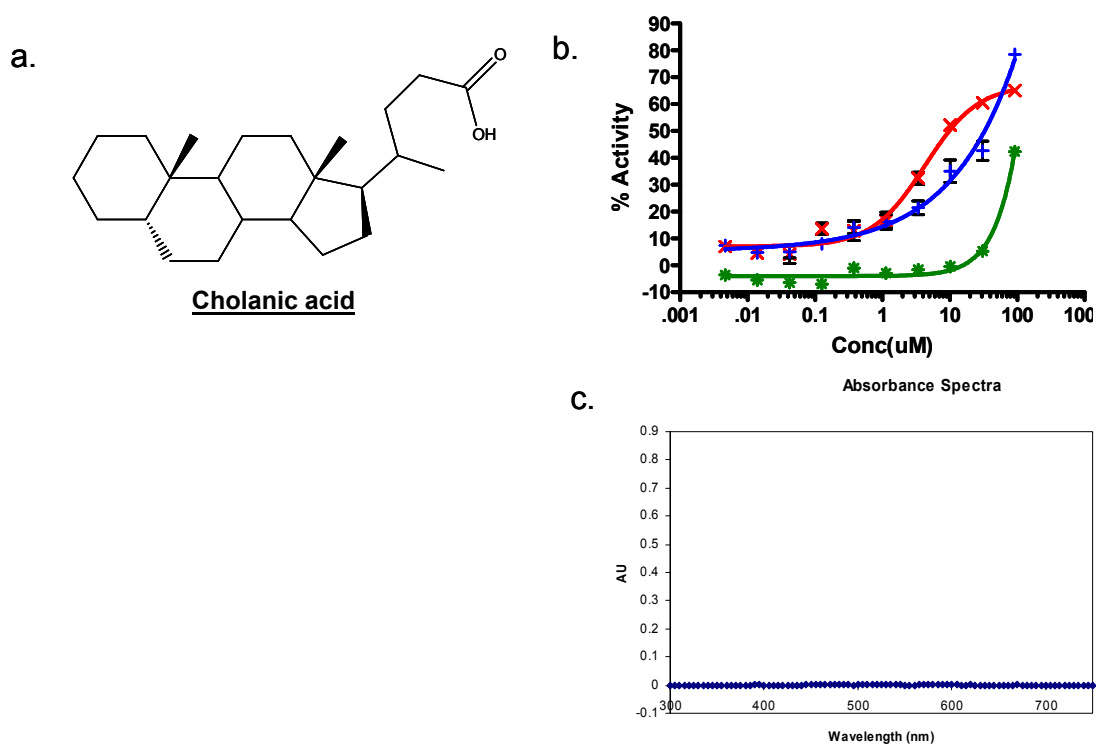


Figure 4-10

Hexachlorophene shows evidence of non-specific aggregation with Granzyme B. The inhibitory activity of hexachlorophene was tested against Granzyme B (GrB) protease in an activity assay. GrB (20 nM), *p*NA substrate (500 μ M), and HEX (30 μ M) were assayed in buffer with varied amounts of detergent Triton X-100.^{18,19} Bar graphs show the ratio of experimental end-point absorbance (A) and un-inhibited end-point absorbance (A0), recorded 30 minutes after addition of substrate. Data represents mean values \pm s.d. (n=3).

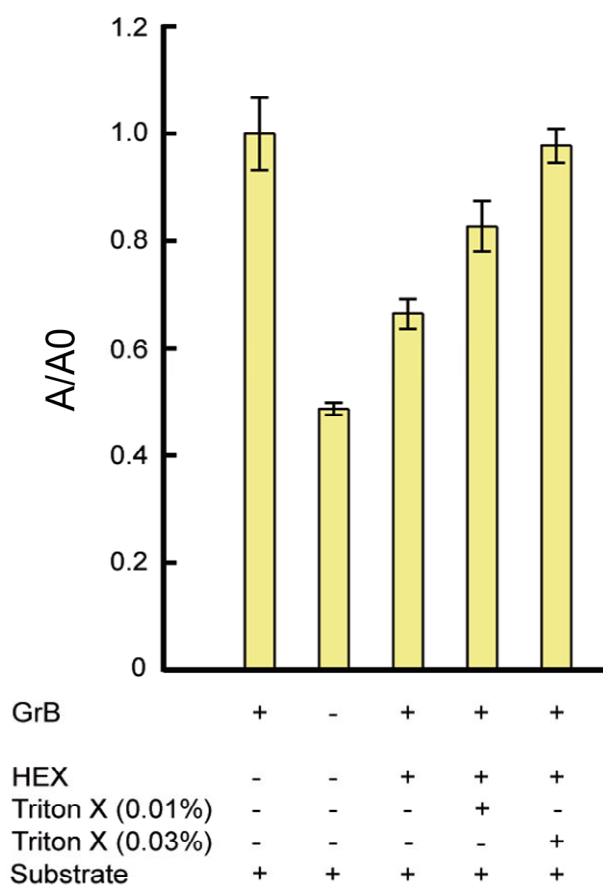
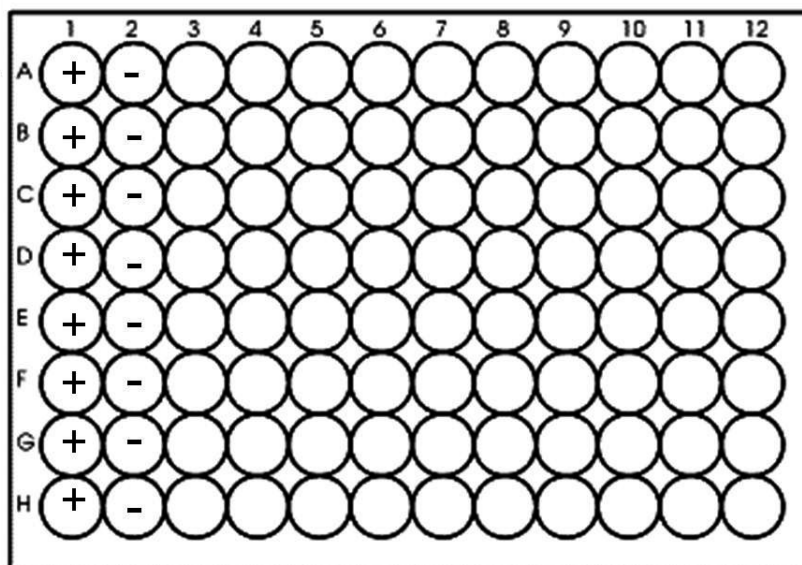


Figure 4-11

The 96-well plate arrangement. Positive (+) and negative (-) controls are located in columns 1 and 2 respectively. Test compounds are screened in columns 3-12. The wells in each row receive substrate at the same time. The controls in each row may be used to accurately calculate % inhibition.



CHAPTER 5: Determining the affects of KSHV Pr inhibition using small molecules in cell culture

Tina Shahian¹, Don Ganem², Charles S. Craik³

¹ Graduate Group in Biochemistry and Molecular Biology University of California San Francisco, CA, 94158-2280 USA

² Head of infectious disease Novartis Vaccines & Diagnostics, Emeryville, CA 94608

³ Department of Pharmaceutical Chemistry, University of California San Francisco, CA 94158-2280 USA

ABSTRACT

Human herpesviruses require the activity of a conserved serine protease for viral replication, making protease inhibition an attractive opportunity for developing novel anti-herpes therapeutics. Previous attempts by pharmaceutical companies to target the protease active-site of β -herpesvirus cytomegalovirus (CMV) were not successful in developing an effective therapeutic. We have developed small molecule dimer disruptor of KSHV Pr that binds a novel allosteric pocket at the interface. We have utilized a KSHV cell assay to measure viral replication in the presence of small molecule protease inhibitors. This viral re-infection assay, as well as a western blot method to detect substrate cleavage in cell culture, is described.

INTRODUCTION

Herpesviruses are a large family of double-stranded DNA viruses that encapsulate their genes in an icosahedral capsid.¹ There are eight types that cause a variety of diseases in humans, one being Kaposi's sarcoma-associated herpesviruses (KSHV), which is the etiological agent of Kaposi's sarcoma (KS), a type of skin neoplasm². KSHV, like other herpesviruses has two replication programs, latent and lytic. During latency only a handful of genes are expressed and no virions are produced. Upon induction of the lytic cycle, the viral genome is replicated, structural components are made, and infectious progeny is generated.

Human herpesviruses (HHV) express a conserved protease that plays a critical role in the lytic cycle. The protease expresses as a fusion to an assembly protein (Pr/AP), while the more abundant AP protein is expressed from a downstream promoter.³⁻⁶ In both forms, AP binds the major capsid protein, and the complex translocates to the nucleus where the immature capsid is assembled around the AP scaffold.⁷⁻¹¹ At this stage Pr cleaves at two sites allowing DNA packaging, formation of the infectious virion, and completion of the lytic cycle.⁷⁻¹¹ Initial studies with herpes simplex virus type 1 (HSV-1), identified a temperature sensitive protease mutant that produced malformed capsids lacking DNA.^{3,9,11-13} Based on these evidence HHV proteases were identified as key targets in drug discovery efforts aimed at treating herpesviral diseases.

Early attempts to target the active-site of cytomegalovirus (CMV) protease lead to variety of peptidic and mechanism-based inhibitors with modest potencies¹⁴. A series of non-peptidic molecules developed based on the mechanism-based β -lactam inhibitors of the serine protease human leukocyte elastase, demonstrated low micromolar potencies in vitro, but poor

efficacy in plaque reduction assays.^{15,16} Other inhibitors based on this scaffold have shown good efficacy and pharmacokinetics in dogs, but have not lead to a clinical trial candidate.^{17,18} Based on the evidence supporting a structural and mechanisml link between the protease active-site and the dimer interface in HHV proteases, we have developed a novel small molecule inhibitor, DD2, that acts as a dimer disruptor.¹⁹ In order to show the utility of this approach for drug development, efficacy data in KSHV cell culture models is needed.

KSHV has a narrow host range and natural infections of non-humans are not observed. In humans, KSHV infects B cells and endothelial (spindle) cells of Kaposi's sarcoma tumors.^{20,21} In cell culture KSHV establishes latency in human endothelial, epithelial, and mesenchymal cells, namely; TIME, 293, HFF, and HeLa cells. Lytic reactivation is achieved by the addition of phorbol esters, sodium butyrate, or valproic acid.^{22,23} In collaboration with Dr. Don Ganem (former Prof. in the UCSF Dept. of Microbiology & Immunology, currently head of infectious disease at Novartis, Emeryville), we used an KSHV cell assay to measure viral replication in the presence of KSHV Pr inhibitor DD2. A western blot assay was also developed to monitor the cleavage of KSHV Pr substrate, AP, in the cell. The poor solubility and permeability of DD2 prevented us from obtaining efficacy data, however both assays are available for validating future small molecule inhibitors.

RESULTS

Assessing the cell toxicity of DD2

Prior to studying the effects of small molecule inhibitor DD2 in cell culture models for KSHV, the cell toxicity of DD2 was measured. The cells used for culturing KSHV are called SLK, an endothelial cell line originating from a KS lesion of an iatrogenically immunosuppressed HIV-negative patient.²⁴ The parental SLK cells have lost the unstable viral episome over time, but can be readily infected with virus. Each well of a 12-well plate was seeded with parental SLK cells and DMSO, 10 μ M, 20 μ M, or 30 μ M DD2 were included in the media. The cells under each experimental condition were a total cell count was carried out after 24, 48, and 72 hours (**Fig. 5-1**). The 72-hour time point was chosen because that is total number of hours the cells will be incubated with DD2. Based on our data both the DMSO and DD2 treated cells showed the same growth over the cell growth over 72 hours, suggesting DD2 is not toxic over this concentration range.

DD2 does not show activity in a KSHV re-infection assay

To see whether the *in vitro* KSHV Pr inhibitor DD2 reduces viral replication in cell culture, we utilized a viral re-infection assay (**Fig. 5-2 and 5-3**).^{25,26} The stably infected rSLK.219 cell line used in this study contains two different fluorescent reporter groups for monitoring (a) latent infection, and (b) the switch to lytic reactivation²⁷. The GFP gene expressed by the human elongation factor 1- α promoter marks cells latently infected with KSHV. Lytic reactivation is induced by ectopic expression of the KSHV replication and transcription

activation gene (RTA) under the control of a doxycyclin inducible promoter.²⁷⁻³⁰ This stage is marked by RFP expression under the control of the viral PAN RNA promoter. Infected rSLK.219 cells were grown to sub-confluency prior to inducing lytic expression with RTA. At the time of induction either DMSO or inhibitor DD2 were introduced into the growth media. After five days growth, the spent media containing mature virions was removed and used for re-infection of freshly plated parental SLK cells. Following 48 hours, the number of latently infected parental SLK cells, which were marked by GFP expression (GFP+) were scored by flow cytometry. Parental SLK cells treated with spent media from un-induced rSLK.219 cells yielded almost zero GFP+ cells (**Fig. 5-4**). However, cells treated with media from doxycyclin induced cells rSLK.219 cells, yielded up to 60% GFP+ cells. DD2 did not exhibit a significant decrease in viral infectivity. The KSHV re-infection assay shows excellent dynamic range and may be used for testing new inhibitors.

Monitoring the processing of AP by western blot

Protease inhibitors that demonstrate antiviral activity in cell culture infectivity assays are expected to act by blocking protease function at the late lytic stage. In order to test this hypothesis we developed a Western blot assay that detects both the cleaved and uncleaved forms of KSHV protease substrates. When KSHV Pr substrate AP (ORF17.5) protein is cleaved at the maturation site (M-site), uncut and cut products at 31kD and 28kD are expected. Cleavage of the less abundant Pr/AP (ORF17) fusion protein at the Release site (R-site) is expected to yield products of sizes 57kD and 55kD.

Stably infected rSLK.219 cells were cultured and induced as described earlier. At various time points post-induction, cells were removed and lysed. Lysates were run on an agarose gel and probed for the presence of AP using a polyclonal antibody that recognizes the AP protein between the R-site and M-site.³¹ At the 48-hr time point a doublet band was observed in the 30kD region that corresponds to the expected cut and uncut AP products (**Fig. 5-5**). A single band is also observed around the 55kD region that most likely corresponds to the uncleaved Pr/AP protein. In future experiments can take advantage of a Cy5-coupled secondary antibody that allows better resolution and quantification of the doublet bands. In the presence of protease inhibitors we expect a reduction in the 28kD band corresponding to cleave AP.

DISCUSSION

Showing efficacy in KSHV cell culture models is a key step in developing novel anti-herpes therapeutics. We have adapted assays for KSHV viral infectivity for testing of our allosteric protease inhibitors in cell culture. A re-infection assay, which measures the viral progeny from cells that underwent lytic reactivation in the presence of small molecule inhibitors, demonstrates a great dynamic range. Furthermore, we have developed a western blot assay to show that a reduction in viral load due treatment with protease inhibitors, is a direct result of a defective protease function. The antibody used can detect the cleaved and uncleaved forms of protein AP, the *in vivo* KSHV Pr substrate, which is visualized as a doublet on the gel. Our studies used chemiluminescence as means for detection, but fluorescently tagged secondary antibodies offer enhanced sensitivity and allow for a more accurate quantification of the cut and un-cut protein bands. The poor solubility and permeability properties of KSHV Pr inhibitor DD2, prevented us from obtaining cell culture data. Screening of small molecule libraries is necessary for discovering additional inhibitors with have properties favorable to cell culture studies.

MATERIALS AND METHODS

Cell toxicity

Parental SLK cells were seeded on each well of a 12-well plate. Each column was treated with either DMSO, 10, 20, or 30 μ M DD2. At 24, 48, and 72 hour time points, cells from each experimental condition were counted using a hemocytometer.

Viral re-infection assay

Recombinant SLK.219 (rSLK.219) cells were obtained from the laboratory of Don Ganem and cultured as described previously.²⁷ Briefly, cells were plated in DMEM supplemented with 10% FBS and 1% penicillin/streptomycin. At 70% confluency cells were induced to enter lytic phase by treating with 1 μ g/mL doxycycline, which switched on the RTA expression. DMSO or compound DD2 were also included at this step. Over the next five days, the expression of RFP and the appearance of dead floating cells were monitored by microscopy. On day five spent media was filtered to remove cell debris and transferred to freshly-plated parental SLK cells. Infection was carried out by spinoculation at 2500 RPM for 120 min, followed by a 1 hour recovery at 37°C. Media was replaced and cells were cultured for 48 hours before GFP expressing cells were scored by FACS analysis.

Flow cytometry

SLK cells were trypsinized and washed with PBS and fixed by 0.5% paraformaldehyde for 5min at room temperature. Cells were then washed in cold PBS and resuspended in FACS

buffer, containing 4% FBS and 0.09% sodium azide. GFP expressing cells were examined on LSR II instrument. Data analysis was performed in FlowJo software.

Western blot analysis

rSLK.219 cells were cultured and lytic cycle was induced as described above. At 12, 24, 48, and 72 hours post induction, cells were collected and lysates were prepared in RIPA buffer. Samples were analyzed by western blot using an antisera (rabbit bleed) to KSHV Pr ORF 17 between the R and M sites.³¹ Antibody was used at a 1/2000 dilution and secondary goat-anti-rabbit/HRP antibody was used at 1/5000 dilution.

AKNOWLEDGMENTS

The authors thank the laboratory of Dr. Don Ganem for providing us with the viral strains and protocols used in this chapter. This work was funded by US National Institutes of Health grants T32 GMO7810 and AIO67423 (C.S.C.).

REFERENCES

1. Ganem, D. Kaposi's sarcoma-associated herpesvirus. in *Fields Virology*, Vol. 1 (eds. Knipe, D.M. & Howley, P.M.) (Lippincott, Williams and Kluwer, Philadelphia, PA, 2007).
2. Edelman, D.C. Human herpesvirus 8--a novel human pathogen. *Virol J* **2**, 78 (2005).
3. Preston, V.G., Coates, J.A. & Rixon, F.J. Identification and characterization of a herpes simplex virus gene product required for encapsidation of virus DNA. *J Virol* **45**, 1056-64 (1983).
4. Preston, V.G., Rixon, F.J., McDougall, I.M., McGregor, M. & al Kobaisi, M.F. Processing of the herpes simplex virus assembly protein ICP35 near its carboxy terminal end requires the product of the whole of the UL26 reading frame. *Virology* **186**, 87-98 (1992).
5. Register, R.B. & Shafer, J.A. A facile system for construction of HSV-1 variants: site directed mutation of the UL26 protease gene in HSV-1. *J Virol Methods* **57**, 181-93 (1996).
6. Rixon, F.J. & McNab, D. Packaging-competent capsids of a herpes simplex virus temperature-sensitive mutant have properties similar to those of in vitro-assembled procapsids. *J Virol* **73**, 5714-21 (1999).
7. Baum, E.Z. et al. Expression and analysis of the human cytomegalovirus UL80-encoded protease: identification of autoproteolytic sites. *J Virol* **67**, 497-506 (1993).
8. DiIanni, C.L. et al. Identification of the herpes simplex virus-1 protease cleavage sites by direct sequence analysis of autoproteolytic cleavage products. *J Biol Chem* **268**, 2048-51 (1993).

9. Gao, M. et al. The protease of herpes simplex virus type 1 is essential for functional capsid formation and viral growth. *J Virol* **68**, 3702-12 (1994).
10. Robertson, B.J. et al. Separate functional domains of the herpes simplex virus type 1 protease: evidence for cleavage inside capsids. *J Virol* **70**, 4317-28 (1996).
11. Welch, A.R., Woods, A.S., McNally, L.M., Cotter, R.J. & Gibson, W. A herpesvirus maturational proteinase, assemblin: identification of its gene, putative active site domain, and cleavage site. *Proc Natl Acad Sci U S A* **88**, 10792-6 (1991).
12. Newcomb, W.W. et al. Isolation of herpes simplex virus procapsids from cells infected with a protease-deficient mutant virus. *J Virol* **74**, 1663-73 (2000).
13. Matusick-Kumar, L. et al. Phenotype of the herpes simplex virus type 1 protease substrate ICP35 mutant virus. *J Virol* **68**, 5384-94 (1994).
14. Waxman, L. & Darke, P.L. The herpesvirus proteases as targets for antiviral chemotherapy. *Antivir Chem Chemother* **11**, 1-22 (2000).
15. Yoakim, C. et al. Potent beta-lactam inhibitors of human cytomegalovirus protease. *Antivir Chem Chemother* **9**, 379-87 (1998).
16. Yoakim, C. et al. beta-Lactam derivatives as inhibitors of human cytomegalovirus protease. *J Med Chem* **41**, 2882-91 (1998).
17. Borthwick, A.D. Design of translactam HCMV protease inhibitors as potent antivirals. *Med Res Rev* **25**, 427-52 (2005).
18. Borthwick, A.D. et al. Design and synthesis of pyrrolidine-5,5'-trans-lactams (5-oxo-hexahydropyrrolo[3,2-b]pyrroles) as novel mechanism-based inhibitors of human cytomegalovirus protease. 4. Antiviral activity and plasma stability. *J Med Chem* **46**, 4428-49 (2003).

19. Shahian, T. et al. Inhibition of a Viral Enzyme by a Small Molecule Dimer Disruptor. *Nature Chemical Biology* **9**, 640-646 (2009).
20. Staskus, K.A. et al. Kaposi's sarcoma-associated herpesvirus gene expression in endothelial (spindle) tumor cells. *J Virol* **71**, 715-9 (1997).
21. Boshoff, C. et al. Kaposi's sarcoma-associated herpesvirus infects endothelial and spindle cells. *Nat Med* **1**, 1274-8 (1995).
22. Shaw, R.N., Arbiser, J.L. & Offermann, M.K. Valproic acid induces human herpesvirus 8 lytic gene expression in BCBL-1 cells. *AIDS* **14**, 899-902 (2000).
23. Yu, Y. et al. Induction of human herpesvirus-8 DNA replication and transcription by butyrate and TPA in BCBL-1 cells. *J Gen Virol* **80** (Pt 1), 83-90 (1999).
24. Herndier, B.G. et al. Characterization of a human Kaposi's sarcoma cell line that induces angiogenic tumors in animals. *AIDS* **8**, 575-81 (1994).
25. Chandriani, S. & Ganem, D. Array-based transcript profiling and limiting-dilution reverse transcription-PCR analysis identify additional latent genes in Kaposi's sarcoma-associated herpesvirus. *J Virol* **84**, 5565-73.
26. Vieira, J. & O'Hearn, P.M. Use of the red fluorescent protein as a marker of Kaposi's sarcoma-associated herpesvirus lytic gene expression. *Virology* **325**, 225-40 (2004).
27. Myoung, J. & Ganem, D. Generation of a doxycycline-inducible KSHV producer cell line of endothelial origin: Maintenance of tight latency with efficient reactivation upon induction. *J Virol Methods* **174**, 12-21.
28. Gradoville, L. et al. Kaposi's sarcoma-associated herpesvirus open reading frame 50/Rta protein activates the entire viral lytic cycle in the HH-B2 primary effusion lymphoma cell line. *J Virol* **74**, 6207-12 (2000).

29. Lukac, D.M., Renne, R., Kirshner, J.R. & Ganem, D. Reactivation of Kaposi's sarcoma-associated herpesvirus infection from latency by expression of the ORF 50 transactivator, a homolog of the EBV R protein. *Virology* **252**, 304-12 (1998).
30. Sun, R. et al. A viral gene that activates lytic cycle expression of Kaposi's sarcoma-associated herpesvirus. *Proc Natl Acad Sci U S A* **95**, 10866-71 (1998).
31. Nealon, K. et al. Lytic replication of Kaposi's sarcoma-associated herpesvirus results in the formation of multiple capsid species: isolation and molecular characterization of A, B, and C capsids from a gammaherpesvirus. *J Virol* **75**, 2866-78 (2001).

Figure 5-1

Cell toxicity data with DD2. Parental SLK cells were seeded on each well of a 12-well plate. Each column was treated with either DMSO, 10, 20, or 30 μ M DD2. At 24, 48, and 72 hour time points, cells from each experimental condition were counted using a hemocytometer. No cell toxicity is observed over the concentration range of DD2 tested.

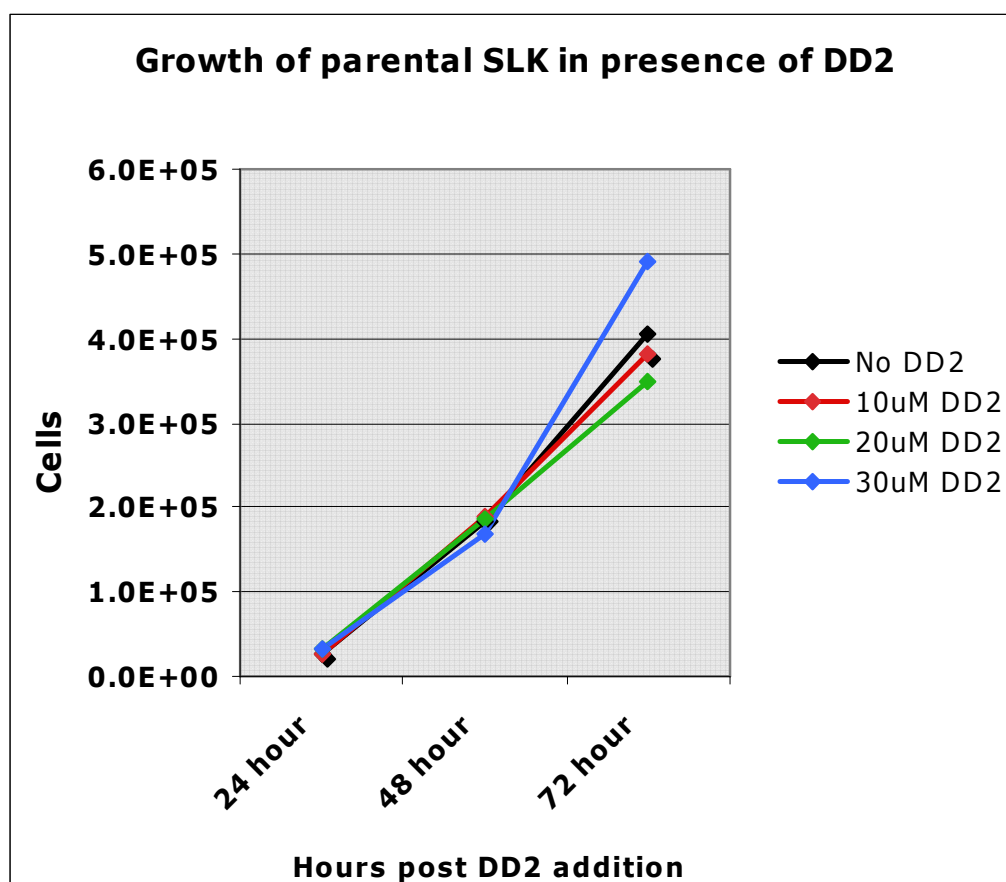


Figure 5-2

Schematic of KSHV re-infection assay. rSLK.219 harbor latent KSHV and constitutively express the GFP marker from the human elongation factor 1-a promoter. Lytic reactivation is induced by ectopic expression of the KSHV replication and transcription activation gene (RTA) under the control of a doxycyclin inducible promoter. Test inhibitors are included at this step. Lytic reactivations is marked by the expression of RFP under the control of the viral PAN RNA promoter. On day 5, supernatant is collected and used to infect freshly plated parental SLK cells using the technique of spinnoculation. After 48 hours, new infections are marked by the expression of GFP.

Figure 5-2

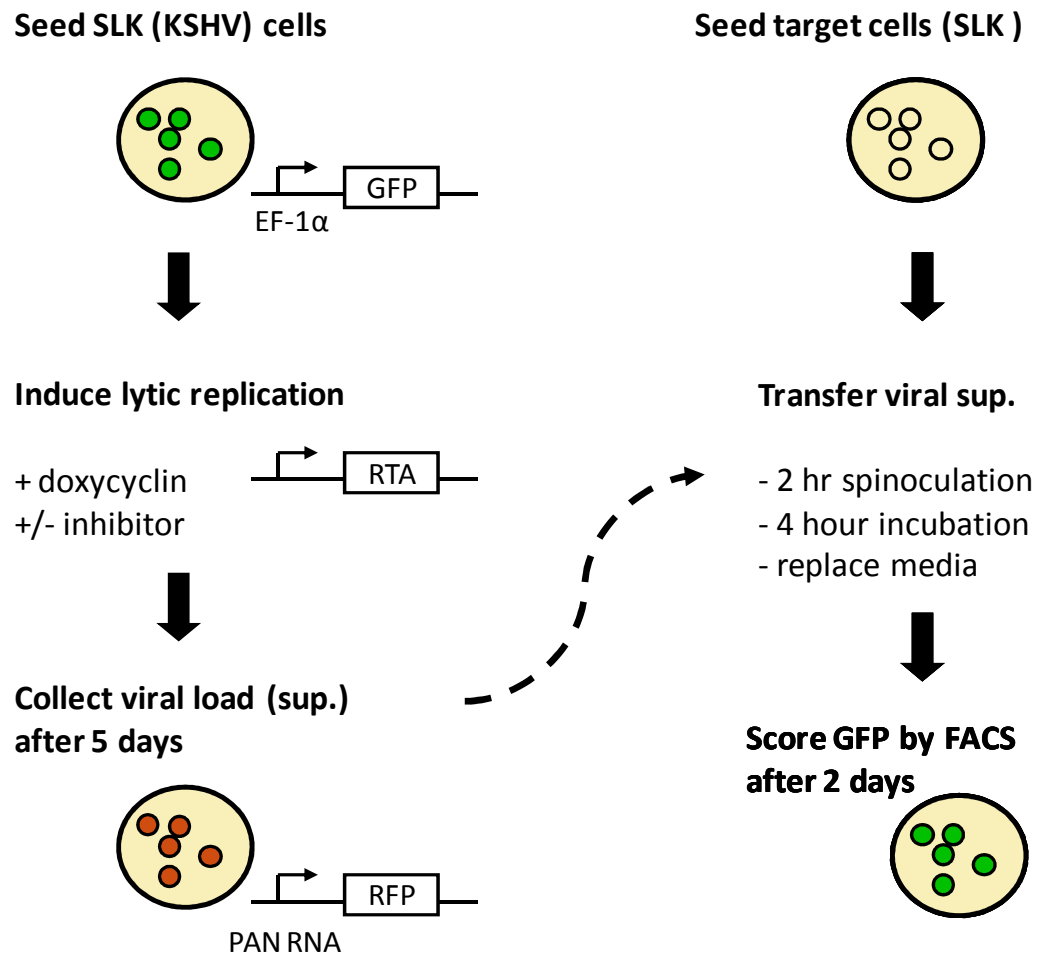


Figure 5-3

Latent and Lytic KSHV219 cells. Sub-confluent rSLK.219 cells were induced doxycyclin. Cells pre and post induction were observed under a fluorescent microscope for the expression of GFP (left) or RFP (right).

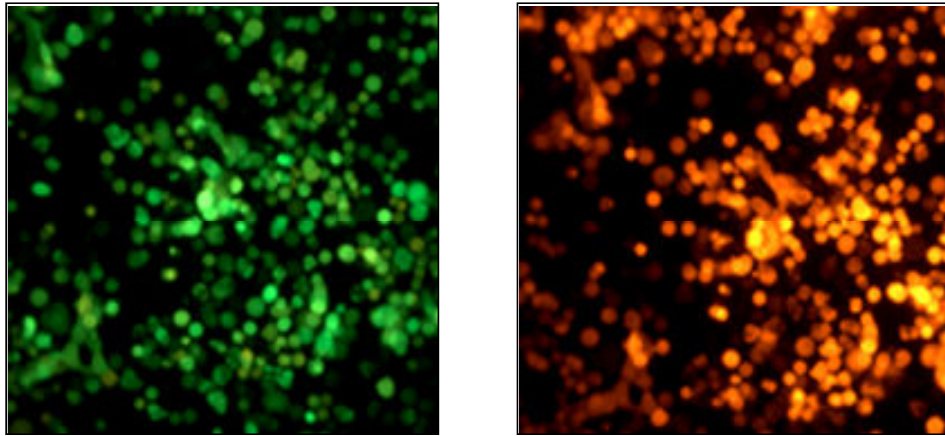


Figure 5-4

KSHV re-infection assay in the presence of DD2. Sub-confluent rSLK.219 cells were induced with either DMSO or doxycyclin in the presence or absence of 20 μ M and 30 μ M DD2. Spent media was transferred to uninfected SLK cells and GFP+ cells were scored after 48 hours by flow cytometry.

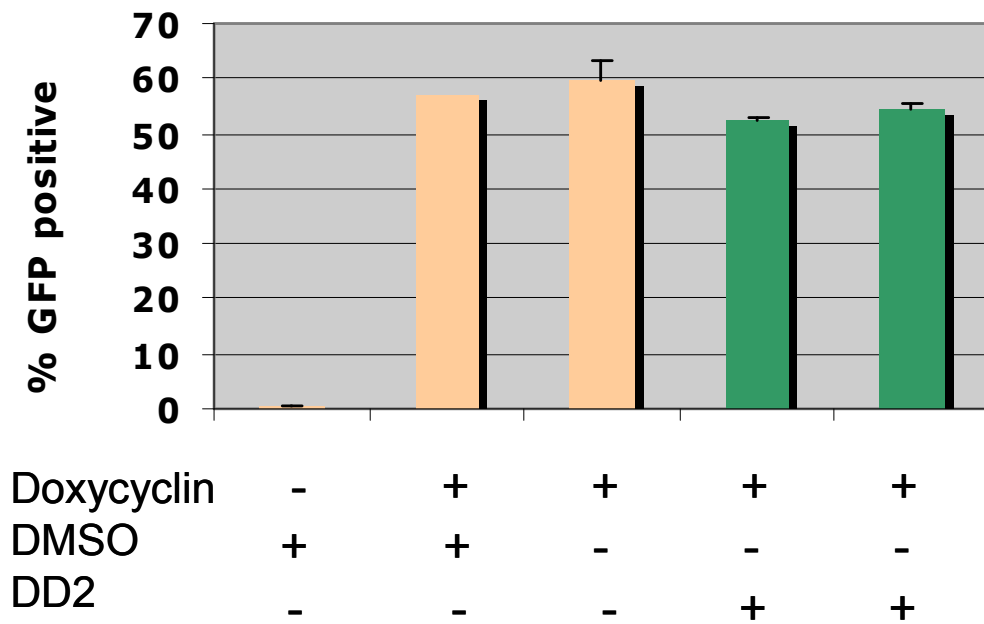
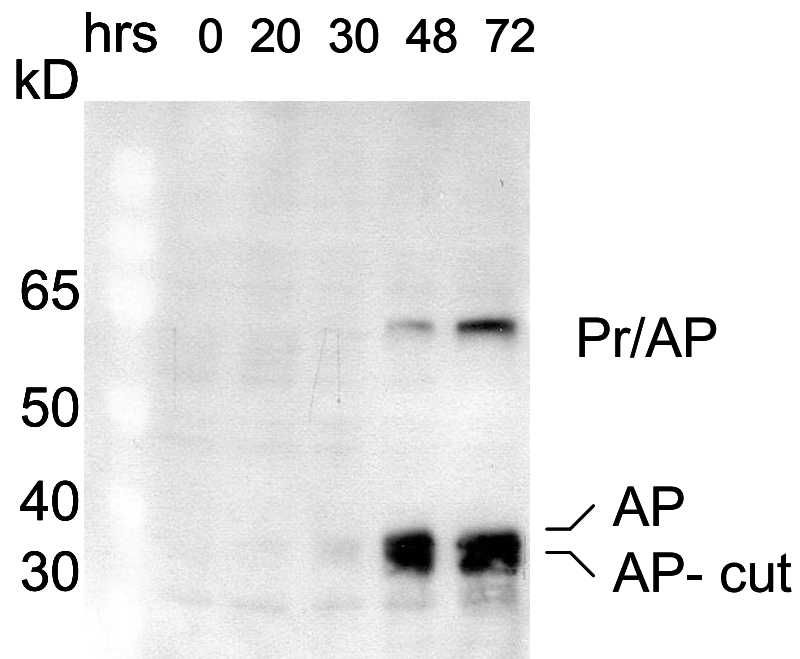


Figure 5-5

Western blot assay to monitor AP cleavage. Sub-confluent rSLK.219 cells were induced with doxycyclin and spent media was collected at the indicated time points. Lysates were prepared and analyzed by western blot for the presence of the AP protein. A rabbit antisera was the source of the polyclonal anti-AP antibody used.



CHAPTER 6: Conclusion and Future Directions in Developing Novel Inhibitors that Target Human Herpesvirus Proteases

Human herpesvirus proteases (HHV Pr) are attractive targets for the development of specific anti-herpes drugs. However, efforts to advance candidate active-site inhibitors to clinical trials have been unsuccessful. Based on evidence supporting a strong linkage between the active-site and dimer interface of KSHV Pr, we have focused on molecules that inhibit dimerization. In Chapters 2 and 3 the development and characterization of the helical mimetic small molecule DD2 was described in detail. DD2 is the first reported inhibitor targeting an HHV Pr that acts by trapping the protease monomer in an inactive state.¹ Furthermore, crystallographic data of the inhibited monomer revealed a novel allosteric pocket at the dimer interface of KSHV Pr that is occluded in the dimeric state.² This finding creates an opportunity to use *in silico* screening to identify additional scaffolds that bind in the novel interfacial DD2 pocket.

All known HHV proteases are structurally and functionally conserved. Therefore it is conceivable to identify a broad-acting inhibitor against this family of enzymes. In Chapters 2 and 3 we present preliminary evidence that DD2 inhibits human cytomegalovirus protease (CMV Pr), a beta sub-family member, with an IC_{50} of $12.8 \pm 1.1 \mu M$.¹ DD2 titration experiments with $^{13}C/^{15}N$ -methyl Ile-labeled monomeric CMV Pr (L222D), or a variant truncated to remove the disordered C-terminal α -helices suggested DD2 binds at the interface.² A close examination of available crystallographic structures shows Tyr128 located at the position congruent to Trp109 of the DD2 binding pocket in KSHV Pr. Importantly, all known HHV Pr structures have an aromatic residue at this position. This suggests that a similar allosteric pocket may be present in other HHV proteases, increasing the likelihood of identifying pan-specific inhibitors.

The poor solubility and permeability of DD2 is a limitation for testing the compound in cell culture antiviral efficacy models. Given that DD2 is our only candidate, high throughput screening (HTS) of large compound libraries is critical to the future of this project. Chapter 4 described the development and pilot test of a HTS activity assay for KSHV Pr. The pilot screen of roughly 3000 “bioactive” compounds only produced two hits, one with inadequate potency and a second that proved to inhibit through a non-specific aggregation mechanism. For future screens robust secondary assays must be in place to eliminate false positive hits that act through non-specific mechanisms.

Secondary assays are essential to HTS for eliminating false positive hits. Compounds that absorb at the emission wavelength of the KSHV Pr hexapeptide coumarin substrate (P6) may cause a signal reduction that mimics protease inhibition. We have developed a quenched substrate named iFRET8 with a different coumarin fluorophore that can be used in conjunction with P6 (**Fig. 6-1a**). The non-prime side P1-P6 peptide sequence is the same as that of the P6 substrate. Two serines are located on the prime P1'-P2' positions. In comparison to the P6 substrate, the iFRET8 substrate has a comparable K_M of 10 μM , but an improved k_{cat} of 0.2469 s^{-1} (**Table 1** and **Fig. 6-1b**). In assays using the iFRET8 substrate, both KSHV Pr inhibitors DD2 (Chapter 2) and cholanic acid (Chapter 4) showed a dose response curve that was comparable to results obtained with substrate P6. Interestingly, the IC_{50} of DD2 was higher than what was recorded with the P6 substrate. When tetrapeptide substrate P4 was tested the opposite result was obtained where the IC_{50} of DD2 was reduced (Table 1). Previous studies have shown that binding of substrate in the active-site stabilizes a network of interactions that support protease dimerization. Hence, longer substrates with tighter binding interactions reduce the apparent activity of DD2, most probably

by reducing the availability of the binding sites on the monomeric proteins. This effect on the IC₅₀ values may be used in the future to identify inhibitors that act as dimer disruptors.

Most HTS have a hit rate of ~1%, therefore a secondary assay that can quickly identify dimer disruptors is of great value. Fluorescence resonance energy transfer (FRET) is an effective technique for monitoring the distance between two proteins. KSHV Pr may be engineered to carry the donor fluorophore Cy3 on one monomer, and the acceptor fluorophore Cy5 on the second monomer, such that dimer dissociation results in a loss of FRET efficiency.³ Previously it was reported that mutating the three surface cysteines, Cys16, Cys138, and Cys179, of KSHV Pr to serines, does not affect protease function.⁴ This variant was the template used to generate two FRET constructs with cysteines at positions for conjugation to the FRET fluorophores (**Fig. 6-2**). The S185C construct contained a new mutation, while the S16C construct contained a back-mutation to the wild type cysteine residue. Even though the expression and purification results of both constructs appeared promising, the final purified products were inactive. In the event that one or both of the inactive proteases can form dimers, they may still be useful for their intended purpose. More studies are needed to determine the utility of the above construct, or the need for a modified strategy.

Using hydrocarbon-stapled α -helices is an alternate route for developing inhibitors that penetrate the cell membrane. These peptides are generated by inserting two substituted non-natural alkenyl amino acids at non-essential $i, i+4$ positions along the peptide chain, followed by cross linking via a ring-closing olefin metathesis reaction.⁵ Previous studies with Avian pancreatic polypeptide (aPP), a 30-amino acid peptide containing an internally stabilized α -helix, was evidence that

helical peptide mimetic of α -helix 5 can disrupt KSHV Pr dimerization and inhibit activity.⁶ However, in addition to the entropic cost associated with folding of the aPP scaffold, this peptide was not an optimal candidate for cell culture studies. Hydrocarbon-stapled peptides have shown desirable metabolic stability and serum half-lives and have been successfully used to target intracellular protein-protein interactions, including the Notch transcription factor complex.⁷ Aileron Therapeutics has recently advanced a stapled α -helical peptide drug candidate that targets the pro-apoptotic BAX protein into clinical trials.^{8,9}

To date we have synthesized six helical peptides to target the KSHV Pr dimer interface and tested them for activity inhibition (**Fig. 6-3** and **Fig. 6-4**). We observed weak inhibition with peptides A1 and A2, but later determined the effect was due to peptide precipitation (**Fig. 6-3**). The next generation of peptides were shorter in length and had a greater number of polar/charged residues. The distribution of charged residues across the entire sequence was also improved (**Fig. 6-1**). Peptides B1-B4 were highly soluble but did not inhibit KSHV Pr activity. Importantly, the percent of helicity of the peptides was not accurately determined for either generation of peptides, either due to poor solubility or insufficient purity. Guiding us in future efforts are Prof. Loren D. Walensky (Assistant Professor of Pediatrics, Harvard Medical School, Boston, MA) and Dr. Evripidis Gavathioti (member of the Walensky laboratory), both of whom are experts in the design and synthesis of stapled peptides. Dr. Gavathioti has provided us with additional peptide sequences that are worth exploring. We propose to generate a library of stapled peptides to screen against KSHV Pr.

Showing evidence of reduced KSHV replication in response to an allosteric KSHV Pr inhibitor, like DD2, is a key milestone. Chapter 5 presented two viral assays that can be used to test cell culture efficacy with future KSHV Pr inhibitor. Even though animal models for KSHV do not exist, Dr. Ren Sun at the University of California, Los Angeles, has developed the murine gammaherpesvirus 68 (MHV-68) as an *in vivo* model for KSHV. Additionally, the closest phylogenetic relative of KSHV is the Rhesus monkey rhadinovirus (RRV), which is the most relevant *in vivo* model and is being studied by Dr. Dean Kedes at the University of Virginia, School of Medicine. The methodologies presented in Chapters 2-5 provide the framework for the development of novel allosteric inhibitors that target not only KSHV Pr, but potentially all HHV proteases.

REFERENCES

1. Shahian, T. et al. Inhibition of a Viral Enzyme by a Small Molecule Dimer Disruptor. *Nature Chemical Biology* **5**, 640-646 (2009).
2. Lee, G.M. et al. Enzyme Inhibition by Allosteric Capture of an Inactive Conformation. *Journal of Molecular Biology* (In Press).
3. Eggers, C.T., Wang, S.X., Fletterick, R.J. & Craik, C.S. The role of ecotin dimerization in protease inhibition. *J Mol Biol* **308**, 975-91 (2001).
4. Nomura, A.M., Marnett, A.B., Shimba, N., Dotsch, V. & Craik, C.S. Induced structure of a helical switch as a mechanism to regulate enzymatic activity. *Nat Struct Mol Biol* **12**, 1019-20 (2005).
5. Kim, Y.W., Grossmann, T.N. & Verdine, G.L. Synthesis of all-hydrocarbon stapled alpha-helical peptides by ring-closing olefin metathesis. *Nat Protoc* **6**, 761-71.
6. Shimba, N., Nomura, A.M., Marnett, A.B. & Craik, C.S. Herpesvirus protease inhibition by dimer disruption. *J Virol* **78**, 6657-65 (2004).
7. Moellering, R.E. et al. Direct inhibition of the NOTCH transcription factor complex. *Nature* **462**, 182-8 (2009).
8. Tse, C. et al. ABT-263: a potent and orally bioavailable Bcl-2 family inhibitor. *Cancer Res* **68**, 3421-8 (2008).
9. Pitter, K., Bernal, F., Labelle, J. & Walensky, L.D. Dissection of the BCL-2 family signaling network with stabilized alpha-helices of BCL-2 domains. *Methods Enzymol* **446**, 387-408 (2008).
10. Lazic, A., Goetz, D.H., Nomura, A.M., Marnett, A.B. & Craik, C.S. Substrate modulation of enzyme activity in the herpesvirus protease family. *J Mol Biol* **373**, 913-23 (2007).

Table 6-1

The effect of substrate length on DD2 activity. The synthesis of peptides P4 and P6, and the kinetic assays with all peptides were performed as reported previously.¹⁰ The numerical values 4 and 6 used in naming peptides P4 and P6 refer to the number of amino acids. The IC₅₀ of DD2 increases when longer substrates are used. ACC = 7-amino-4-carbamoylmethyl coumarin fluorophore group. Ac = acetyl group.

| Name | Sequence | K _{cat} (s ⁻¹) | K _M (μM) | DD2 IC ₅₀ |
|--------|------------------|-------------------------------------|---------------------|----------------------|
| P4 | Ac-YtQA-ACC | 0.0084±0.0003 | 80.0±8.8 | 2.0 |
| P6 | Ac-PVYtQA-ACC | 0.0083±0.0002 | 8.5±0.8 | 2.7 |
| iFRET8 | MCA-PVYtQA-SSdnp | 0.2469 | 10 | 10.2 |

Figure 6-1

Substrate iFRET8 sequence and kinetics. (a) The structure of iFRET8 substrate is shown. A 2,4,-dinitrophenyl quencher group and 7-methoxycoumarin-4-acetyl fluorophore are on the N and C terminus, respectively. The location of the scissile bond is marked with a arrow. The excitation/emission wavelengths of 7-methoxycoumarin-4-acetyl in the unquenched state are 323/393 nm. (b) The Michaelis-Menten plot for the iFRET8 substrate is shown with increasing substrate concentration on the x axis, and initial velocity of KSHV Pr activity on the y axis. The K_m and k_{cat} parameters were calculated as described previously.¹⁰

Figure 6-1

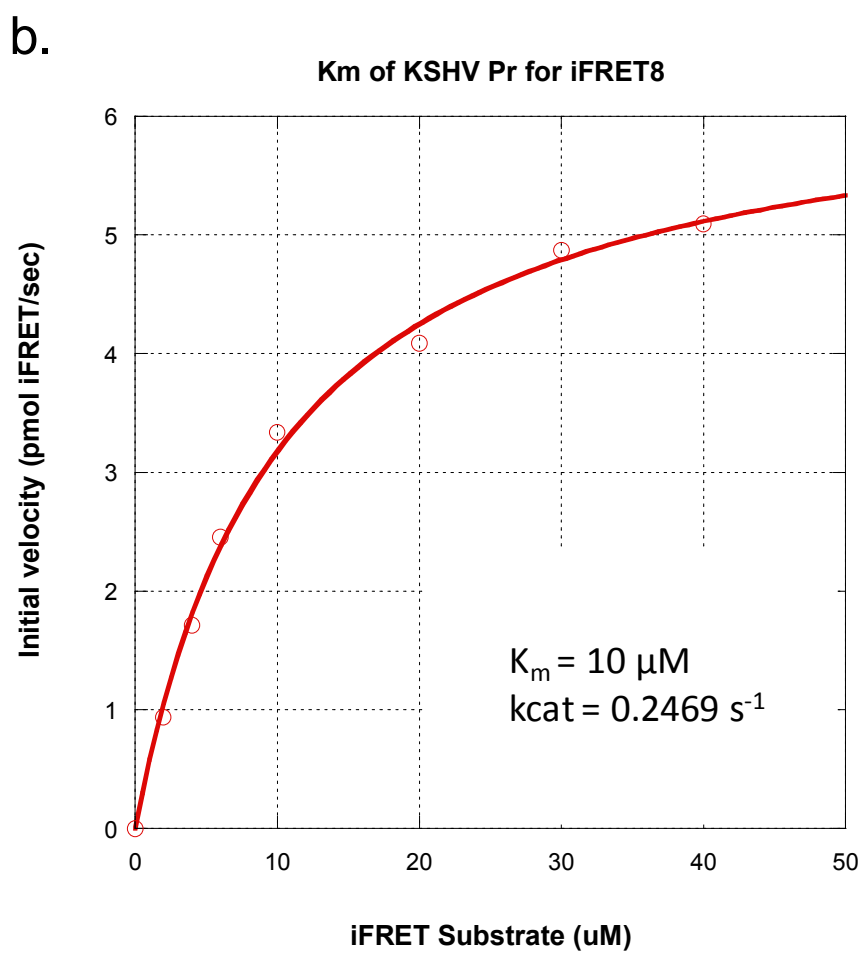
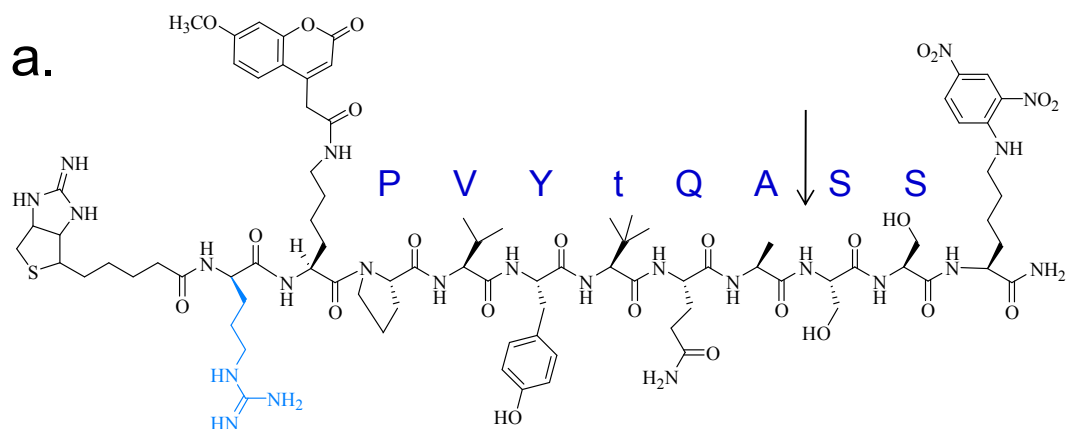


Figure 6-2

Design of KSHV Pr FRET construct. The dimeric crystal structure of KSHV Pr is shown. In each monomer there are four cysteines (red) and two serines (blue). The locations ideal for placing the FRET donor and acceptor dyes are Ser185 (R_0 of 46.9 Å) and Cys16 (R_0 of 44.1 Å). FRET efficiency at these placements is expected to be 67% and 75% respectively. Dimer disruption will result in a decrease in FRET efficiency.

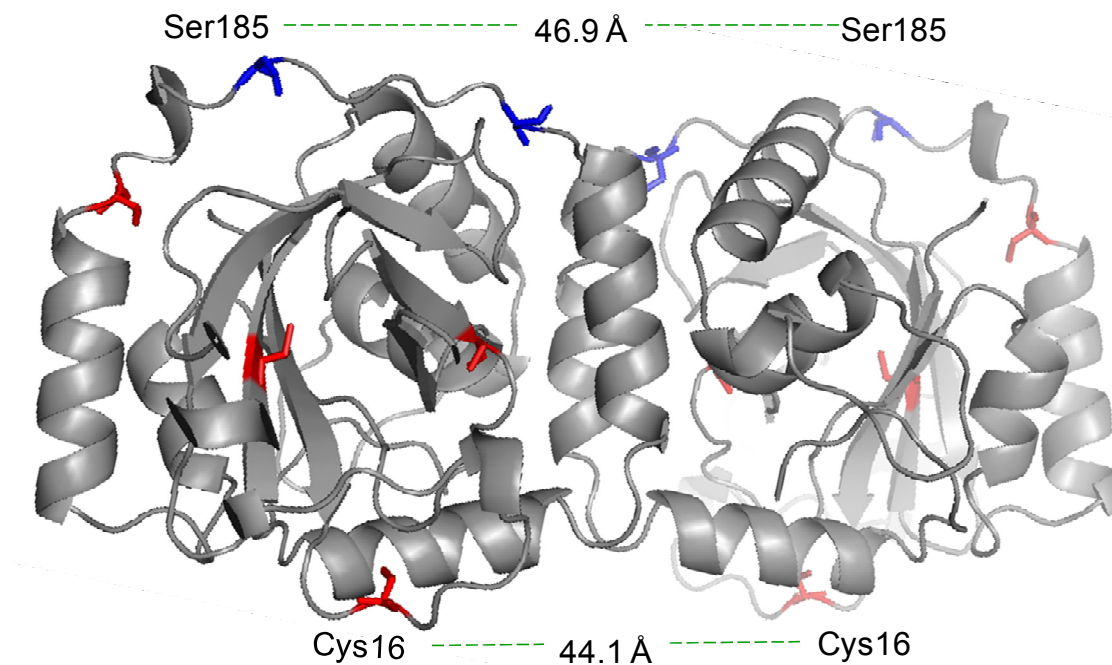


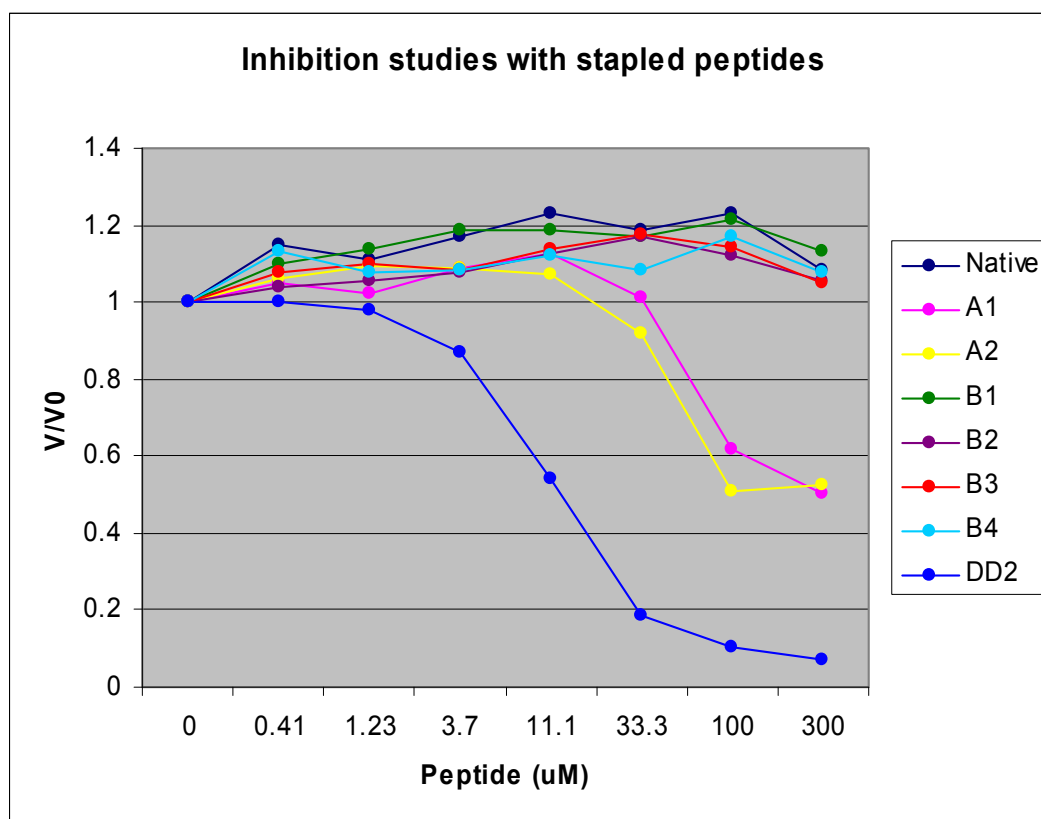
Figure 6-3

Sequences of hydrocarbon-stapled peptides. The first sequence listed, PLETLMAKAIDAGFIRDR, is that of the native α -helix 5. The residues critical to the interface are in blue. Residues that don't form interactions at the dimer interface are marked in black. The non-natural alkenyl amino acid substitutions at the i and $i+4$ positions are marked in green. Other amino acid substitutions or additions are marked in red. Peptide N, serves as the control and mimics the native α -helix 5 sequence with the exception of the M/L substitution, which was made since methionine is not favored in peptide synthesis protocols. Peptides C1-C6 remain to be synthesized and tested. In the columns for % polar and % charge, the number outside the parenthesis refers to the number of polar or charged residues.

| | peptide sequence | residues | %polar | %charge | charge |
|----|---|----------|--------|---------|--------|
| | P L E T L M A K A I D A G F I R D R | 18 | 7(38%) | 6(33%) | 0 |
| N | P L E T L L A K A I D A G F I R R K | 18 | 7(38%) | 6(33%) | +2 |
| A1 | P L E X L L A X A I D A G F I R R K | 18 | 5(27%) | 5(27%) | +1 |
| A2 | P L E T L L A X A I D X G F I R R K | 18 | 6(33%) | 5(27%) | +1 |
| B1 | R L E T R L A X A I D X G F R K | 16 | 7(43%) | 6(37%) | +2 |
| B2 | R L E T R L A X A I D X G Y R K | 16 | 8(50%) | 6(37%) | +2 |
| B3 | R L E X R L A X A I D S G F R K | 16 | 7(43%) | 6(37%) | +2 |
| B4 | R L E X R L A X A I D S G Y R K | 16 | 8(50%) | 6(37%) | +2 |
| C1 | E E X L E T X L A K A I D A G F I R R R | 20 | | | 0 |
| C2 | E E X L E T X L A K A I D T G F I R R R | 20 | | | 0 |
| C3 | L E T S L A K A I D X G F I X R R | 17 | | | +1 |
| C4 | L E T S L A K A I D X G F T X R R R | 18 | | | +2 |
| C5 | L E X E L A X A I D A G F I R R R | 17 | | | 0 |
| C6 | L E T E L A X A I D X G F I R R R | 17 | | | 0 |

Figure 6-4

Inhibition studies with hydrocarbon-stapled peptides. Peptides A1-B4 (see Fig. 6-1) were synthesized using published protocols.⁵ Increasing concentrations of DD2, native peptide control, and hydrocarbon stapled peptides were tested for inhibition of KSHV Pr activity, as reported previously.¹ The stapled peptides do not inhibit KSHV Pr activity when compared to control DD2.

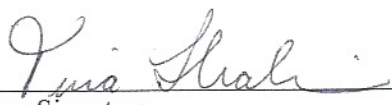


Publishing Agreement

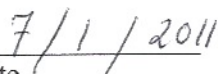
It is the policy of the University to encourage the distribution of all theses, dissertations, and manuscripts. Copies of all UCSF theses, dissertations, and manuscripts will be routed to the library via the Graduate Division. The library will make all theses, dissertations, and manuscripts accessible to the public and will preserve these to the best of their abilities, in perpetuity.

Please sign the following statement:

I hereby grant permission to the Graduate Division of the University of California, San Francisco to release copies of my thesis, dissertation, or manuscript to the Campus Library to provide access and preservation, in whole or in part, in perpetuity.



Author Signature



Date